Model Reduction and Nonlinear Model Predictive Control of Large-Scale Distributed Parameter Systems with Applications in Solid Sorbent-Based CO_2 Capture

Submitted in partial fulfillment of the requirements

for the degree of

Doctor of Philosophy

in

Chemical Engineering

Mingzhao Yu

B.S., Control Science and Engineering, Zhejiang University

Carnegie Mellon University

Pittsburgh, PA

April, 2017

Acknowledgments

I would like to express my sincere thanks to my advisor, Prof. Lorenz T. Biegler, and I feel very fortunate to work with him over the past five years. He is not only an outstanding advisor who provides insightful guidance in research, but also a great mentor who is always willing to listen and help whenever needed. I am extremely grateful for benefiting from his vast knowledge, support and patience. I would also like to thank Prof. Ignacio E. Grossmann, Prof. B. Erik Ydstie, Prof. Nikolaos V. Sahinidis, Prof. Chrysanthos E. Gounaris, and all the faculty and staff in chemical engineering department at Carnegie Mellon for their support during my PhD study.

I would like to thank the members of my committee, Prof. Lorenz T. Biegler, Prof. B. Erik Ydstie, Prof. Nikolaos V. Sahinidis and Prof. Shlomo Ta'asan, for their careful reading of my dissertation and all their comments and suggestions.

I would also like to thank Dr. David Miller, Prof. Debangsu Bhattacharyya, Dr. Andrew Lee, Dr. Benjamin Omell, Dr. Priyadarshi Mahapatra, Dr. Jinliang Ma, Dr. Yang Chen, Dr. Zhihong Yuan and other colleagues in the CCSI and IDAES projects for all their support and help. It is a great experience for me to work in this interdisciplinary team across national laboratories and universities. I would like to express my gratitude to all members of Prof. Biegler's research group for the motivating discussions and enjoyable conversations we had. My thanks also go to all my friends in the U.S. and China for their support and encouragements.

I especially thank my parents for their support and unconditional love during my good and bad times. I would also like to thank my wife Shujia. Her love, patience and sense of humor brightens my life and encourages me to face the challenges and move forward. The love of my family is the very reason that I never lose hope, even in the most difficult time.

I am grateful to the financial support from the National Energy Technology Laboratory and the Department of Energy under grant DE-AC02-05CH11231 for my PhD study.

Abstract

This dissertation deals with some computational and analytic challenges for dynamic process operations using first-principles models. For processes with significant spatial variations, spatially distributed first-principles models can provide accurate physical descriptions, which are crucial for offline dynamic simulation and optimization. However, the large amount of time required to solve these detailed models limits their use for online applications such as nonlinear model predictive control (NMPC). To cope with the computational challenge, we develop computationally efficient and accurate dynamic reduced order models which are tractable for NMPC using temporal and spatial model reduction techniques. Then we introduce an input and state blocking strategy for NMPC to further enhance computational efficiency. To improve the overall economic performance of process systems, one promising solution is to use economic NMPC which directly optimizes the economic performance based on first-principles dynamic models. However, complex process models bring challenges for the analysis and design of stable economic NMPC controllers. To solve this issue, we develop a simple and less conservative regularization strategy with focuses on a reduced set of states to design stable economic NMPC controllers.

In this thesis, we study the operation problems of a solid sorbent-based CO_2 capture system with bubbling fluidized bed (BFB) reactors as key components, which are described by a large-scale nonlinear system of partial-differential algebraic equa-

tions. By integrating dynamic reduced models and blocking strategy, the computational cost of NMPC can be reduced by an order of magnitude, with almost no compromise in control performance. In addition, a sensitivity based fast NMPC algorithm is utilized to enable the online control of the BFB reactor. For economic NMPC study, compared with full space regularization, the reduced regularization strategy is simpler to implement and lead to less conservative regularization weights. We analyze the stability properties of the reduced regularization strategy and demonstrate its performance in the economic NMPC case study for the CO_2 capture system.

Contents

List of Figures

List of Tables

Chapter 1

Introduction

In this chapter, we present the scope of the research work in this dissertation. Firstly we introduce the conventional hierarchy structure for process operations and review research developments to improve the current operational practice. Then we define the research problems tackled in this dissertation and introduce thesis outline.

1.1 Hierarchy Structure for Process Operation

For the process industries, operations of complex processes involve a large number of decisions variables and it is extremely important to find an optimized operation strategy to maximize the overall economic performance. The current practice of operation is the so-called hierarchy planning and operations structure, which is shown in the following figure. The upper layers, planning and scheduling layer, decide what products to produce and in which sequences. These tasks are usually executed on a monthly/daily basis. Then the business decisions are passed down to the real time optimization (RTO) and advanced process control (APC) layer for real-time implementation. Based on these business decisions, RTO finds econom-

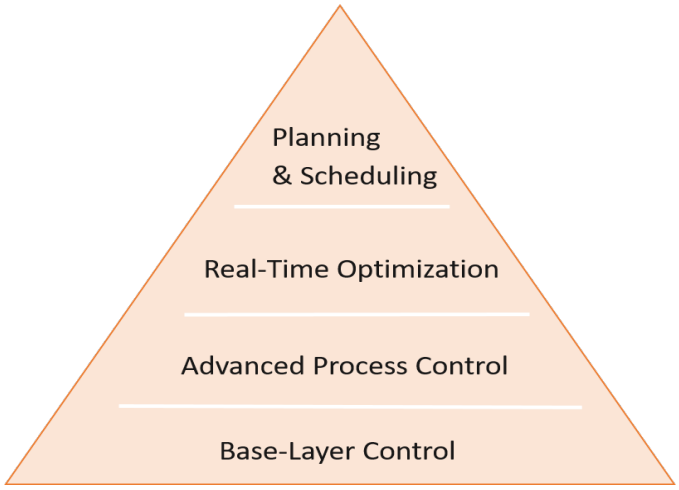

Figure 1.1: Hierarchy structure for process operation

ically optimal operating points by solving an optimization problem which optimizes an economic objective, subject to first-principles steady state process models. Then these operating points are passed down as setpoints to the APC layer and it will drive the process to the setpoints sent by the RTO layer. The APC layer usually utilizes model predictive control (MPC) to determine optimal control moves. The models used in MPC controllers are typically linear data-driven models which are obtained through system identification. Lastly, Base-Layer Control is required to implement the control decisions by APC, which are typically done by PID controllers.

Such a hierarchy has been widely applied in process industry and has various successful applications. However, the operation performances have been limited by several inconsistencies existed between different layers within the structure. One significant inconsistency is in the execution frequency of different layers. For example, the RTO layer usually runs on an hourly basis while APC layer usually executes every minute. Between RTO executions, if disturbances occur, RTO will take no action to handle these disturbances until process measurements get steady and RTO models get updated. Meanwhile APC will still track the old setpoints, which are now suboptimal. External disturbances are very common in the daily oper-

ations of real plants. For example, typical disturbances include the variations in input feed temperature or composition and also limit changes by operators. Since RTO runs relatively infrequently, it lags behind external disturbances and sacrifices the process economic performance between RTO executions. Another inconsistency exists due to different models used in separate layers. Although detailed first-principles models used in RTO layers give accurate prediction of system's economics, the dynamics of the process is not considered. What's more, the setpoints by RTO layer may not be reachable for APC layer since it uses a different set of models which are typically linear data-driven models. To mitigate this issue, a separate steady state optimization is required in the APC layer, but that may lead to sacrifice in the overall economic performance.

1.2 Research Developments

To improve the current process operation structure, much research has been done in this area, aiming at bridging the gaps between different operational layers and improving the overall economic performances of process operations.

Firstly, we can see a trend of tighter integration of different layers to overcome the shortcomings of the current hierarchy structure. For example, the concept of dynamic real time optimization (DRTO) has been proposed to integrate the RTO and APC layers [15, 38]. Compared with the two-layered structure, DRTO directly optimizes the economic performance of process over a prediction time subject to first-principles dynamic models. Similar to this idea, high-level objectives such as process economics are added to MPC, which is denoted as economic model predictive control (eMPC) [5, 71]. More theoretical developments of economic MPC including stability analysis will be discussed in Chapter 5. With this formulation, process economics can be directly optimized in the dynamic control problem and thus the limitations of the conventional RTO-APC structure could be avoided.

Secondly, we can see there are increasing interests in integrating first-principles models into dynamic process operations. For processes with strong nonlinearity and frequent transitions, first-principles process models are crucial to provide accurate predictions for dynamic behaviors. With improved solution algorithms and increasing computing power, detailed first-principles models are being integrated for dynamic optimization purposes. This includes the developments and application of first-principles differential-algebraic equation (DAE) models for off-line dynamic optimization such as optimal recipe optimization [65] and optimal grade transition [79]. For control studies, detailed nonlinear process models are being incorporated into the MPC framework and this strategy is denoted as nonlinear MPC (NMPC). Compared with linear data-driven models in MPC, first-principles models are more accurate in larger ranges and thus NMPC may help improve control performance. Online NMPC strategies have been demonstrated on highly nonlinear industrial chemical processes including batch reactors [64] and polymerization processes [96].

Integration of optimal decision-making for process operations and application of first-principles models are crucial to improve the overall economic performance for complex integrated process systems. However, it should be noted that successful applications of these strategies always require efficient solutions, which could be challenging with tighter integration of separate layers and increasing applications of more detailed first-principles models.

1.3 Research Statement and Thesis Outline

For process with strong nonlinearity, NMPC provides superior performance over MPC in terms of setpoint tracking and disturbance rejection. Economic NMPC provides a novel alternative to integrate the traditional RTO and APC layers and it optimizes the economic performance directly. However, to facilitate the success-

ful application of these ideas, improved computational performance is always required especially for complex integrated systems with detailed first-principles process models.

The objective of this dissertation is to develop systematic approaches to handle the computational and analytic challenges for NMPC brought by large-scale spatially-distributed first-principles process models. Spatially distributed first-principles process models are usually needed to provide accurate physical descriptions for complex chemical processes with significant spatial variations. The integration of such detailed model into dynamic process operations such as NMPC framework requires direct transcription of the first-principles models, which lead to large-scale models whose numerical solution are computationally expensive. To handle these challenges, we develop computational efficient models suitable for the time-critical application using model reduction techniques. Novel formulation for NMPC will be discussed to improve computational efficiency. In addition, economic NMPC is a promising solution to improve the economic performance of process operations. For complex systems with a large number of states, in addition to computational burden, it complicates the analysis and design of stable economic NMPC controller. To solve this issue, we develop a regularization strategy on reduced sets of system states to design stable economic NMPC controller.

In this thesis, we study the operation problems of bubbling fluidized bed (BFB) reactors in a post-combustion CO_2 capture process. Specific tasks for this thesis include dynamic model reduction, computationally efficient formulations for setpoint tracking NMPC and regularization strategy for economic NMPC. The proposed strategies are demonstrated on the setpoint tracking NMPC and economic NMPC of the BFB reactors with applications in CO_2 capture.

This dissertation is organized as follows:

Chapter 2 provides background and literature reviews for the tasks in the disser-

tation. For NMPC, we will introduce the basic notations, formulation and stability results for setpoint tracking NMPC. We also present the formulation of NMPC into nonlinear programming (NLP) problems via direct transcription through high order collocation with finite elements grids. We will also discuss solution strategies for NLP and briefly describe a sensitivity based NMPC algorithm. For model reduction, we will provide a review of general model reduction approaches.

Chapter 3 discusses process modeling and model reduction for the BFB reactor. Firstly we will briefly introduce the application of BFB reactors in CO_2 capture process and the rigorous modeling of BFB reactors. Then we will focus on the model reduction for the rigorous BFB model and discuss the temporally and spatially dynamic reduced models.

Chapter 4 focuses on improving computational efficiency for NMPC of the BFB reactor. We introduce an input and state blocking formulation for NMPC to further reduce the size of NLP problem with stability guarantees. Dynamic reduced models are integrated into NMPC and additive output correction terms are introduced to handle the model mismatch. Case studies show computational cost of NMPC can be reduced by an order of magnitude with almost no compromise in control performance. Lastly, advanced step NMPC is applied to reduce the online computational delay.

Chapter 5 studies the economic NMPC of an integrated CO_2 capture system aiming at reducing operational costs. A regularization strategy with reduced sets of states is proposed for economic NMPC, which is simpler to implement and less conservative compared with full regularization. We discuss the stability properties of the reduced regularization strategy and demonstrate its performance in the economic NMPC case study for the integrated CO_2 capture system.

Chapter 6 concludes this dissertation and discusses recommendations for future work.

Chapter 2

Literature Review

In this chapter, we briefly review the literature in the area of model predictive control (MPC), computational strategies and model reduction, which are closely related with the research work in this dissertation. Firstly we introduce basic notation and formulation of MPC which will be used in the later chapters. Stability properties of setpoint tracking NMPC will also be discussed. After that, we review the computational strategy used to solve NMPC problems and also a fast NMPC algorithm. In the last section, we discuss general approaches for model reduction.

2.1 MPC Formulation

We consider the following discrete-time dynamic model of a plant:

$$\begin{aligned} x(k+1) &= \hat{f}(x(k), u(k), w(k)) \\ &= f(x(k), u(k)) + d(x(k), u(k), w(k)) \end{aligned} \tag{2.1.1}$$

where $x(k) \in \Re^{n_x}$, $u(k) \in \Re^{n_u}$ and $w(k) \in \Re^{n_w}$ are the plant states, controls and disturbance signals, respectively, defined at time steps t_k with integers $k > 0$. The mapping $f : \Re^{n_x+n_u} \mapsto \Re^{n_x}$ represents the nominal model, while the term

$d : \Re^{n_x+n_u+n_w} \mapsto \Re^{n_x}$ is used to describe modeling errors, estimation errors and disturbances.

A general formulation of MPC for this given plant is shown as follows:

$$
\begin{aligned}
V(x(k)) := \min_{z_l, v_l} & \sum_{l=0}^{N-1} \psi(z_l, v_l) \\
\text{s.t.} \quad & z_{l+1} = f(z_l, v_l), l = 0, \ldots N-1 \\
& z_0 = x(k) \\
& v_l \in \mathbb{U}, z_l \in \mathbb{X}.
\end{aligned}
\tag{2.1.2}
$$

where N is the prediction horizon length of MPC, and $x(k)$ are the initial conditions for the dynamic plant model. The nominal plant model $f(\cdot,\cdot)$ is used to predict the trajectory of the plant states. $\psi(\cdot,\cdot)$ is the stage cost. For setpoint tracking MPC, the stage cost is usually a quadratic form which represents the differences between the predicted states and setpoints. By solving the above optimization problem, MPC can find the optimal control moves subject to the constraints on predicted states z and controls u over a specific horizon N in the future.

The key idea of MPC is to solve this dynamic problem in a moving horizon manner. At sampling time t_k, the MPC problem (2.1.2) is solved and the optimal solution is denoted as $\{z_0^*, \cdots, z_N^*, v_0^*, \cdots, v_{N-1}^*\}$. The first control move of the optimal solution is extracted and implemented into the plant as $u(k) = v_0^*$. Then the plant evolves as $x(k+1) = f(x(k), u(k)) + d(x(k), u(k), w(k))$. At next sampling time t_{k+1}, the MPC problem is shifted one step forward by setting $k = k+1$ and the new state estimates $x(k)$ are applied as initial conditions. With this moving horizon strategy, state estimates at each sampling time provide feedback to handle process disturbances and model mismatch.

With this formulation, MPC is suitable to control multivariable plants and can directly handle state and input constraints, which are significant advantages com-

pared with most conventional control strategies like PID controller. Therefore MPC has been widely applied in process industry [69] and become an active area for research study [61].

MPC strategy originates in early 1980s. Cutler and Ramaker proposed the dynamic matrix control (DMC) algorithm [25], where linear step response models are used to predict system dynamic response. Later, we can see more variations of MPC controller such as QDMC [32]. The linear data-driven models are widely used for MPC because they are relatively easy to obtain and have small computational cost. Thus linear MPC has been successfully applied in refining and petrochemical processes where the system dynamics are only slightly nonlinear. Recently, nonlinear MPC (NMPC), which uses nonlinear models for state predictions, are becoming attractive, especially for processes with strong nonlinearity. In this dissertation, we focus on the NMPC strategy using first-principles nonlinear models.

2.2 Stability Property of Setpoint Tracking NMPC

One of the key areas for NMPC study is the stability analysis of the closed-loop system using NMPC. The stability of a system without any disturbances is called *nominal* stability; while the stability of a system under disturbances is called *robust* stability. In this section, we will introduce some basic definitions and assumptions for stability analysis and briefly discuss the nominal and robust stability property of setpoint tracking NMPC.

2.2.1 Notations and Definitions

Firstly we introduce some definitions which will be used in stability analysis.

Definition 2.2.1. *[14] A function $f(.)$: $\Re^n \mapsto \Re$ is continuous in $\Re^n$ if for all $\epsilon > 0$, there exists a value $\delta > 0$ such that $|f(x_1) - f(x_2)| \leq \epsilon$ for all x_1 , x_2 that satisfy $|x_1 - x_2| \leq \delta$.*

A continuous function $f(.)$: $\Re^n \mapsto \Re$ is Lipschitz continuous in $\Re^n$ if there exists a finite $L > 0$ such that $|f(x_1) - f(x_2)| \leq L|x_1 - x_2|$ for all $x_1, x_2 \in \Re^n$.

Definition 2.2.2. *[59] A continuous function $\alpha(.)$: $\Re_{\geq 0} \mapsto \Re_{\geq 0}$ is a $\mathcal{K}$ function if $\alpha(0) = 0, \alpha(s) > 0, \forall s > 0$ and it is strictly increasing. A continuous function $\alpha(.)$: $\Re_{\geq 0} \mapsto \Re_{\geq 0}$ is a $\mathcal{K}_\infty$ if it is a $\mathcal{K}$ function and $\alpha(s) \to \infty$ as $s \to \infty$. A continuous function $\alpha(.)$: $\Re_{\geq 0} \times Z_{\geq 0} \mapsto \Re_{\geq 0}$ is a $\mathcal{KL}$ function if $\alpha(s,k)$ is a $\mathcal{K}$ function in s for any fixed $k > 0$ and for each fixed $s > 0$, $\alpha(s, \cdot)$ is decreasing and $\alpha(s,k) \to 0$ as $k \to \infty$.*

Assumption 2.2.1. *The set $\mathbb{X} \subseteq \Re^n$ is robust positive invariant for the system (2.1.1), namely, $\hat{f}(x, u(x), w) \in \mathbb{X}$ holds for all $x \in \mathbb{X}, w \in \mathbb{W}$.*

Definition 2.2.3. *(Stable Equilibrium Point) [74] The point $x = 0$ is called a stable equilibrium point of the system (2.1.1) if for all $k_0 > 0$ and $\epsilon_1 > 0$, there exists $\epsilon_2 > 0$ such that $|x_{k_0}| < \epsilon_2 \Rightarrow |x_k| < \epsilon_1$ for all $k \geq k_0$.*

Next we consider nominal and robust stability. There are various forms of stability; here we introduce the definitions of asymptotic stability for the nominal case and input-to-state stability and input-to-state practical stability for the robust case.

Definition 2.2.4. *(Asymptotic Stability) [74] The system (2.1.1) is asymptotically stable on $\mathbb{X}$ if $\lim_{k \to \infty} x(k) \to 0$ for all $x_0 \in \mathbb{X}$ and $x = 0$ is a stable equilibrium point.*

Definition 2.2.5. *(Input-to-State Stability) [45, 59] The system (2.1.1) is input-to-state stable (ISS) in $\mathbb{X}$ if there exists a $\mathcal{KL}$ function β, and a $\mathcal{K}$ function γ such that for all w in the bounded set $\mathcal{W}$,*

$$|x(k)| \leq \beta(|x(0)|, k) + \gamma(|w|), \ \forall k \geq 0, \ \forall x(0) \in \mathbb{X}$$

Definition 2.2.6. *(Input-to-State Practical Stability) [56] The system (2.1.1) is input-to-state practically stable (ISpS) in $\mathbb{X}$ if there exists a $\mathcal{KL}$ function β, a $\mathcal{K}$ function γ and a positive constant c such that for all w in the bounded set $\mathcal{W}$,*

$$|x(k)| \leq \beta(|x(0)|, k) + \gamma(|w|) + c, \ \forall k \geq 0, \ \forall x(0) \in \mathbb{X}$$

Lyapunov stability theorems provide a powerful tool for the stability analysis of closed-loop systems using NMPC. The following are the definitions for Lyapunov functions and the theorems to establish stability property based on Lyapunov functions.

Definition 2.2.7. *(Lyapunov Function) [74] A function $V(\cdot)$ is called a Lyapunov function for the system (2.1.1), if there exist $\mathcal{K}_\infty$ functions $\alpha_1, \alpha_2, \alpha_3$ such that for all $x \in \mathbb{X}$,*

$$\begin{aligned} &\alpha_1(|x|) \leq V(x) \leq \alpha_2(|x|) \\ &V(\hat{f}(x, u(x), w)) - V(x) \leq -\alpha_3(|x|) \end{aligned} \tag{2.2.1}$$

Definition 2.2.8. *(ISS-Lyapunov Function) [45, 59] A function $V(\cdot)$ is called an ISS-Lyapunov function for the system (2.1.1), if there exist $\mathcal{K}_\infty$ functions $\alpha_1, \alpha_2, \alpha_3$, a $\mathcal{K}$ function σ such that for all $x \in \mathbb{X}$ and $w \in \mathbb{W}$,*

$$\begin{aligned} &\alpha_1(|x|) \leq V(x) \leq \alpha_2(|x|) \\ &V(\hat{f}(x, u(x), w)) - V(x) \leq -\alpha_3(|x|) + \sigma(|w|) \end{aligned} \tag{2.2.2}$$

Definition 2.2.9. *(ISpS-Lyapunov Function) [56] A function $V(\cdot)$ is called an ISpS-Lyapunov function for the system (2.1.1), if there exist $\mathcal{K}_\infty$ functions $\alpha_1, \alpha_2, \alpha_3$, a $\mathcal{K}$ function σ and positive constants c_1, c_2 such that for all $x \in \mathbb{X}$ and $w \in \mathbb{W}$,*

$$\begin{aligned} &\alpha_1(|x|) \leq V(x) \leq \alpha_2(|x|) + c_1 \\ &V(\hat{f}(x, u(x), w)) - V(x) \leq -\alpha_3(|x|) + \sigma(|w|) + c_2 \end{aligned} \tag{2.2.3}$$

Theorem 2.2.1. *[74] If system (2.1.1) admits a Lyapunov Function in $\mathbb{X}$ that satisfies Assumption 2.2.1, then it is asymptotically stable in $\mathbb{X}$.*

Theorem 2.2.2. *[45, 59] If system (2.1.1) admits an ISS-Lyapunov Function in $\mathbb{X}$ that satisfies Assumption 2.2.1, then it is ISS in $\mathbb{X}$.*

Theorem 2.2.3. *[56] If system (2.1.1) admits an ISpS-Lyapunov Function in $\mathbb{X}$ that sat-*

isfies Assumption 2.2.1, then it is ISpS in $\mathbb{X}$.

2.2.2 Nominal Stability

The value function $V(x)$ of NMPC (2.1.2) is a good candidate for Lyapunov functions, which can be used to establish the stability property of NMPC. To ensure the stability of NMPC, different formulations of NMPC have been proposed, i.e. infinite-horizon MPC; finite horizon NMPC with terminal constraint/terminal cost; and quasi-infinite horizon NMPC. By adding appropriate modifications on NMPC (2.1.2), $V(x)$ can be shown to be a Lyapunov function and thus the nominal asymptotic stability of MPC can be established. A review of stability property of MPC can be found in [61].

In this section, we focus on a specific formulation of NMPC to illustrate the outline of a stability proof, which provides a basis for the research in this dissertation. The following is a finite horizon formulation for NMPC with terminal equality constraints.

$$\begin{aligned} V(x(k)) := \min_{z_l, v_l} & \sum_{l=0}^{N-1} \psi(z_l, v_l) \\ \text{s.t.} \quad & z_{l+1} = f(z_l, v_l), l = 0, \ldots N-1 \\ & z_0 = x(k), z_N = x_s \\ & v_l \in \mathbb{U}, z_l \in \mathbb{X}. \end{aligned} \tag{2.2.4}$$

Compared with the NMPC formulation (2.1.2), only terminal equality constraints $z_N = x_s$ are imposed to facilitate the stability analysis, where x_s are setpoints for tracking NMPC. Here we assume that the states and controls are restricted to the domains $\mathbb{X}$ and $\mathbb{U}$, respectively. The set $\mathbb{U}$ is compact and contains the origin; the set $\mathbb{X}$ is closed and contains the origin in its interior. We consider a stage cost given by $\psi(\cdot,\cdot) : \Re^{n_x+n_u} \to \Re$, which is assumed to be Lipschitz continuous.

Stability properties of setpoint tracking NMPC can be found in [46, 59], with the following assumption:

Assumption 2.2.2. *(Nominal Stability Assumptions for NMPC)*

- *The optimal stage cost $\psi(x,u)$ satisfies $\alpha_p(|x|) \leq \psi(x,u) \leq \alpha_q(|x|)$ where $\alpha_p(\cdot)$ and $\alpha_q(\cdot)$ are $\mathcal{K}_\infty$ functions.*

Nominal stability of NMPC can be established by the following theorem.

Theorem 2.2.4. *(Nominal Stability) Consider the moving horizon problem (2.2.4) that satisfies Assumption 2.2.2. Then, $V(x)$ from the controller (2.2.4) is a Lyapunov function and the closed-loop system is asymptotically stable.*

To prove this theorem, we rely on a key property called the recursive feasibility of NMPC. Namely, if we obtain optimal solutions $\{z_0^*, \cdots, z_N^*, v_0^*, \cdots, v_{N-1}^*\}$ of NMPC (2.2.4) at t_k, then these solutions can serve as feasible solutions for NMPC problem at t_{k+1} with some mild assumptions. For NMPC (2.2.4), we can construct a feasible solution $\{z_1^*, \cdots, z_N^*, x_s, v_1^*, \cdots, v_{N-1}^*, u_s\}$ for NMPC at t_{k+1}. Then we compare the value function $V(x(k))$ at two consecutive sampling times. Based on recursive feasibility and the principle of optimality, we can derive the following inequality:

$$V(x(k+1)) - V(x(k)) \leq -(\psi(x(k), u(k)) - \psi(x_s, u_s)) \tag{2.2.5}$$

For setpoint tracking NMPC, the stage cost is usually a quadratic form $\psi(z_l, v_l) = |z_l - x_s|^2_{Q_x} + |v_l - u_s|^2_{Q_u}$. Therefore, (x_s, u_s) are the global minimum for all $z \in \mathbb{X}, v \in \mathbb{U}$. Thus the right hand side of equation (2.2.5) is always negative and $V(x)$ will be non-increasing and it will converge to a fixed value. Then, we can show that $\lim_{k\to\infty} \psi(x(k), u(k)) \to \psi(x_s, u_s)$ and with Assumption 2.2.2, we have $\lim_{k\to\infty} x(k) \to x_s$.

2.2.3 Robust Stability

We also make the following assumptions and establish robust stability of the NMPC controller from the following theorem [45, 59].

Assumption 2.2.3. *(Robust Stability Assumptions)*

- *The value function $V(x)$ of moving horizon problem (2.2.4) is continuous and differentiable with respect to x, with a positive Lipschitz constant L_V*
- *$d(x,u,w)$ is Lipschitz with respect to its arguments, with $|d(x,u,w)| \leq |d(x,u,0)| + L_g|w|$ and $|d(x,u,0)| \leq \frac{\rho}{L_V}\alpha_p(|x|)$, where $\alpha_p(|x|)$ is a $\mathcal{K}_\infty$ function and $\rho \in (0,1)$.*

Theorem 2.2.5. *(Robust ISS Stability of NMPC Under Assumptions 2.2.2 and 2.2.3, the cost function $V(x)$ obtained from the solution of (2.2.4) is an ISS-Lyapunov function and the resulting closed-loop system is ISS stable.*

Under Assumption 2.2.3, the setpoint tracking NMPC with nominal asymptotic stability will automatically inherit the ISS property under robust cases. The outline to prove Theorem 2.2.5 is as follows:

Proof: We compare the value functions of two consecutive NMPC problems and bound the changes in the value functions using the following inequality:

$$\begin{aligned}
&V(x(k+1)) - V(x(k)) \qquad (2.2.6)\\
&= V(x(k+1)) - V(f(x(k),u(k))) + V(f(x(k),u(k))) - V(x(k))\\
&\leq L_V|d(x(k),u(k),w(k))| - \psi(x(k),u(k))\\
&\leq L_V|d(x(k),u(k),0)| + L_V L_g|w(k)| - \alpha_p(|x(k)|)\\
&\leq -(1-\rho)\alpha_p(|x(k)|) + L_V L_g|w(k)|
\end{aligned}$$

The derivation of inequality for the first pair relies on the nonlinear programming (NLP) sensitivity and Assumption 2.2.3; while the second inequality follows the proof for nominal stability. Therefore, we can show that $V(x)$ is an ISS Lyaponuv

function and the closed-loop system is ISS stable.

2.3 Computational Methods

Efficient solution strategies are always required for NMPC. In this section, we discuss the solution strategies for dynamic optimization and focus on the formulation of NMPC into nonlinear programming (NLP) problems via direct transcription. Then we will briefly introduce solution algorithms for NLP and the concept of NLP sensitivity.

2.3.1 Solution Approaches for Dynamic Optimization

As discussed earlier, NMPC can be set up as a dynamic optimization problem. For dynamic chemical processes, differential-algebraic equation (DAE) models are typically used to describe their dynamic behaviors. DAE models consist of differential equations including mass and energy balances and algebraic equations such as thermodynamic relations. The following is a general form of DAE-constrained dynamic optimization problems:

$$\begin{aligned} \min_{z,y,v} \quad & \psi(z,y,v) \\ \text{s.t.} \quad & \frac{dz}{dt} = f(z,y,v) \\ & 0 = g(z,y,v) \\ & c_l \leq c(z,y,v) \leq c_u \end{aligned} \tag{2.3.1}$$

where z, y, u represent differential variables, algebraic variables and control inputs; $f(\cdot)$ are differential equations and $g(\cdot)$ are algebraic equations; $c(\cdot,\cdot)$ represent additional constraints imposed on all variables.

Many solution strategies have been proposed to solve the above DAE-constrained dynamic optimization problem. Analytic solutions of problem (2.3.1) can be obtained based on Pontryagin's maximum principle. However, this is inefficient for large-scale problems and difficult to handle inequality constraints. To compensate for this issue, various direct methods are developed, which convert the dynamic optimization problem into a nonlinear programming problem. For direct methods, they can be separated into two major categories - sequential and simultaneous approaches, based on how DAE models are solved.

For the sequential approach, only control variables are discretized and DAE models are solved using numerical integration methods with fixed control variables. Then optimization is performed with respect to discretized control variables. The gradients of the objective function can be obtained by solving direct sensitivity equations or integrating the adjoint sensitivity equations. However, several limitations exist for this type of methods; e.g. it's difficult to handle unstable DAE systems and inequality constraints. Instead multiple shooting approaches have been proposed to handle the issues with the sequential methods. Similar to sequential methods, only control variables are discretized for multiple shooting method. However, instead of integrating DAE over entire time domain, multiple shooting divides the time domain into multiple finite elements and integrates DAEs separately within each finite element.

Moreover, simultaneous approaches are proposed, with a central idea of discretizing both control variables and state variables and solving the optimization problem simultaneously. Compared with the sequential approach, the simultaneous approach has many advantages. With this formulation, no DAE integrator is needed and thus excessive integration efforts can be avoided. The simultaneous approach is also suitable to handle unstable and ill-conditioned DAE systems. In addition, constraints on states and controls can be directly enforced. On the other hand, simultaneous approach may lead to a large-scale nonlinear programming prob-

lem with significant variable size and degrees of freedom. Therefore efficient NLP solvers are required, which will be discussed in the following section. A more detailed comparison of sequential and simultaneous methods can be found in [14].

In this work, we utilize the simultaneous approach to solve dynamic optimization problem. The discretization of state variables can be achieved using orthogonal collocation on finite elements (OCFE). In this formulation, time domain is separated into multiple finite elements and state profiles are approximated using a weighted sum of orthogonal polynomials within each finite element. It can be shown that such approximation is equivalent to implicit Runge-Kutta method with high order accuracy and excellent stability.

Next we introduce the NLP formulation for dynamic optimization problem (2.3.1) using OCFE. Over the time domain, we introduce discrete points, $0 = t_0 < t_1 ... < t_i \ldots < t_N = t_f$. Applying orthogonal collocation to the finite elements $h_i = t_i - t_{i-1}$, we approximate the differential variables $z(t)$ using Lagrange interpolation polynomials $l_j(\cdot)$ within each element.

$$
\begin{aligned}
& t = t_{i-1} + h_i \tau \\
& z^K = \sum_{j=0}^{K} l_j(\tau) z_{i,j} \\
& t \in [t_{i-1}, t_i], \tau \in [0, 1]
\end{aligned}
\tag{2.3.2}
$$

where $j \in \{0, \ldots, K\}$ is the index of the polynomials used in finite element i, $z_{i,j}$ are the coefficients for the approximation.

Lagrange interpolations polynomials $l_j(\tau)$are defined as follows:

$$
l_j(\tau) = \prod_{k=0,\neq j}^{K} \frac{(\tau - \tau_k)}{(\tau_j - \tau_k)} \tag{2.3.3}
$$

By using Lagrange interpolation polynomials for state approximation, the coeffi-

cients $z_{i,k}$ are the state values at collocation points $\tau_k,\ k = 1, \ldots, K$.

Then we substitute the approximated states into the original dynamic optimization problem (2.3.1) and enforce the resulting algebraic equations at the collocation points τ_k. This leads to the discretized system shown in equation (2.3.4b) - equation(2.3.4e). The continuity of the differential states is guaranteed by equation(2.3.4e).

$$\min_{z_{i,j}, y_{i,j}, v_{i,j}} \quad \psi(z_{i,j}, y_{i,j}, v_{i,j}) \tag{2.3.4a}$$

$$\text{s.t.} \quad \sum_{j=0}^{K} z_{i,j} \frac{dl_j(\tau_k)}{d\tau} = h_i f(z_{i,j}, y_{i,j}, v_{i,j}) \qquad i = 1 \cdots N, k = 1 \cdots K \tag{2.3.4b}$$

$$0 = g(z_{i,j}, y_{i,j}, v_{i,j}) \qquad i = 1 \cdots N, k = 1 \cdots K \tag{2.3.4c}$$

$$c_l \leq c(z_{i,j}, y_{i,j}, v_{i,j}) \leq c_u \qquad i = 1 \cdots N, k = 1 \cdots K \tag{2.3.4d}$$

$$z_{i+1,0} = z_{i,K}, \qquad i = 1 \cdots N - 1 \tag{2.3.4e}$$

where h_i is the length of finite element i; $z_{i,k}$, $y_{i,k}$ and $v_{i,k}$ are the values of differential, algebraic and control variables at collocation points τ_k, respectively.

By converting NMPC problem into the NLP formulation via direct transcription, we obtain the NMPC formulation as shown in (2.1.2). For NMPC case studies in this work, we use a 3-point Radau-collocation formulation. For control variables, we use a piecewise constant formulation. Such transformation usually leads to a large-scale NLP problem, which requires efficient NLP solvers. In the next section, we will briefly introduce the optimization method to solve the above NLP problem.

2.3.2 IPOPT and NLP Sensitivity

In this section, we will discuss solution methods to the NLP resulting from the simultaneous collocation formulation. A general formulation for the NLP problem

can be written as follows:

$$\begin{aligned} \min_{x} \quad & \psi(x,p) \\ \text{s.t.} \quad & c(x,p) = 0 \\ & x \geq 0 \end{aligned} \tag{2.3.5}$$

where x are variables and p are parameters.

NLP can be solved by different optimization strategies and there exist a number of NLP solvers. Here we consider IPOPT algorithm which is very efficient in solving large-scale NLPs. IPOPT is an interior point method based NLP solver [85]. For IPOPT algorithm, NLP (2.3.5) is reformulated into an equality constrained optimization problem using a barrier approach.

$$\begin{aligned} \min_{x} \quad & \psi(x,p) - \mu \sum_{i=0}^{n} ln(x^{(i)}) \\ \text{s.t.} \quad & c(x,p) = 0 \end{aligned} \tag{2.3.6}$$

where μ is a positive barrier parameter and $x^{(i)}$ denotes the ith component of the vector x. In the reformulated problem, the inequality constraints are removed by logarithmic barrier terms and added into the objective function. Under mild assumptions, $x(\mu)$ converges to a local optimal solution of the original problem as $\mu \to 0$. IPOPT algorithm applies this strategy and uses Newton's method to solve the KKT conditions derived from NLP (2.3.6), which leads to the following large-scale linear system at iteration j:

$$\begin{bmatrix} W_j & A_j & -I \\ A_j^T & 0 & 0 \\ V_j & 0 & X_j \end{bmatrix} \begin{bmatrix} \Delta x \\ \Delta \lambda \\ \Delta v \end{bmatrix} = - \begin{bmatrix} \nabla \psi(x_j) + A_j \lambda_j - v_j \\ c(x_j) \\ X_j V_j e - \mu e \end{bmatrix} \tag{2.3.7}$$

where we define $e = [1, 1, \cdots, 1]^T$, $X = diag(x)$, $V = diag(v)$, the Hessian $W_j = \nabla_{xx} L(x_j, \lambda_j, v_j)$, the Lagrange function $L(x, \lambda, v) = \psi(x) + c(x)^T \lambda - x^T v$ and the Jacobian of equality constraint $A_j = \nabla c(x_j)$.

For every barrier problem with a fixed μ, IPOPT finds the search directions by solving a smaller symmetric linear system after removing the last block row in (2.3.7). Then a line-search filter method is used to obtain the steps. After a barrier NLP is converged, then barrier parameter μ decreases and IPOPT solves another barrier problem. This loop continues until the original NLP is solved as μ approaches to 0.

IPOPT is very efficient in solving large-scale and sparse NLPs, since it exploits the sparsity of large-scale systems. In addition, the analytic Jacobian and Hessian information provided by modeling platforms such as AMPL can be used to improve the performance of IPOPT. Therefore we utilize IPOPT to solve the NMPC problems. More detailed discussions about IPOPT can be found in [85].

In addition to the interior point methods, there are other solution methods for NLPs, e.g. sequential quadratic programming and generalized reduced gradient methods, and corresponding solvers including SNOPT and CONOPT. A detailed review and comparison of different NLP solution strategies can be found in [14].

After discussing the NLP solution strategy, we will introduce the concept of NLP sensitivity. For a parametric NLP (2.3.5) with a nominal parameter vector p_0, the optimal solution with a perturbed parameter vector p could be obtained based on NLP sensitivity.

Assume that $\psi(x, p)$ and $c(x, p)$ are at least twice differentiable in x and once differentiable in p. $x^*(p_0)$ is the optimum solution to NLP (2.3.5), with $p = p_0$. As shown in [67], assume that linear independence constraint qualification (LICQ), strict complementarity (SC) and strong second-order sufficient conditions (SSOSC) hold at $x^*(p_0)$. Then the optimal triplet vector $s(\mu, p)^T = [x(\mu, p)^T, , \lambda(\mu, p)^T, v(\mu, p)^T]$ is continuous and differentiable for p in a neighborhood of p_0.

Based on the implicit function theorem, we can find the sensitivity matrix given by the following equation:

$$\frac{s(\mu, p_0)^T}{dp} = -M(s(\mu, p_0))^{-1} N_p(s(\mu, p_0)) \tag{2.3.8}$$

where $M(\cdot)$ and $N_p(\cdot)$ are defined as:

$$M(s(\mu, p_0)) = \begin{bmatrix} W(s(\mu, p_0)) & A(x(\mu, p_0)) & -I \\ A(x(\mu, p_0))^T & 0 & 0 \\ V(\mu, p_0) & 0 & X(\mu, p_0) \end{bmatrix} \tag{2.3.9}$$

$$N_p(s(\mu, p_0)) = \begin{bmatrix} \nabla_{xp} L(s(\mu, p_0)) \\ \nabla_p c(x(\mu, p_0))^T \\ 0 \end{bmatrix} \tag{2.3.10}$$

Then we can get a first order approximation $\tilde{s}(\mu, p)$ of the perturbed optimal solution $s^*(\mu, p)$:

$$\tilde{s}(\mu, p) = s(\mu, p_0) - M(s(\mu, p_0))^{-1} N_p(s(\mu, p_0))(p - p_0) \tag{2.3.11}$$

The approximation error can be bounded by:

$$|\tilde{s}(\mu, p) - s^*(\mu, p)| \leq L_s |p - p_0|^2 \tag{2.3.12}$$

where L_s is a positive Lipschitz constant.

Based on the above idea, sIPOPT [67] has been implemented to provide optimal sensitivity of solutions of parametric NLPs. sIPOPT reuses the matrix factorization results from IPOPT, so that the sensitivity can be obtained with minimal computational cost. This provides opportunities for very fast NLP sensitivity based

approximations, which could be used for fast NMPC algorithms.

2.4 Advanced Step NMPC

Nonlinear model predictive control (NMPC) uses nonlinear process models to predict system behavior and find an optimal sequence of values for the manipulated variables by solving the dynamic optimization problem. Compared with linear MPC, NMPC may lead to better performance since the nonlinear first-principles models are more robust than the linear data-driven models in larger operation ranges. However, solving NMPC problems with detailed first-principles process models can be computationally challenging. The computational time to solve NMPC is usually not negligible; and this computational delay may degenerate control performance and even destabilize the process [29]. Therefore, computationally efficient NMPC algorithms are needed to reduce the online computational cost. Several fast NMPC strategies have been developed, including hierarchical NMPC and distributed NMPC. A review of fast NMPC strategies is given in [87]. Recently, NMPC with fast updates based on NLP sensitivity becomes attractive since the online computational cost is negligible. In this section, we focus on a fast advanced step NMPC (asNMPC) algorithm proposed in [95].

As discussed earlier, NMPC problems are solved in a moving horizon manner. At each sampling time, problem (2.2.4) is solved with $z_0 = x(k)$ as initial conditions. Therefore, a NMPC problem can be treated as a parametric NLP and an approximated optimal solution can be obtained based on NLP sensitivity. The key idea of asNMPC is to solve the NMPC problem one sampling time in advance using the predicted state as initial conditions and generate a perturbed optimal solution when true states are obtained. The implementation of asNMPC algorithm can be divided into the following two steps:

- Background calculation

Within the sampling interval from t_k to t_{k+1}, obtain the predicted states $f(x(k), u(k))$ one step ahead and solve the NMPC problem in background by setting $z_0 = f(x(k), u(k))$.

- Online update

  At the sampling time t_{k+1}, obtain the true states $x(k+1)$. Calculate the perturbed solutions given by (2.3.11) and implement the first control move.

In this algorithm, the predicted states $f(x(k), u(k))$ are the nominal parameters p_0 while the true states $x(k+1)$ are treated as parametric perturbations. Expensive computation for the nominal NMPC problem is put into background. The online update step is very cheap to get from sIPOPT, since the sensitivity matrix (2.3.8) has already been factorized at the nominal optimum and only a backsolve is required. Usually, the computational cost of online update step is one to two orders of magnitude smaller than the background calculation. Therefore, the computational delay for NMPC can be avoided by asNPMC. In terms of stability analysis, the nominal asymptotic stability and robust ISS stability are established for asNMPC in [95].

In addition, an advanced-multi-step NMPC (amsNMPC) algorithm has been proposed in [90], with the central idea of extending the background calculation step from one sampling time to multiple sampling times. A parallel and sequential implementation of amsNMPC has also been proposed. This algorithm is suitable to handle the cases where NMPC may take more than a sampling time to solve. For the online update step, a single sensitivity update may cause infeasible input and active set changes. This issue can be handled by a simple clipping strategy [90] or introducing several subsequent sensitivity updates in a path-following manner [44].

2.5 Model Reduction

Mathematical models are mathematical abstractions of physical systems. A proper mathematical model of process is important to understand the system's behavior and it is crucial for numerical simulation, optimization and control of these systems. However, modeling physical systems can lead to complex high-order dynamic models. For systems with little spatial variation, lumped parameters models can provide a good approximation of the system behavior, and they are commonly used for chemical units. However, for systems with multiple components and complicated physical behavior, lumped parameter models can have significant dimension and complexity. What's more, to accurately describe the dynamic behavior of processes with strong spatial-temporal dynamics, distributed parameter fist-principles models are usually required, which may pose computational challenges for numerical solutions and limit their applications in real-time optimization and control tasks.

Model reduction provides a systematic way to find a lower dimensional approximation of complex models with reasonable accuracy and it offers an attractive solution to integrating these complicated models into time-critical applications, such as nonlinear model predictive control and dynamic real time optimization. For model reduction, there are generally two types of methodologies. One is the black-box approach, which generates surrogate models using data-driven techniques, such as principal component analysis, artificial neural networks and Kriging methods. There are also software implementations to generate data-driven surrogate models [24, 58]. The other is the physics-based approach, which manipulates the structure and equations of the rigorous model to find a lower dimensional approximation. The physics-based approach provides not only accurate input-to-output mapping but also access to all the states in the rigorous model.

In this dissertation, we focus on the physics-based approach to generate fast and

accurate dynamic reduced order models which can be used for equation-based applications. For linear dynamic systems, model reduction techniques are well established. Antoulas et al. reviewed approximation approaches for large-scale linear systems in [7]. The general idea is to first transfer the original model using state transformation into a new system, where important and unimportant states can be easily separated. Then, truncation or residualization can be used to generate the reduced model. For nonlinear model reduction, Marquardt provided an overview of a large variety of nonlinear model order reduction and model simplification methods from an optimization-based control perspective [60]. Despite various model reduction methods, there is no generic approach that is appropriate for all process systems. It is also emphasized that the proper way to assess model reduction quality for online nonlinear model-based control is to compare the closed loop performance.

For nonlinear model reduction, one representative method is nonlinear balancing, introduced by Scherpen [76], that generalizes the idea of balancing of linear systems. The key idea is to transform a system into an equivalent form where the importance of states can be assessed in terms of the energy in its input and output signals, but difficulty in determining the nonlinear controllability and observability functions limits its practical applications. Lall et al. introduced empirical balancing of nonlinear systems by using empirical Gramians as equivalent linear Gramians [51]. Hahn and Edgar elaborated on model order reduction by balancing empirical Gramians and showed significant model order reduction on a small-scale distillation column model [35].

Another important model reduction technique, especially for models with multiple time scale behavior, is the singular perturbation method [47]. The underlying idea is the quasi-steady state approximation for fast states, which converts the differential equations describing the states with fast dynamics to algebraic equations. However, the major challenge is to identify the time scale differences that exist in

different chemical processes, which requires prior knowledge and first hand experiences with the corresponding processes. Chemical processes are characterized by phenomena on separate time scales, which is due to both the physical characteristics and the operation of the processes. By reviewing the literature, we can identify the following principles and observations for time scale separation in chemical processes.

On the unit level, significant time scales may exist in the following aspects:

- Differences in the orders of magnitude for reaction rates/reaction time constant, e.g. Ozone decomposition reaction system [84]
- Time scale differences in multi-phase processes, e.g. air separation unit [43]
- Time scale differences in mass and heat transfer rates, e.g. fixed bed reactor [23]

On the system level, chemical processes usually involve multiple units such as reactors and separators. For the integrated system, the design and operation of such system may lead to additional multiple time scale behavior. For example, for chemical processes with large recycles, by introducing the concept of recycle number as the perturbed parameter, the fast and slow dynamics can be easily separated [11, 48].

For a distributed parameter system modeled by partial differential equations (PDEs), Li et al. presented an overview of model reduction techniques from a view of time-space separation [55]. The spatial-temporal variables of the distributed parameter systems can be expanded into a set of spatial basis functions and the corresponding temporal models. Then the original infinite-dimensional PDE system can be converted to a finite order temporal models using weighted residual methods. The selection of spatial basis functions is crucial for model reduction and it directly affects the size and accuracy of the approximated model. Spatial basis functions with different properties lead to different type of approximation methods such as or-

thogonal collocation, finite element, finite difference and Karhunen-Loeve method. A more detailed discussion will be presented in Chapter 3.

Chapter 3

Dynamic Reduced Order Models for Bubbling Fluidized Bed Reactors

Spatially distributed first-principles process models provide an accurate physical description of chemical processes, but lead to large-scale models whose numerical solution can be challenging and computationally expensive. Therefore fast reduced order models are required for model-based real-time applications, such as advanced process control and dynamic real-time optimization. In this chapter, we focus on the model reduction of bubbling fluidized bed (BFB) adsorbers, which are the key components of a post-combustion carbon capture system. In the following sections, we will briefly introduce the background for the solid sorbent-based carbon capture system and the rigorous BFB reactor model. Then we will introduce temporal and spatial model reduction for the BFB reactors. From a temporal aspect, dynamic reduced models are generated using nullspace projection and eigenvalue analysis methods, with the basic idea of quasi-steady state approximation for the states with fast dynamics. From a spatial aspect, dynamic reduced models are

developed using orthogonal collocation and proper orthogonal decomposition to reduce the size of the rigorous model. We demonstrate the performances of the dynamic reduced models in simulation case studies.

3.1 Introduction

Anthropogenic carbon dioxide (CO_2) emission is regarded as one of the major causes of global climate change in the scientific community. In the United States, approximately one third of anthropogenic CO_2 emission is produced from the use of fossil fuels in power plants for electricity generation [28] and the demand for electric power will keep growing as the U.S. and global economies grow. Therefore it is crucial to develop techniques to reduce the amount of anthropogenic CO_2 emitted from power plants and considerable research has been conducted in the area of carbon capture and storage (CCS). To improve carbon capture for power plants, three major pathways are being actively studied, including post-combustion capture, pre-combustion capture and oxy-combustion. These three pathways have pros and cons and a comprehensive comparison is given in a review paper [28] by the US Department of Energy. Among these pathways, post-combustion is applicable to most existing coal-fueled power plants that are air fired and is most suitable for retrofit. However, post-combustion capture requires an efficient separation process to remove CO_2 from power plant flue gas, which has a low CO_2 concentration. One popular choice is to use an amine-based solvent considering its good reactivity and absorption capacity. Monoethanolamine (MEA) is the most commonly used solvent for CO_2 recovery. In addition, emerging technologies are being developed to improve the energy efficiency of conventional technology. For example, amine-based solid sorbents are considered because they may require a relatively small amount of energy for regeneration compared with liquid solvents. National Energy Technology Laboratory (NETL) has initiated Carbon Capture Sim-

ulation Initiative (CCSI) to develop computational tools and models to accelerate the development and commercialization of CCS technology [62]. A solid-sorbent-based post-combustion CO_2 capture technology has been utilized to demonstrate how the computational models can be used to develop a carbon capture system integrated with a coal-fired power plant [22]. The process diagram for the carbon capture system is shown in Figure 3.1. The flue gas coming from the power plant is fed into the carbon capture system to remove CO_2. The solid sorbent is desorbed in the regenerator and the captured CO_2 can be compressed for geological storage.

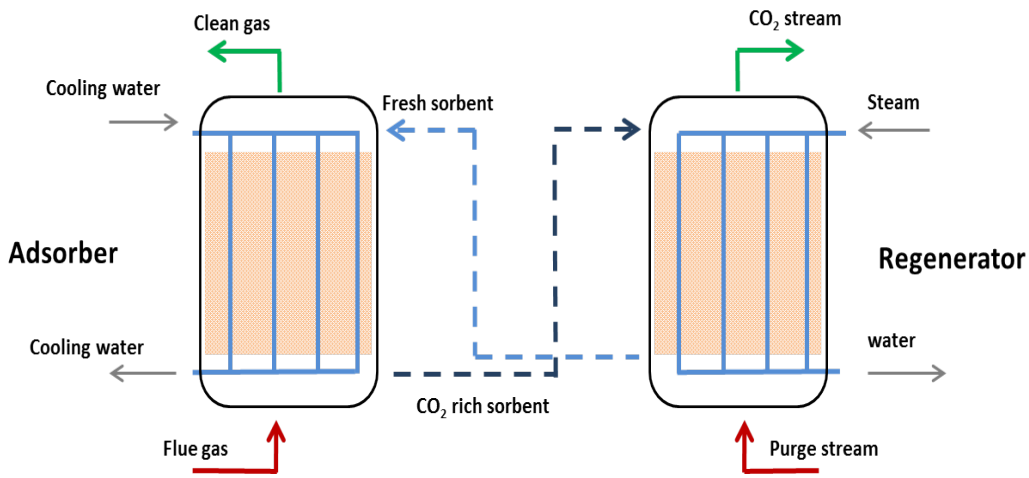

Figure 3.1: Process diagram for a post-combustion, solid sorbent-based CO_2 capture system

The carbon capture system proposed in [22] consists of bubbling fluidized bed (BFB) reactors which are used as adsorber and regenerator to remove CO_2 and recycle sorbent. The BFB reactor is chosen as the key reactor type for post-combustion carbon capture because it has large contact area and offers efficient mass and heat transfer. The process feasibility of solid sorbent-based CO_2 capture has also been demonstrated in [57]. For their study, the authors use a Ca-based sorbent loop technology and construct a pilot-scale dual fluidized bed system to remove the CO_2 from flue gas.

When operating a post-combustion carbon capture system for power plants, spe-

cific requirements on CO_2 capture fraction (e.g. 90%) should be satisfied. However, changing loads will pose significant disturbances on the carbon capture system. Efficient controllers are needed to reject the disturbances and meet the environmental constraints. In addition, economic issues such as high energy consumption are major bottlenecks for the commercial application of carbon capture systems [28]. Therefore flexible operation and control strategies are required to improve the performance of carbon capture systems. Bui et al. [16] gave a comprehensive review of dynamic modeling and optimization of flexible operation in post-combustion CO_2 capture plants. Included in that paper is related research work on amine-based solvent carbon capture systems, which is applicable to other types of CO_2 capture plants as well. Representative examples of strategies for flexible operation consider variations in the electricity market and, thus, implement different operational modes with varied set points for CO_2 recovery to balance the trade-off between profit and CO_2 emissions [86]. These flexible operational strategies of the capture plant impose additional process disturbances as the setpoint of the capture facility is changing with energy demand. Thus robust process control and online optimization need to be developed to reject process disturbances and tracking setpoint change. Such control techniques require dynamic models that can provide accurate predictions of the process to improve and optimize transient performance.

First-principles dynamic models arise in a wide variety of process applications such as dynamic simulation and off-line optimization. However, the large amount of time required to solve the detailed models limits their use for process control. As a result, dynamic reduced order models with reasonable accuracy are required for model-based real-time applications, such as advanced process control and dynamic real-time optimization. In the area of post-combustion capture, the need for reduced dynamic models, which are used for process control, is getting increased attention. A reduced order model of a CO_2 absorption unit was developed based on physical analysis and integrated with nonlinear model predictive control

(NMPC) of the process [2]. A dynamic model of a pilot carbon capture plant was simplified by using equilibrium based modeling instead of rate based modeling for process control applications [54]. In this chapter, we study model reduction approaches and develop dynamic reduced order models of the BFB adsorber which will be used for time-critical applications such as model-based online control. Next, we introduce the full scale model of the BFB adsorber. Following that, we discuss the model reduction for the BFB reactor.

3.2 Full Scale Model of Bubbling Fluidized Bed Adsorber

Comprehensive theoretical studies of bubbling fluidized bed reactors were initiated by Kunii and Levenspiel. They developed a three-region model to describe the behavior within a BFB reactor [49, 50]. The model identified three distinct regions within a fluidized bed, including bubble, cloud-wake and emulsion regions, as shown in Figure 3.2(a). In their model, the solid phase was assumed to be well-mixed and isothermal. Following this approach, other researchers developed models for fluidized bed reactors for application to catalytic processes and polymerization reactions [77, 82]. Their models only consider the bubble and emulsion regions, and the assumption for isothermality in solid phase holds. However, temperature and pressure are key factors that have strong effects on adsorption processes.

To better describe the dynamic behavior of adsorption process, a one-dimensional, three-region, pressure-driven model for a BFB adsorber has been developed by researchers at NETL, which considers axial variations in the solid phase and the bed hydrodynamics [53, 63]. The kinetic model used in the BFB model assumes that the adsorption of CO_2 and water occurs through a three-reaction scheme [52]. Water and CO_2 diffuse into the pores of the solid sorbent and react with impregnated

amines to form carbamate and bicarbonate, as shown below:

$$H_2O_{(g)} \rightleftharpoons H_2O_{(phys)} \tag{3.2.1}$$

$$2R_2NH + CO_2 \rightleftharpoons R_2NH_2^+ + R_2NCO_2^- \tag{3.2.2}$$

$$R_2NH + CO_2 + H_2O_{(phys)} \rightleftharpoons R_2NH_2^+ + HCO_3^- \tag{3.2.3}$$

The kinetic parameters are determined based on experimental data. The reactions are assumed to take place in the solid phase. These three reactions show different time scales, which will be further discussed in temporal reduction section.

The hydrodynamic behavior in the reactor is described by partial differential and algebraic equations (PDAEs), constructed from mass and heat conservation and hydrodynamic equations. This model can be represented by the following general PDAEs.

$$\frac{\partial z}{\partial t} = \frac{\partial z}{\partial x} + f(z, y) \tag{3.2.4a}$$

$$g(z, y) = 0 \tag{3.2.4b}$$

where z are differential variables, y are algebraic variables. The detailed equations and boundary conditions are presented in the Appendix.

For a differential slice in the model shown in Figure 3.2(b), mass and heat balances are written for each phase and region. The differential equations consider the effect of axial material flow and transfer terms between different regions. The gas phase mass balance equation in the bubble region is shown below as an example:

$$\frac{\partial c_{b,j}}{\partial t}\delta A_x = -\frac{\partial G_b y_{b,j}}{\partial x} - A_x \delta K_{bc,j}(c_{b,j} - c_{c,j}) + K_{g,bulk,j} \tag{3.2.5}$$

The term on the left hand side of equation (3.2.5) is the accumulation term for the component concentration in the bubble region. The three terms on the right hand side represent the effect of upwards gas flow through the bubble region, mass

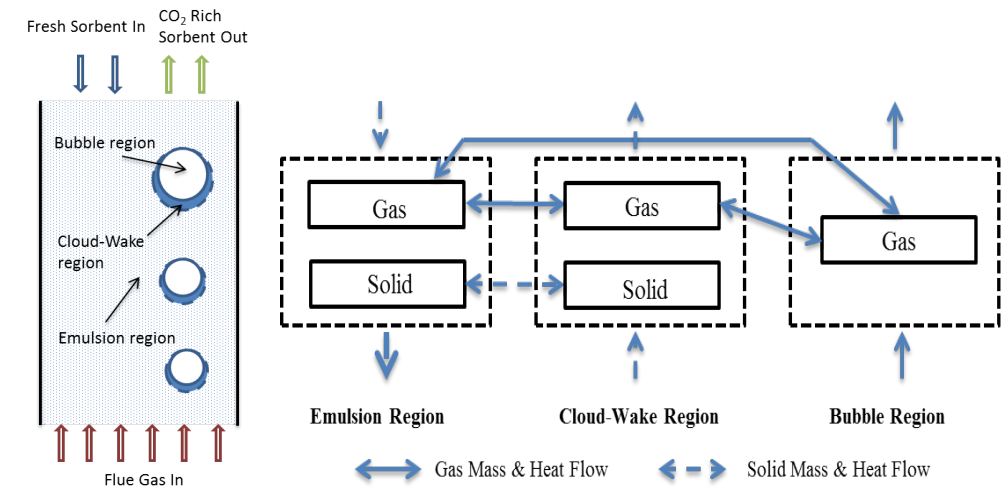

(a) Sketch of the BFB adsorber

(b) Mass and energy relations in a differential slice

Figure 3.2: Three-region BFB model

transfer between the bubble and the cloud-wake region, and the bulk flow between the bubble and the emulsion region, respectively. Here $c_{b,j}$ and $c_{c,j}$ represent the concentrations of component j in the bubble and the cloud-wake region. G_b is the axial flow rate of gas through the bubble region; $y_{b,j}$ is the gas mole fraction. A_x is the cross sectional area; δ is the volume fraction of the bubble region; $K_{bc,j}$ is the mass-transfer coefficient for component j; $K_{g,bulk,j}$ is the flow rate of component j into the bubble region from the emulsion region due to a bulk flow of gas. The component mass and energy balances are enforced as boundary conditions at the bottom ($x = 0$) and the top ($x = L$) of the reactor. For equation (3.2.5), since the flue gas is fed at the bottom, the gas flow rate and component mole fraction at $x = 0$ are the same as the input flue gas. In addition to differential equations, a set of algebraic equations are included to calculate hydrodynamic properties, heat and mass transfer coefficients, reaction kinetics, gas phase properties and the sizing of the reactor and heat exchanger. Most algebraic equations are correlations based on experimental studies with high nonlinearities. A brief summary of the algebraic equations in the BFB model is also given in the Appendix.

The BFB model [53, 63] was implemented in Aspen Custom Modeler (ACM), an equation-based process model development and simulation environment developed by Aspen Technology. Here we denote this model as *original full scale BFB model*. The *original full scale BFB model* is discretized using the finite difference method over 100 nodes. After spatial discretization, the BFB model becomes a system of differential and algebraic equations (DAEs) as described by the following:

$$\frac{dz}{dt} = f(z, y) \tag{3.2.6a}$$

$$g(z, y) = 0 \tag{3.2.6b}$$

A first order backward difference method is used for all upwards flow within the reactor, and a forward finite difference method is used for downwards flow. The discretized system consists of more than 10,000 differential and algebraic equations. Solving such a large-scale DAE model is computationally expensive for real-time applications. Thus, a dynamic reduced order model of the BFB adsorber is needed for model-based control and optimization of the carbon capture system.

In the *original full scale BFB model*, a number of physical properties in the gas phase are used within the model, such as gas phase viscosity and molar heat capacity. These properties are calculated using Aspen properties. The equation of state used in the *original full scale BFB model* is the Peng-Robinson equation with Boston-Mathias modifications. With the large physical and thermodynamic properties database in Aspen, the property functions give accurate predictions of the gas phase physical properties; however, these functions are implicit subroutines, and the explicit form of equations are inaccessible. Moreover, it's desired to have explicit forms for model equations in many cases. Firstly, some physics-based model reduction approaches, such as proper orthogonal decomposition, require the explicit form of all model equations. In addition, access to the full explicit equations

will enable implementation of the model in various algebraic modeling environments, such as AMPL [31] and PYOMO [36], where state-of-art solvers can be easily used. Considering that the BFB model will be used for equation-based control and optimization studies, we introduce some model simplifications to replace these implicit functions, before any model reduction is performed. With reactor pressure and temperature within a limited range, linear regression models can give accurate predictions of gas phase properties. Linear regression models are developed off-line based on the training data given by the Aspen property functions, and they are included in the BFB model to replace the implicit property functions. For more extreme operating conditions, more sophisticated models such as Kriging models can be used for accurate approximations. The BFB model *after the manipulations* described above serves as the *reference model* on which we apply model reduction. Compared with the *original full scale BFB model*, the *reference BFB model* can achieve about 30% reduction in simulation time and the maximum relative errors for key outputs are within 2%.

Since there is no generic model reduction technique for nonlinear process systems, careful analysis of the reference BFB model is required to find the most appropriate techniques and achieve successful model reduction. For the reference BFB model described by large-scale DAEs, there are some characteristics which we could manipulate. First is the stiffness ratio of a DAE system, which is defined as the ratio of the largest real part of eigenvalues to the smallest in the local Jacobian matrix. A high stiffness ratio limits the integration step size due to stability considerations [9]. In the BFB model, system dynamics shows multiple time scales due to factors such as the reaction kinetics and phase differences, which lead to high stiffness. In addition, the huge number of differential and algebraic equations after spatial discretization also increases the simulation time. In this work, time scale decomposition is utilized to reduce the stiffness of the system from a temporal aspect. Orthogonal collocation on finite elements and proper orthogonal decomposition

(POD) reduction are applied to reduce the number of differential and algebraic equations discretized in space. Next we will discuss the derivation of temporally reduced models using time scale decomposition techniques. Case studies are conducted to validate the temporally reduced models. Then we will introduce spatial model reduction using collocation and POD. Simulation results of reduced models by spatial decomposition and combining temporal and spatial methods are presented.

3.3 Temporal Model Reduction for BFB Adsorber

As mentioned in chapter 2, singular perturbation is a useful tool for the reduction of models with separate time scales. The standard singularly perturbed form of ordinary differential equation (ODE) systems [47] is defined as follows.

$$\begin{aligned} \dot{z_s} &= f(z_s, z_f, t, \varepsilon) \\ \varepsilon \dot{z_f} &= g(z_s, z_f, t, \varepsilon) \end{aligned} \tag{3.3.1}$$

Here ε is a very small parameter, z_s and z_f denote slow and fast states. As $\varepsilon \to 0$, the original ODE system collapses to a reduced DAE system with fewer differential equations:

$$\begin{aligned} \dot{z_s}^r &= f(z_s^r, z_f^r, t, \varepsilon) \\ 0 &= g(z_s^r, z_f^r, t, \varepsilon) \end{aligned} \tag{3.3.2}$$

The reduced system is less stiff and has nearly the same dynamic behavior when ε is sufficiently small. A major challenge in using this method is the conversion of process models to the standard perturbed form, which is not trivial and requires sufficient prior knowledge. In chapter 2, we summarize a few guidelines for singular perturbation in modeling of chemical processes. For our case, the BFB reactor is

Table 3.1: Forward and backward equilibrium reaction rates

	$r_f(mol/m^3s)$	$r_b(mol/m^3s)$
Reaction 1	10^6	10^6
Reaction 2	10^0	10^0
Reaction 3	10^{-1}	10^{-1}

r_f - forward equilibrium reaction rates
r_b - backward equilibrium reaction rates

modeled by PDAEs to describe its spatial and temporal features. To deal with this complex process model after spatial discretization, two general approaches are utilized to analyze and manipulate the time scale differences within the BFB model. In this section, we directly perform model reduction on the reference BFB model described by DAE system (3.2.6).

3.3.1 Temporally Reduced Model Using Nullspace Projection

When modeling dynamic chemical processes, we often encounter synergistic fast and slow modes which cause difficulties in numerical solutions. Nie et al. [65] proposed a nullspace projection method which provides a systematic way to reformulate a system of complex reaction equations with multiple time scales, and it has been successfully applied to simplify polymer reaction systems. This method inherits an idea similar to quasi-steady state approximation from singular perturbation but focuses on the time scale differences in equilibrium reaction rates. The kinetics model used in the BFB adsorber includes three equilibrium reactions, as shown in equation (3.2.1) - equation (3.2.3). From simulation results, we find that multiple time scales exist in these reactions. As shown in Table 3.1, we can see that the forward and backward reaction rates of reaction 1, the water physisorption reaction, are much larger than the other two reactions, which indicates the physisorption of water is much faster. Based on this observation, the nullspace projection method, as described in the following, is utilized to simplify the reaction kinetics in the BFB model.

The mass balance equation systems can be described by the following equation:

$$\dot{z} = A\, r(z) + g(z,t) \tag{3.3.3}$$

where z are component concentrations, A is the stoichiometric matrix, $r(z)$ are reaction terms and $g(z,t)$ are additional terms including mass transfer. By partitioning the irreversible and equilibrium reactions, we can obtain the following system:

$$\dot{z} = \begin{bmatrix} A_1 & A_2 \end{bmatrix} \begin{bmatrix} r_1(z) \\ \sigma r_2(z) \end{bmatrix} + g(z,t) \tag{3.3.4}$$

where $r_1(z)$ and $\sigma r_2(z)$ represent reaction rates for irreversible and equilibrium reactions. σ is a very large number which makes the corresponding reactions much faster than the others. Then we multiply both sides of equation (3.3.4) with a non-singular matrix $\begin{bmatrix} Y & Z \end{bmatrix}^T$, where $Z^T A_2 = 0$, which leads to a reformulated system:

$$Y^T \dot{z} = Y^T A_1 r_1(z) + \sigma Y^T A_2 r_2(z) + Y^T g(z,t) \tag{3.3.5}$$

$$Z^T \dot{z} = Z^T A_1 r_1(z) + Z^T g(z,t) \tag{3.3.6}$$

In equation (3.3.6), fast equilibrium reaction rates $\sigma r_2(z)$ are removed, but they still exist in equation (3.3.5). The term $\sigma Y^T A_2 r_2(z)$ can be separated into zero and non-zero parts and Y can be partitioned accordingly, which gives the following formulation:

$$\begin{bmatrix} Y_a^T \\ Y_b^T \end{bmatrix} \dot{z} = \begin{bmatrix} Y_a^T \\ Y_b^T \end{bmatrix} A_1 r_1(z) + \begin{bmatrix} 0 \\ \sigma f(z) \end{bmatrix} + \begin{bmatrix} Y_a^T \\ Y_b^T \end{bmatrix} g(z,t) \tag{3.3.7}$$

When $\sigma \to \infty$, $f(z)$ is required to equal zero in order to get a stable solution; this describes the equilibrium manifold of the fast reaction system. Thus, we can get the reformulated DAE system shown in equation (3.3.8) - equation(3.3.10), which

is less stiff but with the same asymptotic behavior.

$$Y_a^T \dot{z} = Y_a^T A_1 r_1(z) + Y_a^T g(z,t) \tag{3.3.8}$$

$$f(z) = 0 \tag{3.3.9}$$

$$Z^T \dot{z} = Z^T A_1 r_1(z) + Z^T g(z,t) \tag{3.3.10}$$

As mentioned before, physisorption of water is several orders of magnitude faster than the other two reactions, and the nullspace projection $Z^T A_2 = 0$ is applied to remove these fast dynamics. The physical basis is that the fast reaction is assumed to be always at equilibrium, and only slow reactions need to be described by differential equations. After the nullspace projection, the mass balance equation for gaseous and physisorbed water in both the cloud-wake region and the emulsion region, as shown in equations (A.3), (A.5), (A.7) and (A.9) in the Appendix, are removed. A quasi-steady state approximation for the fast reaction is introduced which forces the forward rates of the water physisorption reaction to be equal to the backward reaction rate. The nullspace projection also generates pseudo species s_1 and s_2 defined in equations (3.3.11) and (3.3.12), which are described by new differential equations (3.3.13) and (3.3.14).

$$s_1 = c_{c,H_2O} \frac{\varepsilon_d}{1-\varepsilon_d} + n_{c,H_2O}\rho_s \tag{3.3.11}$$

$$s_2 = c_{e,H_2O} \frac{\varepsilon_d}{1-\varepsilon_d} + n_{e,H_2O}\rho_s \tag{3.3.12}$$

$$\begin{aligned} \dot{s_1} = -r_{2,c} &+ \frac{K_{bc,H_2O}(c_{b,H_2O} - c_{c,H_2O}) - K_{ce,H_2O}(c_{c,H_2O} - c_{e,H_2O})}{f_{cw}(1-\varepsilon_d)} \\ &- \frac{\partial J_c n_{c,H_2O}}{\partial x} \frac{1}{f_{cw}\delta(1-\varepsilon_d)} - \frac{\rho_s K_{ce,bs}(n_{c,H_2O} - n_{e,H_2O})}{f_{cw}(1-\varepsilon_d)} \\ &- \frac{K_{s,bulk,H_2O}}{A_x f_{cw}\delta(1-\varepsilon_d)} \end{aligned} \tag{3.3.13}$$

$$\begin{aligned}\dot{s_2} = & -r_{2,e} + \frac{\delta K_{ce,H_2O}(c_{c,H_2O} - c_{e,H_2O})}{(1 - f_{cw}\delta - \delta)(1 - \varepsilon_d)} - \frac{K_{g,bulk,H_2O}}{(1 - f_{cw}\delta - \delta)(1 - \varepsilon_d)A_x} \\ & + \frac{\partial J_e n_{e,H_2O}}{\partial x}\frac{1}{(1 - f_{cw}\delta - \delta)(1 - \varepsilon_d)} - \frac{\delta \rho_s K_{ce,bs}(n_{c,H_2O} - n_{e,H_2O})}{(1 - f_{cw}\delta - \delta)(1 - \varepsilon_d)} \\ & + \frac{K_{s,bulk,H_2O}}{A_x(1 - f_{cw}\delta - \delta)(1 - \varepsilon_d)}\end{aligned} \tag{3.3.14}$$

In these reformulated differential equations, the first terms on the right hand sides are the reaction rates of the second reaction shown in equation (3.2.2), which represent the slow time scale; the other terms are the mass transfer terms. Compared with the original mass balance equations for gaseous and physisorbed water, the reaction rates of the fast reaction are removed. In terms of model size, the reduced model using nullspace projection achieves a 10% reduction in the number of differential equations.

Next, a case study is conducted to validate the temporally reduced model. The BFB adsorber is designed to remove CO_2 from flue gas emitted by power plants. CO_2 removal fraction and sorbent loading are key outputs which indicate the efficiency of the adsorber. However, when operating the CO_2 capture plant, changing input conditions of the flue gas stream will cause disturbances to the BFB adsorber. For example, the load of power plants may change in response to fluctuations in power demand. This load following leads to variations in the flue gas flow rate, which is a major disturbance to the BFB adsorber. In this study, multiple step changes in the flow rate of flue gas and flow rate of solid sorbent are introduced, and we compare the dynamic behavior of two key outputs, CO_2 removal fraction and sorbent loading, predicted by both the reduced and the reference BFB model. Both models are implemented in Aspen Custom Modeler (ACM) V7.3. The base case conditions are given in Table 3.2. All dynamic simulations were performed on an Intel i7-3770 3.40 GHz personal computer. The ACM integrator uses the implicit Euler method, with an integration error tolerance of 10^{-5}. The equation and variable tolerance is 10^{-7}. These settings apply for all dynamic simulation tests in this chapter.

Table 3.2: Base case conditions

Design parameters		Gas conditions		Solid conditions	
D_t	9 m	$G_{b,in}$	9950 mol/s	$F_{sorb,in}$	166.67 kg/s
L_b	5 m	$T_{g,in}$	313 K	$T_{sorb,in}$	323 K
d_x	0.02 m	$y_{g,CO_2,in}$	0.13	$n_{HCO_3,in}$	0.01 mol/kg solid
N_x	940	$y_{g,H_2O,in}$	0.06	$n_{H_2O,in}$	0.7 mol/kg solid
N_{or}	2500 m^{-2}	$y_{g,N_2,in}$	0.81	$n_{NHCO_2,in}$	0.7 mol/kg solid

Table 3.3: Dynamic simulation results

	Simulation time (s)	MRE1 (%)	MSE1($\%^2$)	MRE2(%)	MSE2(mol^2/kg^2)
Reference model	193	-	-	-	-
RM-1	122	0.017	2.45E-5	0.0081	3.06E-8

RM-1 - temporally reduced model using nullspace projection
MRE - maximum relative error, MSE - mean squared error
1 - CO_2 removal fraction, 2 - sorbent loading

Figure 3.3 shows the dynamic behavior of both the reference model and temporally reduced model RM-1 under disturbances. We can see that the dynamic response of both models are nearly the same, but the reduced model requires about 35% less simulation time because the reduced system becomes less stiff. The performance data are listed in Table 3.3. From these simulation results, we can conclude that the nullspace projection technique is applicable to the model reduction of the BFB adsorber, and the reduced model can greatly reduce the computational cost with very small error in the model's key outputs.

3.3.2 Temporally Reduced Model Using Eigenvalue Analysis

In addition to manipulating the time scale differences in the reaction kinetics, we also investigate the system's overall dynamics, which can be well characterized by the eigenvalues of the Jacobian matrix. Fast states, which quickly reach steady state, are usually associated to eigenvalues with real parts, $Re(\lambda)$, that are negative and large in magnitude. If the system contains two distinct groups of eigenvalues $\lambda_1 \cdots \lambda_i$ and $\lambda_{i+1} \cdots \lambda_n$ such that,

$$\cdots < Re(\lambda_{i-1}) < Re(\lambda_i) \ll Re(\lambda_{i+1}) < Re(\lambda_{i+2}) < \cdots$$

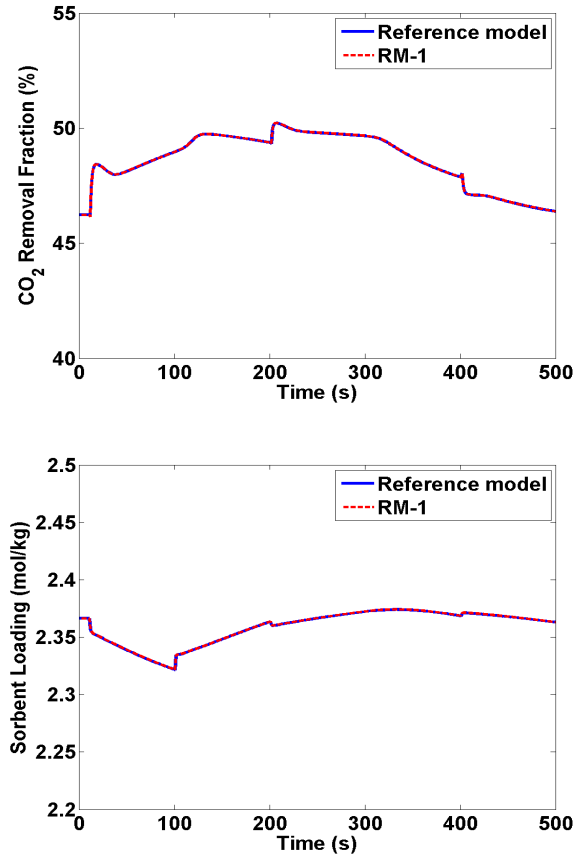

Figure 3.3: Comparison of output profiles of the reduced and reference BFB model

then fast and slow time scales exist when the separation ratio ζ, defined as the ratio of $Re(\lambda_i)$ to $Re(\lambda_{i+1})$, is large, usually greater than one order of magnitude [4].

The spatially discretized reference BFB model is a nonlinear DAE system defined by equation (3.2.6). By making perturbations, we can obtain the locally linearized system. The Jacobian matrix A of the DAE system (3.2.6) is determined by computing the Schur complement of the linearized system.

$$\Delta\dot{z} = A\Delta z, \qquad A = \frac{\partial f}{\partial z} - \frac{\partial f}{\partial y} \cdot \frac{\partial g}{\partial y}^{-1} \cdot \frac{\partial g}{\partial z} \tag{3.3.15}$$

Using equation (3.3.15), we can calculate the Jacobian matrix and its eigenvalues to see if different time scales exist . Robertson and Cameron [75] empirically re-

lated the separation ratio to the model reduction error and presented a homotopy-continuation technique to identify the eigenvalue-state association; however this method can only be used for one-to-one association between eigenvalues and states. For complicated systems, a group of eigenvalues may be associated with a group of states. Here the unit perturbation spectral resolution (UPSR) matrix [19] is used to obtain a quantitative measure of the levels of association between all eigenvalues and states. The key idea is to use the response of a state to a perturbation in itself to measure the eigenvalue-to-state association. The UPSR matrix P is defined as the element by element product of eigenvector matrix of Jacobian A and the transpose of its inverse matrix. The element P_{ij} can be calculated by:

$$P_{ij} = V_{ij}(V^{-1})_{ji} \tag{3.3.16}$$

where V is the eigenvector matrix of the Jacobian A defined by equation (3.3.15). P_{ij} measures the strength of association between state x_i and eigenvalue λ_j. The larger P_{ij} is, the stronger the association between state x_i and eigenvalue λ_j. In this way we can associate fast/slow states with eigenvalue groups with large/small real parts. Then we convert the differential equations of fast states to algebraic equations. The resulting DAE system may become high index after the conversion. Index reduction is needed if the index of the reduced DAE system is greater than 1, especially because consistent initial conditions are required.

In general, the dynamics of mass and heat transfer in different phases have different time scales. Focusing on the different time scales of states in different phases and regions, we further simplify the BFB model and build a single stage model in which the spatial distribution is ignored. By fixing the incoming and outgoing flow variables in a differential slice of BFB model, as shown in Figure 3.2(b), we obtain the single stage model. The original BFB model can be treated as a series connection of the single stage model. Next the Jacobian matrix of the single stage model is calculated using automatic differentiation with Matlab objects (adiff). We

introduce step changes in the input conditions to generate the transient response of the model. Eigenvalue variations of the system are calculated using dynamic simulation data. It should be noted that the following eigenvalue variations only correspond to a representative dynamic trajectory. However, different input disturbances will not significantly change the underlying physics for this solid-gas reaction system. Therefore, we use a representative case to analyze the time scale differences in system states. From Figure 3.4(a), we can find a clear separation of two distinct eigenvalue groups in the reference system. The absolute values of the three eigenvalues in the bottom of the figure are several orders of magnitude larger than the other eigenvalues, which corresponds to the fast dynamics in the reference system. The criterion to classify the slow and fast modes is to choose a separation which gives the largest separation ratio. In that way, less error will be introduced if the corresponding fast dynamics are removed. Based on this criterion, the fast and slow mode separation is shown in Figure 3.4(a). The separation ratio of the two groups is 843, which shows that fast and slow modes exist. By analyzing the UPSR matrix, the 3 eigenvalues in the fast mode are associated with the gaseous water concentration in the emulsion and the cloud-wake regions as described by equation (A.3) and equation (A.7) and the nitrogen concentration in the bubble region as described by equation (A.1). It is noted that all the fast eigenvalues are associated with states in the gas phase. The physical basis is that the dynamics of states in the gas phase are usually faster than the solid phase. The gaseous water concentration states in the emulsion and the cloud-wake regions are identified as fast states because of the fast kinetics of water physisorption, which is consistent with the previous analysis. The nitrogen concentration is identified as a fast state because nitrogen is not involved in any reaction and the bubbles move very quickly upwards and nitrogen mass transfer is nearly instantaneous. In the reduced model, the differential equations for these fast states are converted to (index 1) algebraic equations. By comparing the curves shown in Figure 3.4(b), we can tell that, in the reduced system, all the eigenvalues in fast mode are removed, which validates our

eigenvalue-to-state association.

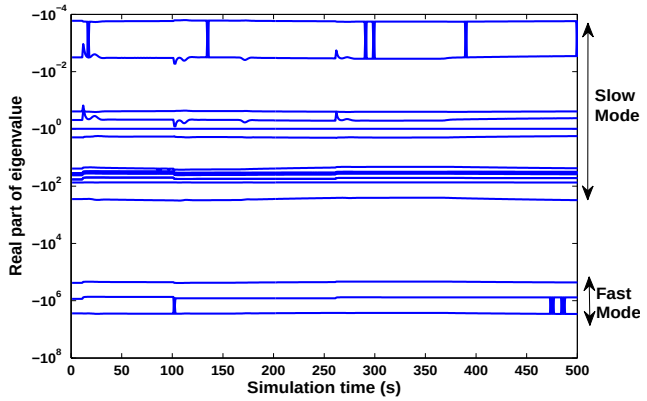

(a) Original model

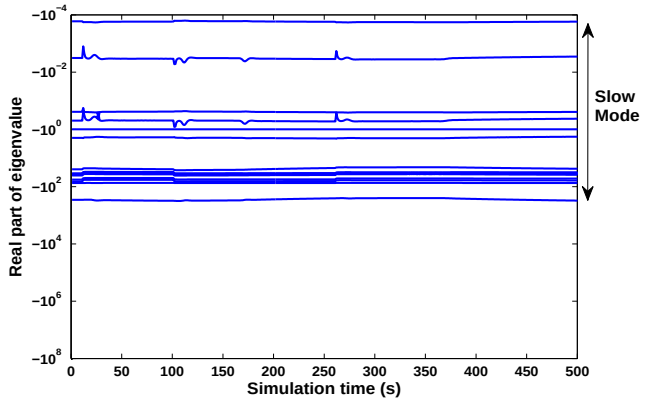

(b) Reduced model

Figure 3.4: Eigenvalue variation during transient response

Neglecting axial variations in temperature and pressure, the time scale decomposition of the single stage model is applied to the reference BFB model to generate the reduced model RM-2. Then, we test the performance of RM-2 in the case study. The simulation data are listed in Table 3.4. From Figure 3.5, we can see that the predicted response of the reference and reduced models have nearly the same dynamic behavior. The major difference is caused by the approximation of fast dynamics during transient response. The simulation time of the reduced model RM-2 is reduced by about 15%. Based on simulation tests and physical analysis, we conclude that the reduced model generated by eigenvalue analysis reduces the

Table 3.4: Dynamic simulation results

	Simulation time (s)	MRE1(%)	MSE1($\%^2$)	MRE2(%)	MSE2(mol^2/kg^2)
Reference model	193	-	-	-	-
RM-2	168	0.32	1.67E-4	0.023	4.31E-8

RM-2 - temporally reduced model using eigenvalue analysis

computational cost with only small error in predicting the model's key outputs.

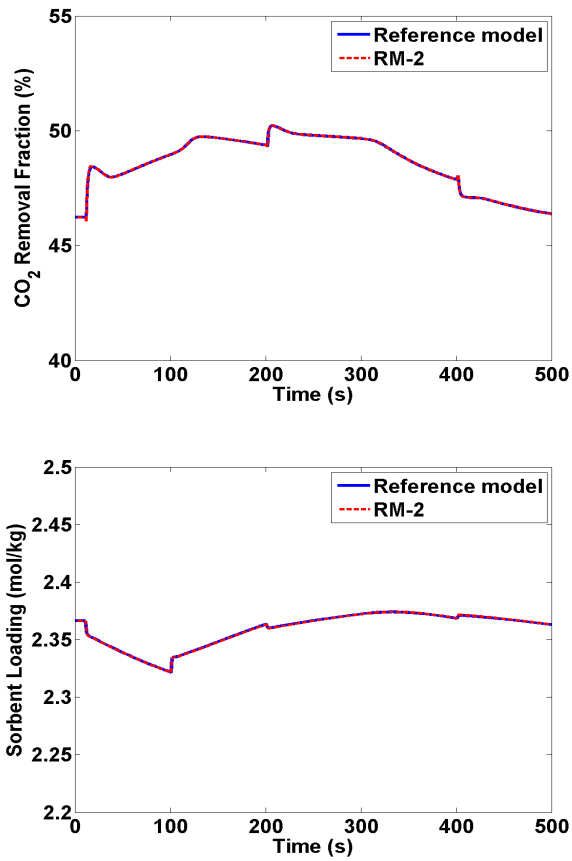

Figure 3.5: Comparison of output profiles of the reduced and reference BFB model

3.3.3 Summary of Results

In this section, a nullspace projection scheme is used to simplify the reaction kinetics and an eigenvalue analysis technique is utilized to study time scale differences in the system's overall dynamics. Simulation results in Table 3.5 show that both techniques lead to reducing simulation time while maintaining good accu-

Table 3.5: Dynamic simulation results

	Simulation time (s)	MRE1 (%)	MSE1 ($\%^2$)	MRE2 (%)	MSE2 (mol^2/kg^2)
Reference model	193	-	-	-	-
RM-1	122	0.017	2.45E-5	0.0081	3.06E-8
RM-2	168	0.32	1.67E-4	0.023	4.31E-8
RM-3	117	0.32	2.02E-4	0.0093	2.59E-8

RM-1 - temporally reduced model using nullspace projection
RM-2 - temporally reduced model using eigenvalue analysis
RM-3 - combined temporally reduced model

racy. We also observe that the temporally reduced model using nullspace projection achieves better performance than eigenvalue analysis. One reason is that the time scale difference in reaction rates is more significant than those in the eigenvalue groups, while the performance of the reduced model is dependent on the time scale differences that exist in the reference model. Usually, the larger the difference, the better the approximation. We can further improve the performance of the reduced model by combining these two methods. Since the fast dynamics of gaseous water has already been removed by nullspace projection, in the combined temporally reduced model, we only introduce the quasi-steady state approximation for nitrogen concentration based on eigenvalue analysis. Dynamic simulation results are listed in Table 3.5. By comparing the results, we find that the reduced model RM-3 with combined techniques is faster than RM-1 or RM-2 and maintains reasonable prediction accuracy.

Considering the generalization of these methods, both methods can be applied to model reduction of general first-principles process models apart from the BFB adsorber. The performance of reduced model depends on the inherent features of the rigorous model. The nullspace projection method is effective for models with significant differences in reaction rates. Prior knowledge about the reaction kinetics is needed, which can be achieved by simulating rigorous models or by experiments. The eigenvalue analysis and spectral association technique give general insight to a system's dynamic modes. For nonlinear systems, this method relies on local linearization, but it can help understand the dynamics at certain local operat-

ing points.

3.4 Spatial Model Reduction for BFB Adsorber

As described previously, the reference BFB model is discretized using the finite difference method, leading to a large-scale DAE system with over 10,000 equations. The large number of equations contributes to the high simulation cost. In this section, we reduce the number of DAEs by introducing a relatively sparse discretization grid while maintaining reasonable accuracy. The model reduction is conducted on the reference BFB model represented by the PDAE system (3.2.4).

3.4.1 Spatially Reduced Model Using Orthogonal Collocation

Orthogonal collocation uses high order orthogonal polynomials to approximate state profiles. Orthogonal collocation on finite elements (OCFE) combines the benefits of orthogonal collocation and finite difference method [20]. Over the spatial domain, $x \in [0, L]$, we introduce discrete points, $0 = x_0 < x_1 ... < x_i \ldots < x_{NE} = L$. Applying orthogonal collocation to the finite elements $h_i = x_i - x_{i-1}$, we approximate the states $z(x,t)$ through basis polynomials $l_j(.)$ within each element.

$$z^K = \sum_{j=0}^{K} l_j(\xi) z_{i,j} \tag{3.4.1}$$

where $j \in \{0, \ldots, K\}$ is the index of the polynomials used in finite element i, $z_{i,j}$ are the coefficients for the approximation which needs to be calculated. In this work, Lagrange polynomials are used for state space approximation. The coefficients $z_{i,k}$ are the state values at collocation points ξ_k, $k = 1, \ldots, K$. We substitute the approximated states into the original PDAE system (3.2.4) and enforce the resulting algebraic equations at the collocation points ξ_k. This leads to the discretized system shown in equation (3.4.2a) - equation (3.4.2b). The continuity of the differential

state is guaranteed by equation (3.4.2c).

$$\frac{\partial z_{i,k}}{\partial t} h_i = \sum_{j=0}^{K} z_{i,j} \frac{\partial l_j(\xi_k)}{\partial \xi} + h_i f(z_{i,k}, y_{i,k}) \qquad i = 1 \cdots N, k = 1 \cdots K \tag{3.4.2a}$$

$$g(z_{i,k}, y_{i,k}) = 0 \qquad i = 1 \cdots N, k = 1 \cdots K \tag{3.4.2b}$$

$$z_{i+1,0} = z_{i,K}, \qquad i = 1 \cdots N - 1 \tag{3.4.2c}$$

where h_i is the length of finite element i, $z_{i,k}$ and $y_{i,k}$ are the values of differential and algebraic variables at collocation points ξ_k.

The collocation method is a high order method, and the truncation error for Radau collocation is $O(h^{2K-1})$, where K is the number of collocation points in a single finite element. Therefore, it needs fewer discretization points than the finite difference method to achieve a similar accuracy. Considering the characteristics of fluidization, since the solids are circulated in the reactor, there exist upward and downward flows for the solids. For a counter-current flow configuration, special treatment is needed for discretization. For upward flow of gas and solid, the spatial partial differential terms are discretized at collocation points and boundary conditions are enforced at the bottom boundary ($x = 0$). For the downward flow, the boundary condition is applied at the top ($x = L$) and spatial partial differential terms are discretized at collocation points including the bottom boundary. The discretization scheme for the BFB model is shown in Figure 3.6.

Simulation results show dramatic changes for spatial states, such as solid molar flux, in the lower region near the bottom of the reactor ($0 \leq x \leq 0.1L$). Figure 3.7 shows the spatial profile of the solid molar flux in the emulsion region. We can see that with a small increase in bed length near the lower region, the value of the solid molar flux changes greatly. Since we discretize the partial differential terms at the bottom boundary, an accurate approximation for spatial gradients is required, especially in the lower region. To handle this issue, we introduce an unevenly distributed finite element scheme. In the case study, a total of 12 finite elements

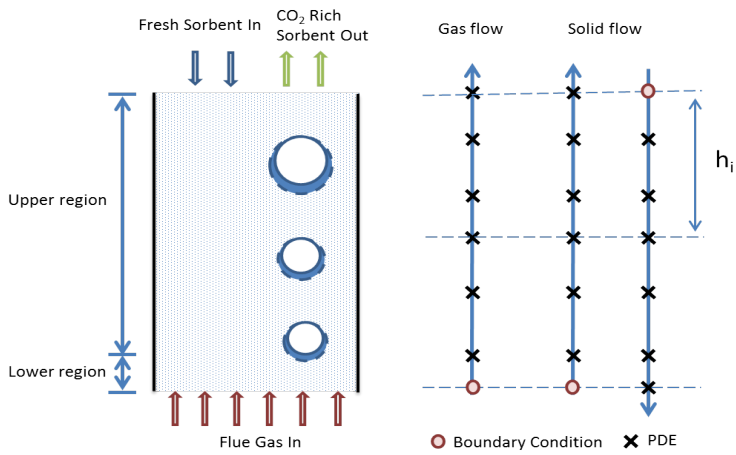

Figure 3.6: Discretization scheme for BFB adsorber using OCFE

is introduced, with 2 finite elements located in the lower region. Thus, a denser discretization grid is used in the lower region of the reactor to better approximate steep gradients for state variables. The finite elements in the lower region are almost half the size as in the upper region, and the overall system is more sparse than the finite difference case. In each finite element, 3 Radau collocation points are used. Thus, the total number of equations in the spatially reduced model using OCFE is only about 40% of the original model discretized using the finite difference method. The element mesh can also be tuned to balance model size and accuracy.

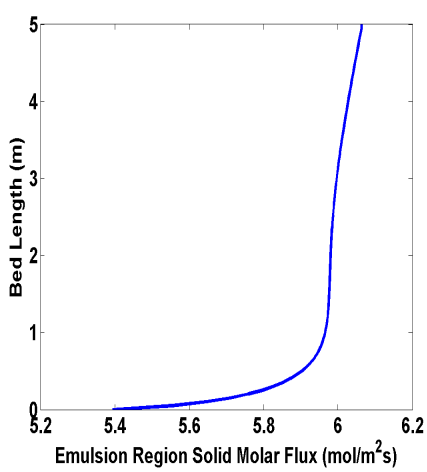

Figure 3.7: Spatial profile of solid molar flux in the BFB adsorber

We test the performance of the spatially reduced model RM-4 using the same sim-

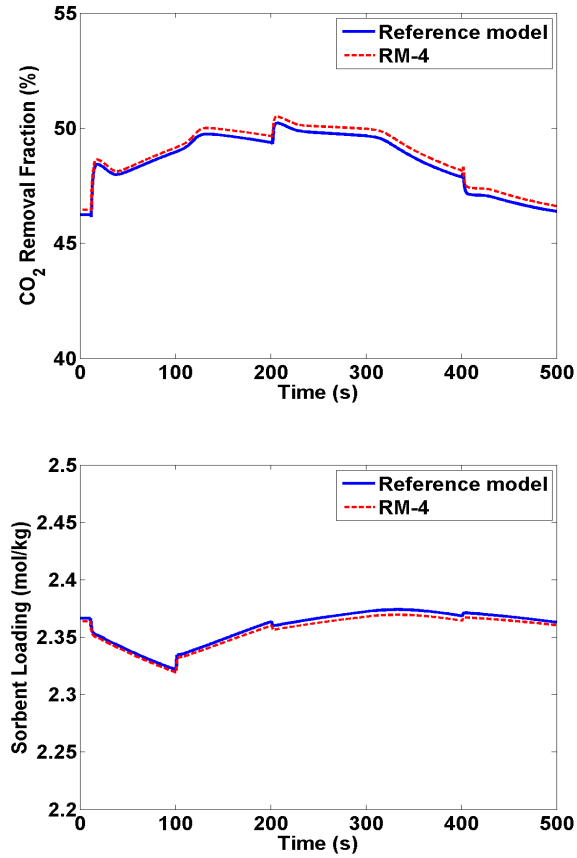

Figure 3.8: Comparison of output profiles of the reduced and reference BFB model

ulation test as for the temporally reduced models. From Figure 3.8, we can see that the dominant dynamic behavior is captured by the reduced model. The detailed simulation results are listed in Table 3.6. The MRE for CO_2 removal is only 0.68%, and the MSE is 0.071%. For sorbent loading, the MRE is within 0.19%. The reduced model can achieve about 65% reduction in simulation time because of a similar reduction in model size. In addition, we compare the discretized model us-

Table 3.6: Dynamic simulation results

	Simulation time (s)	MRE1(%)	MSE1($\%^2$)	MRE2(%)	MSE2(mol^2/kg^2)
Reference model	193	-	-	-	-
RM-4	69	0.68	0.071	0.19	1.19E-5
RM-5	54	8.91	15.54	1.46	1.04E-3

RM-4 - spatially reduced model using orthogonal collocation on finite elements (36 nodes)
RM-5 - discretized model using finite difference method (36 nodes)

ing finite differences with same number of discretization points as OCFE. Hence, we reduce the number of discretization points in the upper region, with the number in the lower region unchanged. From simulation results shown in Table 3.6, we can see that there are much higher prediction errors when using finite differences with 36 discretization points. Although this approach reduces the simulation time, the accuracy is much worse than with the collocation method. So we can achieve a computationally efficient reduced model with good accuracy using OCFE.

3.4.2 Model Reduction Using Proper Orthogonal Decomposition

In addition to using general spatial basis functions such as Lagrange polynomials, we also investigate specific spatial basis functions based on the model's characteristics. Proper orthogonal decomposition (POD), also called the Karhunen-Loeve method, is a powerful model reduction tool to create an accurate low dimensional approximation of spatially distributed models based on dynamic simulation data. The basic idea of POD is to find the dominant empirical eigenfunctions that represent the spatial features of the original states. POD is introduced by Lumley [13] to find coherent structures in turbulent flows. This approach has been applied to model reduction and numerical simulation of many complex distributed systems, such as the rapid thermal processing system [3] and a lithium-ion battery [18]. POD has also been applied to control and optimization problems such as the control of diffusion-reaction processes [8], optimization of diffusion-convection-reaction processes [12] and optimization of pressure swing adsorption systems [1]. The procedure of POD is illustrated as follows. The spatio-temporal state variables $z(x,t)$ of a distributed parameter system given by equation (3.2.4a) can be expanded by a set of spatial basis functions as follows:

$$z(x,t) = \sum_{i=1}^{M} a_i(t)\phi_i(x) \tag{3.4.3}$$

where $\phi_i(x)$ is a spatial basis function, $a_i(t)$ is a time dependent coefficient. In this way, the temporal and spatial information of z is decomposed. The key idea of POD is to find a low dimensional set of orthogonal basis functions, in which the spatial distribution information is captured, to represent the original high dimensional system. In this case study, we use the method of snapshots [81] to find the spatial basis functions. Snapshots are the numerical solutions to a large-scale system after spatial discretization of the PDEs. The snapshot matrix Z is given by:

$$Z = \{z(x, t_1), \cdots, z(x, t_{N_t})\} \tag{3.4.4}$$

Each column $z(x, t_j)$ represents the spatial profile of the state variable at time t_j, and each row $z(x_i, t)$ represents the time trajectory of the state variable at spatial location x_i. The POD basis functions are generated by performing singular value decomposition (SVD) of the snapshot matrix Z:

$$Z = UDV^T = \sum_{i=1}^{N} \sigma_i u_i v_i^T \tag{3.4.5}$$

where u_i is the eigenvector, and σ_i is the singular value. The first M vectors of the orthogonal eigenvector matrix U, which capture most spatial distribution information, are chosen as the POD basis functions $\phi_i(x), i = 1 \cdots M$. This approximation will lead to a projection error ε which can be quantified by:

$$\varepsilon = 1 - \frac{\sum_{i=1}^{M} \sigma_i^2}{\sum_{i=1}^{N} \sigma_i^2} \tag{3.4.6}$$

After finding appropriate basis functions, the method of weighted residuals [30] is used to solve the unknown time dependent coefficient $a_i(t)$ by enforcing the inner product of residuals of the approximated PDEs with an orthonormal set of weighted basis function set to zero. The Galerkin method is the most popular choice used for POD applications, where the weighted basis functions are the same

Table 3.7: Dynamic simulation results

	Simulation time (s)	MRE1(%)	MSE1($\%^2$)	MRE2(%)	MSE2(mol^2/kg^2)
Reference model	193	-	-	-	-
RM-6	741	0.35	0.0051	0.080	2.77E-6
RM-7	395	8.47	12.64	8.54	0.034

RM-6 - spatially reduced model using POD (L^2 inner product over 100 nodes)
RM-7 - spatially reduced model using POD (5 point quadrature)

as the POD basis functions. Next we consider a PDE described by equation (3.4.7) to demonstrate how POD can reduce model size. The approximated state given by equation (3.4.3) is substituted into equation (3.4.7). The residuals are projected onto the orthonormal basis function $\phi_i(x)$ and this leads to a reduced system with only M sets of ordinary differential equations (ODE), as shown in equation (3.4.8). For the original system, however, there will be N sets of ODEs after spatial discretization over N nodes. Since M is significantly less than N, a much smaller reduced model with reasonable accuracy is created using POD.

$$\frac{\partial z}{\partial t} = f(z, \frac{\partial z}{\partial x}) \tag{3.4.7}$$

$$\frac{da_i}{dt} = \int f(\sum_{j=1}^{M} a_j(t)\phi_j(x), \sum_{j=1}^{M} a_j(t)\frac{d\phi_j}{dx})\phi_i dx, \qquad i = 1 \ldots M \tag{3.4.8}$$

For the POD reduction of the BFB model, the reference BFB model discretized by the finite difference method is used to generate dynamic simulation data as snapshots. The method of snapshots is then applied to find the POD basis functions. We find that all the states can be represented with only 6 to 7 POD basis functions, instead of 100 discretization points. The projection error ε, defined by equation (3.4.6), is less than 0.1%. These results show great potential for reducing the model size and maintaining good accuracy. The Galerkin method is then utilized to project the model equations onto the basis functions. In the dynamic simulation case study, we approximate the gas temperature in the bubble region using 5 POD basis functions to study POD's performance. The bubble region energy balance equation, as shown in equation (A.2), has been projected onto the basis functions.

From the simulation results in Table 3.7, we can see that spatially reduced model RM-6 by POD has good prediction accuracy. Only 5 basis functions are needed to capture most of the spatial information. However, the simulation time of RM-6 is much higher than the reference model. The first reason for this inconsistency is that the Galerkin method enforces the integral of residuals to be zero. At every iteration, the integral of the residuals needs to be calculated, and it is very time-consuming for a highly nonlinear system like the BFB model. To reduce the computational cost of calculating the integral, we can use the quadrature method to approximate the integral, instead of the L^2 inner product. Results from RM-7 show that this takes less simulation time than RM-6, but its accuracy is worse due to the integral approximation. After using the quadrature approximation, however, the simulation time of RM-7 is still higher than the reference model. This is due to the fact that the sparsity of Jacobian $\partial f/\partial a$ in equation (3.4.8) is destroyed by POD projection. POD can generate a smaller model, but the Jacobian is denser compared with normal discretization methods. This may become a serious issue especially for systems having many states with strong couplings. To potentially improve the effectiveness of the POD method,there are several ways to reduce the computational cost of approximating L^2 inner products, such as missing point estimation [10] and discrete empirical interpolation method [21] , with a central idea of using a small selected set of spatial nodes to avoid directly calculating L^2 inner products. These methods have been shown to be effective on models developed for applications such as glass melting furnaces, and we will consider applying them on the reference BFB model in future work.

3.4.3 Summary of Results

In this section, two spatial model reduction methods are utilized to reduce the number of equations in the reference BFB model. Orthogonal collocation is a higher order discretization method and requires fewer discretization points compared

with the finite difference method to achieve a similar accuracy in space. Orthogonal collocation with finite elements adds more flexibility into the discretization framework. Fewer finite elements can be used in spatial areas with small spatial variations in spatial states. Thus, the total number of discretization nodes can be further reduced based on the spatial distribution features of the rigorous model. For the POD method, dominant spatial basis functions can be found using the method of snapshots. This shows great potential for reducing model size. Despite the reduction in model dimension, the projection scheme of POD destroys the sparsity of the Jacobian, and it does not achieve significant reduction in computational cost for doing subsequent simulation.

To further reduce the simulation time, both temporal and spatial model reduction approaches are combined. We test the performance of the reduced model generated by combining temporal and spatial model reduction. Detailed simulation results are listed in Table 3.8. By comparing the results, we find that the reduced model with combined techniques is faster than those with spatial or temporal reduction applied separately, and the reduced model has reasonable prediction accuracy. For the reference BFB model, the most significant contribution to reducing simulation time is by orthogonal collocation on finite elements. Thus, the dominant factor causing high simulation time is the large number of equations. Temporal model reduction can also help reduce the simulation cost by reducing stiffness. For models of small size, such as the discretized model using orthogonal collocation, temporal model reduction does not improve as much as for large-scale models, since the stiffness issue becomes less serious for Jacobians of lower dimension.

3.5 Concluding Remarks

In this chapter, we developed temporally and spatially reduced order dynamic models for a large-scale and highly nonlinear model of a bubbling fluidized bed

Table 3.8: Dynamic simulation results

	Simulation time (s)	MRE1(%)	MSE1($\%^2$)	MRE2(%)	MSE2(mol^2/kg^2)
Reference model	193	-	-	-	-
RM-3	117	0.32	2.02E-4	0.0093	2.59E-8
RM-4	69	0.68	0.071	0.19	1.19E-5
RM-8	64	0.68	0.072	0.18	9.91E-6

RM-3 - combined temporally reduced model
RM-4 - spatially reduced model using orthogonal collocation on finite elements
RM-8 - combined reduced model using spatial and temporal model reduction

adsorber. The reduced models can achieve significant reduction in simulation time while maintaining good accuracy. Time scale decomposition methods, including nullspace projection and eigenvalue analysis, can help remove the fast dynamics of the system and reduce system stiffness. Orthogonal collocation on finite elements can reduce the number of model equations with reasonable accuracy. An unevenly distributed finite element scheme helps further reduce the model size based on process features. On the other hand, POD shows the potential to reduce the model size but does not reduce the simulation time, since it destroys the sparsity of the original system.

The computationally efficient and accurate reduced dynamic models developed in this chapter will be incorporated into time-critical applications in advanced process control to reduce the computational cost. Nonlinear model predictive control (NMPC) uses nonlinear process models to predict system behavior and find an optimal sequence of values for the manipulated variables by solving the dynamic optimization problem. However, solving the dynamic optimization problem with detailed first-principles process model is time-consuming and may lead to computational delay that will degenerate control performance and even destabilize the process [29]. Therefore, incorporating dynamic reduced models into the NMPC framework can help improve the computational efficiency of NMPC and make it applicable for online-control applications.

Chapter 4

NMPC of BFB Adsorber

In the previous chapter, we have developed accurate and computationally efficient dynamic reduced models. In this chapter, we will study the nonlinear model predictive control (NMPC) problem of the BFB adsorber using first-principles dynamic reduced models developed in the previous section. In addition to model reduction, we also introduce an input and state blocking formulation to reduce the size of nonlinear programming (NLP) problem and the computational cost for NMPC. Next we will apply a fast NMPC algorithm based on NLP sensitivity which could significantly reduce the online computational cost of NMPC. In the case study, we will demonstrate the performance of NMPC for BFB adsorber. Also we will focus on improvements in computational time brought by model reduction, NMPC blocking strategy and fast NMPC algorithm.

4.1 Input and State Blocking for NMPC

4.1.1 Introduction

As we mentioned before, the computational burden of solving large-scale optimization problems is one of the major challenges for practical applications of NMPC.

For larger process systems, computationally efficient solution of NLP subproblems are always required to avoid computational delay for NMPC. In addition to model reduction, we will introduce an input and state blocking strategy to further improve the computational efficiency for NMPC.

As discussed in Chapter 2.3.1, the dynamic optimization problem in NMPC can be reformulated to NLP via temporal discretization of the dynamic models using orthogonal collocation on finite elements. In standard NMPC formulation, dynamic models are discretized over uniformly distributed finite elements whose lengths equal the sampling time. This reformulation could lead to a large-scale NLP especially if the dynamic model has significant size and the prediction horizon is long.

For *offline* implementation of dynamic optimization, nonuniform grids are frequently considered for temporal discretization of state and control profiles to obtain accurate approximation and reduce the size of NLP problem. The construction of these nonuniform grids usually depends on the dynamics of particular applications. With appropriate nonuniform grids, nonuniform discretizations of state and control profiles, through high order collocation with finite elements grids, are essential to approximate the discretized DAE system, capture multiple time scales of the state profiles and reduce the size of NLP problem.

In this work, we expand this task to *on-line* NMPC controllers. As we mentioned earlier, uniform grids are typically used for temporal discretization when formulating the NMPC problem. The benefit of uniform discretization is that recursive feasibility is guaranteed in the moving horizon framework under mild assumptions, which is a key property to establish the stability of NMPC controller.

In this section, we denote NMPC with nonuniform discretization for control and state profiles as *input and state blocking strategies* for NMPC. A closely related problem to input and state blocking for NMPC is the use of *input blocking* or *move blocking* in MPC. This formulation is widely applied in commercial implementations of

DMC and other MPC controllers. A common strategy is to specify a shorter horizon for manipulated variables than the prediction horizon for states and outputs (see, e.g, [68]). With this formulation, the degrees of freedom in the optimization problem for MPC can be reduced, but not the size of the NLP problem. On the other hand, applying input blocking into the moving horizon framework raises several challenges with respect to stability and robustness properties, especially when terminal costs and constraints are imposed for MPC. In particular, for most moving horizon blocking (MHB) schemes, recursive feasibility cannot be guaranteed and this can complicate the stability analysis.

To solve this issue, stability and robustness properties of input blocking schemes have been analyzed over the past decade for linear MPC, mainly focusing on finding specific input blocking strategies that can guarantee recursive feasibility. In [17], the authors developed a general cyclic blocking scheme based on input deviations from an unconstrained feedback controller. This blocking scheme cycles over a time period and maintains recursive feasibility, even for terminal conditions. However, the controller moves are more restricted through these input deviations and optimal performance of the blocked MPC strategy is not guaranteed. A blocking scheme is established in [33] that applies to all blocking patterns by initially establishing feasible regions for the blocked controller. The approach then finds the least restrictive moves for a given blocking scheme. The approach ensures recursive feasibility but without stability guarantees. In [78], the authors develop a blocking framework for variable horizon MPC, which allows shifting and transformation of blocking patterns as the horizons evolve. They include a robust stability analysis using contraction properties and require terminal constraints on the MPC problem.

These studies show that an alternative shifted blocking (SB) scheme, where the left-most interval is removed and a right-most interval is added as the horizon shifts, is recursively feasible if appropriate terminal conditions are imposed. A

particular case considered in [88] is based on approximations to infinite horizon NMPC, where a shrinking horizon is maintained over infinite time. Under these conditions approximations to MHB and SB schemes are equivalent and recursively feasible.

With our input and state blocking formulation, recursive feasibility may not be maintained, which makes stability analysis more difficult. In this study, we will modify the NMPC formulation and show how nominal stability and input-to-state stability (ISS) can still be preserved with input and state blocking. In the next section we describe our MHB and SB schemes for nonuniform grids. Based on these we modify the NLP subproblem for blocked NMPC to enforce strong descent of the Lyapunov function at each sampling time. This leads to an NMPC strategy that embeds both MHB and SB schemes and leads to robust stability guarantees. Then we will demonstrate the performance of blocking strategy on the bubbling fluidized bed adsorber process.

4.1.2 Input and State Blocking Formulation

Consider the following discrete-time nonlinear dynamic model of the plant with uncertainties:

$$\begin{aligned} x(k+1) &= \hat{f}(x(k), u(k), w(k)) \\ &= f(x(k), u(k)) + d(x(k), u(k), w(k)) \end{aligned} \tag{4.1.1}$$

where $x(k) \in \Re^{n_x}$, $u(k) \in \Re^{n_u}$ and $w(k) \in \Re^{n_w}$ are the plant states, controls and disturbance signals, respectively, defined at time steps t_k with integers $k > 0$. The mapping $f : \Re^{n_x+n_u} \mapsto \Re^{n_x}$ with $f(0,0) = 0$ represents the nominal model, while the term $d : \Re^{n_x+n_u+n_w} \mapsto \Re^{n_x}$ is used to describe modeling errors, estimation errors and disturbances. We assume that $f(\cdot,\cdot)$ and $d(\cdot,\cdot,\cdot)$ are Lipschitz continuous, and that the noise $w(k)$ is drawn from a bounded set $\mathcal{W}$.

Then we introduce a blocking pattern $\mathbf{v} = Mq$ where $\mathbf{v} = [v_0^T, v_1^T, \ldots, v_{N-1}^T]^T$ and q are the blocked inputs. After N_0 intervals, the blocking matrix M incorporates n_b blocks, each of length $N_j, j = 1, \ldots, n_b$ as follows:

$$M = \begin{bmatrix} I_{n_u \times N_0} & 0 & 0 & \ldots & 0 \\ 0 & E_1 & 0 & \ldots & 0 \\ \ldots & \ldots & \ldots & \ldots & \ldots \\ 0 & 0 & 0 & \ldots & E_{n_b} \end{bmatrix} \tag{4.1.2}$$

where the matrices $E_j, j = 1, \ldots n_b$ consist of N_j stacked identity matrices of order n_u.

This blocked NMPC controller is defined by the following nonlinear programming problem (NLP):

$$V(x(k)) := \min_{z_l, v_l} \quad \Psi(z_N) + \sum_{l=0}^{N-1} \psi(z_l, v_l) \tag{4.1.3a}$$

$$\text{s.t. } z_{l+1} = f(z_l, v_l), l = 0, \ldots N_0 - 1 \tag{4.1.3b}$$

$$\begin{aligned} z_{l+1} &= f^j(z_l, v_l), j = 1, \ldots n_b, \\ l &= \sum_{j'=0}^{j-1} N_{j'}, \ldots, \sum_{j'=0}^{j} N_{j'} \end{aligned} \tag{4.1.3c}$$

$$z_0 = x(k), \mathbf{v} = Mq, z_l \in \mathbb{X}, v_l \in \mathbb{U}, z_N \in \mathbb{X}_f. \tag{4.1.3d}$$

where the horizon length is $\sum_{j'=0}^{n_b} N_{j'} = N$.

We assume that the states and controls are restricted to the domains $\mathbb{X}$ and $\mathbb{U}$, respectively. $\mathbb{X}_f$ is the terminal set with $\mathbb{X}_f \subset \mathbb{X}$. The set $\mathbb{U}$ is compact and contains the origin; the sets $\mathbb{X}$ and $\mathbb{X}_f$ are closed and contain the origin in their interiors. The stage cost is given by $\psi(\cdot, \cdot) : \Re^{n_x + n_u} \to \Re$, while the terminal cost is denoted by $\Psi(\cdot) : \Re^{n_x} \to \Re$; both are assumed to be Lipschitz continuous.

Moreover, we apply the robust problem formulation in [91] and relax $\mathbb{X}$ and $\mathbb{X}_f$ with ℓ_1 penalty terms. Writing $\mathbb{X}$ and $\mathbb{X}_f$ as inequalities $g(z_l) \leq 0$ and $g(z_N) \leq$

0, respectively, and redefining $g_+^{(j)}(z_l) = max(0, g^{(j)}(z_l))$, $\psi(z_l, v_l) := \psi(z_l, v_l) + \rho\|g_+(z_l)\|$ and $\Psi(z_N) := \Psi(z_N) + \rho\|g_+(z_N)\|$, we obtain the following MHB reformulation:

$$
\begin{aligned}
V(x(k)) = \min_{v_l, z_l} \quad & \Psi(z_N) + \sum_{l=0}^{N-1} \psi(z_l, v_l) && (4.1.4a)\\
\text{s.t. } z_{l+1} &= f(z_l, v_l), l = 0, \ldots N_0 - 1 && (4.1.4b)\\
z_{l+1} &= f^j(z_l, v_l),\ j = 1, \ldots, n_b, \\
l &= \sum_{j'=0}^{j-1} N_{j'}, \ldots, \sum_{j'=0}^{j} N_{j'} && (4.1.4c)\\
z_0 &= x(k), \mathbf{v} = Mq, v_l \in \mathbb{U}. && (4.1.4d)
\end{aligned}
$$

Note that the redefined objective function in (4.1.4) is no longer differentiable everywhere, but still Lipschitz continuous, with Lipschitz constant L_V, which is sufficient for the stability analysis in the following sections.

In the reformulated MHB problem (4.1.4), we can find a coarser approximation for the discretized differential-algebraic equation model, given by $z_{l+1} = f^j(z_l, v_l)$. For $f^j(\dot{;})$, the dynamic model is discretized by collocation on nonuniform finite elements with the length of element equal to N_j. Within the finite element that covers multiple sampling times, the states at each sampling time are calculated via interpolation. We denote this as *state blocking*.

This formulation leads to state profiles described by finite elements of different length in each block. These longer elements are sufficient for slower time scales and lead to a significant reduction in NLP variables. It should be noted that the accuracy of the discretized models depends on the blocking pattern. In this study, we assume that the blocked state model based on collocation on nonuniform finite elements is a high fidelity approximation to the plant since the blocking pattern can be determined offline based on the system dynamics.

Figure 4.1 shows a graphical representation of state and input profiles in the pro-

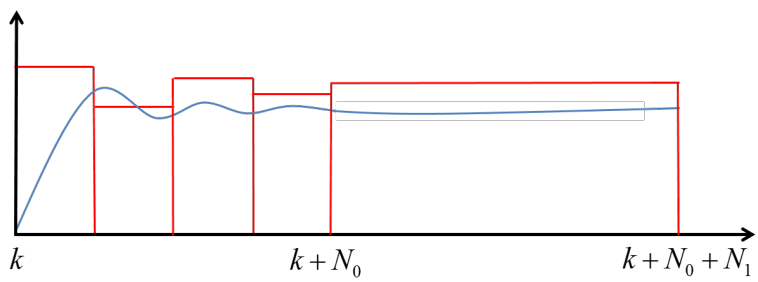

Figure 4.1: Representation of input and state blocking scheme

posed blocking scheme. The blue curve represents state profiles and red rectangle represents control moves. For the initial part (k to $k+N_0$) in the prediction horizon, where fast dynamics may dominate, uniform grids with small lengths are applied for temporal discretization. For the rest of prediction horizon ($k+N_0$ to $k+N_0+N_1$) , we introduce a larger finite element to discretize dynamic model equations and control inputs. In this region, states with slow time scales evolve less significantly and the larger finite element can still provide sufficient approximation.

Then we apply the input and state blocking into the moving horizon framework. At time step k, we solve the blocked NMPC problem (4.1.4). At next sampling time $k+1$, we move the optimization problem one step forward and solve the NMPC with the same blocking scheme. The scheme for MHB strategy is shown in Figure 4.2.

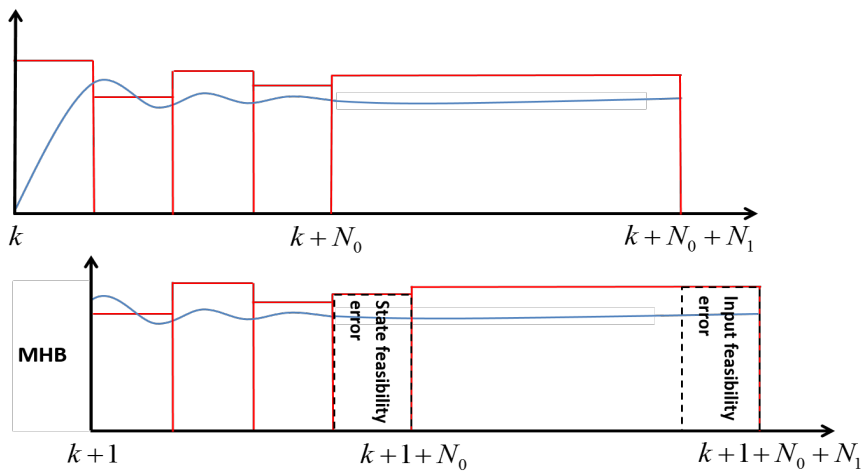

Figure 4.2: Representation of moving horizon blocking scheme

From Figure 4.2 we can see that MHB is not recursively feasible, neither for inputs nor states due to the input and state blocking introduced. In this figure, we denote state feasibility error and input feasibility error, which will be discussed in the following section.

Moreover, we also consider a Shifted Blocking (SB) strategy with $\mathbf{v} = \bar{M}\bar{q}$. The input blocking matrix $\bar{M}$ for shifted blocking strategy is defined as follows:

$$\bar{M} = \begin{bmatrix} I_{n_u \times (N_0-1)} & 0 & 0 & \dots & 0 \\ 0 & E_1 & 0 & \dots & 0 \\ \dots & \dots & \dots & \dots & \dots \\ 0 & 0 & \dots & E_{N_b} & 0 \\ 0 & 0 & \dots & 0 & I_{n_u} \end{bmatrix}. \tag{4.1.5}$$

As shown in Figure 4.3, the shifted blocking pattern modifies the moving horizon blocking pattern by removing the sampling time on the left and adding a sampling interval on the right. The SB strategy is recursively feasible for the inputs and states, as well as the terminal conditions. The NLP subproblem for the SB pattern

is given by:

$$\bar{V}(x(k)) = \min_{v_l, z_l} \quad \Psi(z_N) + \sum_{l=0}^{N-1} \psi(z_l, v_l) \tag{4.1.6a}$$

$$\text{s.t. } z_{l+1} = f(z_l, v_l), l = 0, \ldots N_0 - 2 \tag{4.1.6b}$$

$$z_{l+1} = f^j(z_l, v_l), j = 1, \ldots n_b,$$

$$l = (\sum_{j'=0}^{j-1} N_{j'}) - 1, \ldots (\sum_{j'=0}^{j} N_{j'}) - 1 \tag{4.1.6c}$$

$$z_N = f(z_{N-1}, v_{N-1}) \tag{4.1.6d}$$

$$z_0 = x(k), \mathbf{v} = \bar{M}\bar{q}, v_l \in \mathbb{U} \tag{4.1.6e}$$

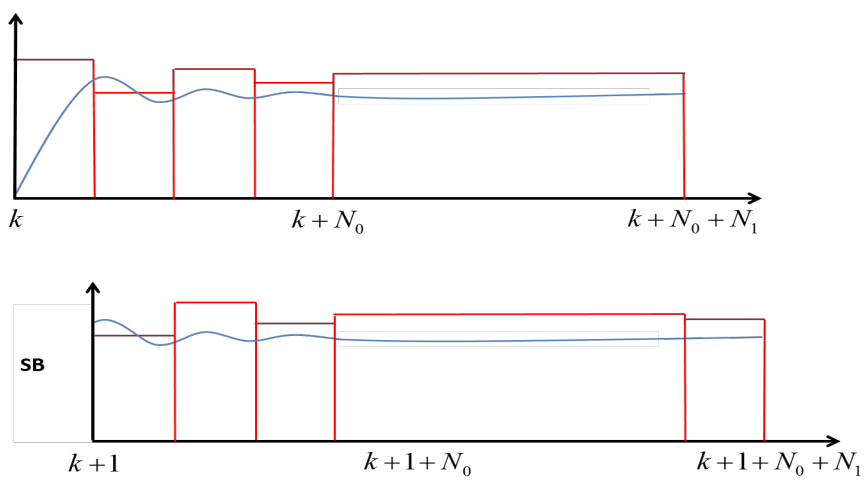

Figure 4.3: Representation of shifted blocking scheme

4.1.3 Nominal and ISS Stability Properties

Stability properties of blocked NMPC are adapted from well-known properties of the standard NMPC controller [46, 59], with the following assumptions:

Assumption 4.1.1. *(Nominal Stability Assumptions for NMPC)*

- *The terminal penalty* $\Psi(\cdot)$*, satisfies* $\Psi(z) > 0, \forall z \in \mathbb{X}_f \backslash \{0\}$*,*
- *There exists a local control law* $u = \kappa_f(z)$ *defined on* $\mathbb{X}_f$*, such that* $f(z, \kappa_f(z)) \in \mathbb{X}_f, \forall z \in \mathbb{X}_f$*, and* $\Psi(f(z, \kappa_f(z))) - \Psi(z) \leq -\psi(z, \kappa_f(z)), \forall z \in \mathbb{X}_f$*.*

- *The optimal stage cost $\psi(x,u) = \psi(x,\kappa(x))$ satisfies $\alpha_p(|x|) \leq \psi(x,u) \leq \alpha_q(|x|)$ where $\alpha_p(\cdot)$ and $\alpha_q(\cdot)$ are $\mathcal{K}$ functions.*

Nominal stability can be paraphrased by the following theorem.

Theorem 4.1.1. *(Nominal Stability [74]) Consider the unblocked moving horizon problem (Problem (4.1.4) with $M = I$) and associated control law $u = u^{id}$, that satisfies Assumption 4.1.1. Then, $V(x)$ from the unblocked controller is a Lyapunov function and the closed-loop system is asymptotically stable.*

For unblocked NMPC, under Assumption 4.1.1, we have the following descent condition by comparing two neighboring value functions:

$$\begin{aligned} V(x(k+1)) - V(x(k)) &\leq \Psi(f(z_N, \kappa_f(z_N))) + \sum_{l=1}^{N} \psi(z_l, v_l) \\ &\quad - \Psi(z_N) - \sum_{l=0}^{N-1} \psi(z_l, v_l) \\ &= -\psi(x(k), u(k)) + \Psi(f(z_N, \kappa_f(z_N))) - \Psi(z_N) + \psi(z_N, \kappa_f(z_N)) \\ &\leq -\psi(x(k), u(k)) \end{aligned} \tag{4.1.7}$$

Relying on the recursive feasibility of unblocked NMPC, most terms in $V(x(k))$ and $V(x(k+1))$ cancel out. With the above inequality, the nominal asymptotic stability of unblocked NMPC can be established.

For blocked NMPC, however, the above inequality may not hold because recursive feasibility is not guaranteed. Here we assume that the solutions $[v_0, \cdots, v_{N-1}]$ from NMPC at t_k provide feasible inputs to the NMPC problem at t_{k+1}. Namely, the control $[v_1, \cdots, v_{N-1}, v_N]$ with $v_N = v_{N-1}$ are feasible inputs to NMPC at t_{k+1}. Note that at t_{k+1}, the blocking is moved one step forward and it doesn't match the previous discretization grids. Therefore the overlapping states for two consecutive NMPC problems are different due to blocking in state approximation. Then we compare the value functions at two consecutive sampling time t_k and t_{k+1}. Since

the overlapping states are not completely the same, additional error terms appear in the value function difference.

$$\begin{aligned} V(x(k+1)) - V(x(k)) &\leq \Psi(f(z_N, \kappa_f(z_N))) + \sum_{l=1}^{N} \psi(z_{l,blocked}, v_l) \\ &\quad - \Psi(z_N) - \sum_{l=0}^{N-1} \psi(z_l, v_l) \\ &= -\psi(x(k), u(k)) + \epsilon_f \\ &\quad + \Psi(f(z_N, \kappa_f(z_N))) - \Psi(z_N) + \psi(z_N, \kappa_f(z_N)) \\ &\leq -\psi(x(k), u(k)) + \epsilon_f \end{aligned} \tag{4.1.8}$$

where ϵ_f are the feasibility errors brought by the state blocking. In addition, the input may not be recursively feasible as well, which will introduce a similar input feasibility error term, as shown in Figure 4.2.

Therefore, the inequality (4.1.7) may not hold due to the input and state blocking. However, if the feasibility errors ϵ_f can be bounded by $\rho\psi(x(k), u(k))$, with $0 \leq \rho < 1$, which leads to the following inequality

$$V(x(k+1)) \leq V(x(k)) - (1-\rho)\psi(x(k), u(k)) \tag{4.1.9}$$

where $\rho \in [0, 1)$ is chosen to reflect the inaccuracy caused by input and state blocking as well as other sources of model mismatch.

With constraint (4.1.9) being satisfied, the value function of blocked NMPC will be decreasing monotonically and thus the stability of blocked NMPC controller can be established. In addition, it is easy to show that the nominal stability can be maintained if the inequality (4.1.9) is violated for a finite number of times. This can be shown by summing the left hand side of (4.1.9) over k. If (4.1.9) is allowed to be

violated for no more than a finite subsequence (say, $k \in K_f$), which leads to:

$$
\begin{aligned}
V(x(k_0)) &\geq \sum_{k=k_0}^{\infty} V(x(k)) - V(x(k+1)) \qquad (4.1.10)\\
&= \sum_{k\in K_f}^{\infty} V(x(k)) - V(x(k+1)) + \sum_{k=k_0\setminus K_f}^{\infty} V(x(k)) - V(x(k+1))\\
&= C_f + \sum_{k=k_0\setminus K_f}^{\infty} (V(x(k)) - V(x(k+1)))\\
&\geq C_f + \sum_{k=k_0\setminus K_f}^{\infty} (1-\rho)\psi(x(k), u(k)).
\end{aligned}
$$

Then we can see that $\lim_{k\to\infty} \psi(x(k), u(k)) \to 0$, and $\lim_{k\to\infty} x(k) \to 0$.

For the analysis of robust stability properties of NMPC, we consider Input-to-State Stability (ISS) ([45, 59]). We also make the following assumptions and establish robust stability of the NMPC controller from the following theorem.

Assumption 4.1.2. *(Robust Stability Assumptions)*

- *The value function $V(x(k))$ of (4.1.4) is continuous with respect to $x(k)$, with a positive Lipschitz constant L_V.*
- *$d(x, u, w)$ is Lipschitz with respect to its arguments, with $|d(x, u, w)| \leq |d(x, u, 0)| + L_g|w|$ and $|d(x, u, 0)| \leq \alpha_0(|x|)$, where $\alpha_0(|x|)$ is a $\mathcal{K}_\infty$ function.*

Theorem 4.1.2. *(Robust ISS Stability of Unblocked NMPC (Theorem 2 in [59], see also [45]) Under Assumptions 4.1.1 and 4.1.2 with $\alpha_0(|x|) \leq \frac{\eta}{L_V}\alpha_p(|x|)$ and $\eta \in (0, 1)$, the cost function $V(x)$ obtained from the solution of (4.1.4) with $M = I$ is an ISS-Lyapunov function and the resulting closed-loop system is ISS stable.*

The result from Theorem 4.1.2 with unblocked NMPC leads to the following in-

equality:

$$
\begin{aligned}
&V(x(k+1)) - V(x(k)) \\
&= V(x(k+1)) - V(f(x(k),u(k))) + V(f(x(k),u(k))) - V(x(k)) \\
&\leq \epsilon_w - \psi(x(k),u(k))
\end{aligned}
\tag{4.1.11}
$$

where $\epsilon_w \geq |V(x(k+1)) - V(f(x(k),u(k)))|$ is an additional ISS term that represents the influence of disturbances $w(k)$. The inequality for the second pair follows the inequality (4.1.7) in Theorem 4.1.1.

However, for blocked NMPC, recursive feasibility doesn't hold. Therefore, we have the following relationship, with additional feasibility error ϵ_f as shown in (4.1.8):

$$
\begin{aligned}
&V(x(k+1)) - V(x(k)) \\
&= V(x(k+1)) - V(f(x(k),u(k))) + V(f(x(k),u(k))) - V(x(k)) \\
&\leq \epsilon_w - \psi(x(k),u(k)) + \epsilon_f
\end{aligned}
\tag{4.1.12}
$$

Similarly, if the feasibility error ϵ_f can be bounded by $\rho\psi(x(k),u(k))$, with $0 \leq \rho < 1$, we can have the following inequality, which still guarantees ISS property of blocked NMPC.

$$
V(x(k+1)) \leq V(x(k)) - (1-\rho)\psi(x(k),u(k)) + \epsilon_w \tag{4.1.13}
$$

The ISS term ϵ_w can be bounded by $L_V\|x(k+1) - f(x(k),u(k))\|$ based on NLP sensitivity, where L_V can be determined by off-line NLP sensitivity analysis.

4.1.4 Blocked NMPC Strategy

To show under what conditions (4.1.9) and (4.1.13) hold, we first consider the quasi-infinite horizon formulation in [88]. Here $n_b = 1$ after N_0 sampling times, and the single blocked stage takes the process to (near) steady state where $x_s = f(x_s, u_s)$. Assuming that N_1 is sufficiently long, we do not need to impose a terminal constraint. As shown in Figure 4.4 the quasi-infinite blocking pattern is recursively feasible for the inputs. On the other hand, there is a slight error in the approximation of the states. We will assume this error and other model mismatch effects can be bounded above by the $\rho\psi(x(k), u(k))$ term in (4.1.13).

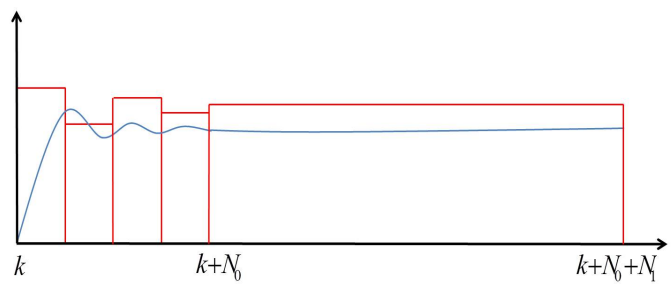

Figure 4.4: Representation of quasi-infinite blocking scheme

On the other hand, if an arbitrary blocking pattern is used with $n_b > 1$, we no longer have recursive feasibility and the descent conditions (4.1.13) for moving horizon blocking problem (4.1.4) need to be checked. If stability condition (4.1.13) is not satisfied, then we will apply the solutions to the shifted blocking problem (4.1.6). Figure 4.5 illustrates the cyclic pattern for shifted blocking, which maintains recursive feasibility.

Based on these characteristics, we apply the following blocked NMPC approach:

While $k > 0$

- At time k obtain $x(k), u(k)$, $\psi(x(k), u(k))$ and $V(x(k))$.
- At time $k+1$ obtain $x(k+1)$ and $\|x(k+1) - f(x(k), u(k))\|$.

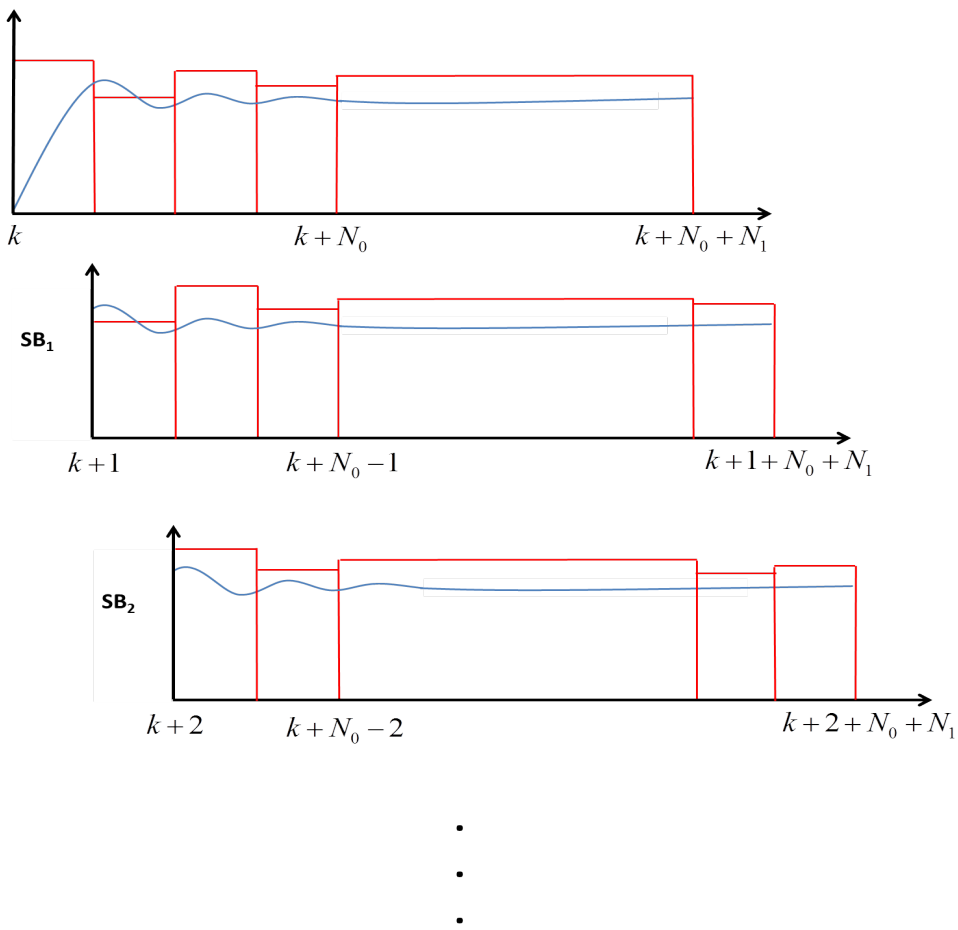

Figure 4.5: Representation of cyclic shifted blocking scheme

- Obtain (an approximate) solution of SB$_n$ problem (4.1.6).
- Solve the MHB problem (4.1.4) and obtain $V(x(k+1))$.
- For $k > k_0$ if (4.1.13) is satisfied, implement $u(k+1)$ from the solution of the MHB problem (4.1.4), set $n = 1$. Else, implement $u(k+1)$ from the solution of SB$_n$ problem (4.1.6), set $n = n+1$.
- Set $k := k+1$.

Note that by checking (4.1.13) at $k > k_0$ where time k_0 is some settling time after a setpoint change or upset, we allow (4.1.13) to be violated a finite number of times, and still satisfy the stability guarantees. Also note that cyclic shifted block-

ing scheme shown in Figure 4.5 cannot guarantee recursive feasibility forever. In the worst case, shifted blocking becomes fully unblocked NMPC.

4.1.5 NMPC Case Study on Nonuniform Grids

In this section, we discuss the NMPC case study using nonuniform grids formulation. In the case study, we consider the NMPC problem for the BFB adsorber discussed in chapter 3. For the BFB adsorber, the controlled variable is the CO_2 removal fraction and the manipulated variable is the inlet flowrate of the solid sorbent. The dynamic optimization problem for NMPC is formulated as NLP (4.1.4), with a traditional setpoint tracking objective. In the case study, we use the reference BFB model in chapter 3 as both control model and plant model. The sampling time for NMPC in the case study is 50 seconds and the prediction horizon is 600 seconds.

Two input and state blocking strategies are considered in the case study. For blocking strategy A, $n_b = 1, N_0 = 4$ and $N_1 = 8$, i.e., we introduce 4 short finite elements whose length equals 50 seconds and one long finite element at the end. For blocking strategy B, $n_b = 2, N_0 = 4, N_1 = 4$ and $N_2 = 4$, i.e., we introduce 4 short finite elements and 2 long finite elements to cover the prediction horizon. The discretized BFB models are implemented in AMPL [31] and the NMPC problem is solved using IPOPT [85]. The computational tests are conducted on an Intel i7-3770 3.40 GHz PC.

In the nominal cases, no additional disturbances or noises are introduced. In the robust cases, we study a comprehensive scenario with measurement noises and setpoint changes as disturbances. Using the proposed algorithm, stability constraints are checked in all simulation cases to guarantee the stability of the controller. The effect on the stability, induced by the blocking strategy and disturbances, is handled by ρ and ϵ_w.

Firstly we look at the nominal cases with no external disturbances. In nominal case 1, blocking strategy A is applied to discretize the BFB model. Figure 4.6 shows the variation of cost function in every NMPC cycle for nominal case 1. As we can see from Figure 4.6, $V(x(k+1))$ is always smaller than $V(x(k))$, which means we can always find ρ so that stability constraint (4.1.9) is satisfied. Since the state blocking is introduced at the end of the prediction horizon, where the states are close to steady state, the errors introduced by state blocking are relatively small. For the case using blocking strategy B, as shown in Figure 4.7, the cost function variations during NMPC iterations are very similar to the cases using blocking strategy A. Moreover, for all of the nominal cases the shifted blocking strategy was not invoked.

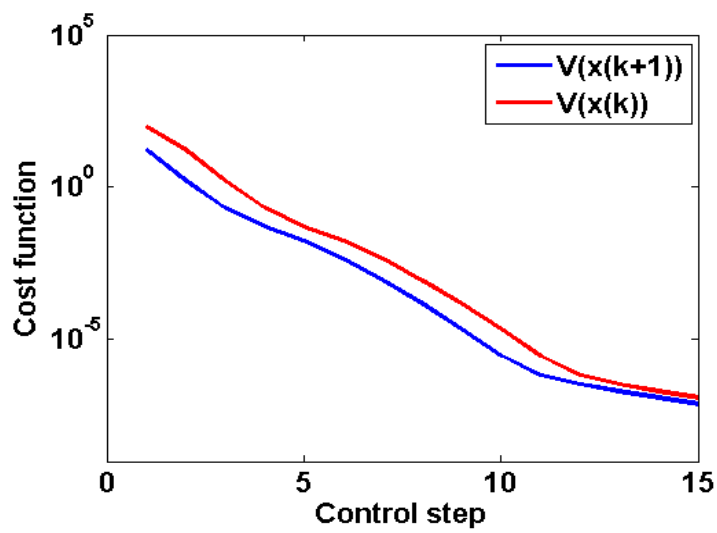

Figure 4.6: Cost function variation in nominal case 1

In addition, we compare the control performance of nonuniform NMPC cases to those with uniform grids. We also present the benefits in computational cost reduction given by the nonuniform grids formulation. Control performance for all nominal cases is shown in Figure 4.8. Uniform grids with a length equal to 50 are applied to discretize BFB model in the nominal base case; this provides the best control performance for this simulation scenario. From Figure 4.8 we see hardly

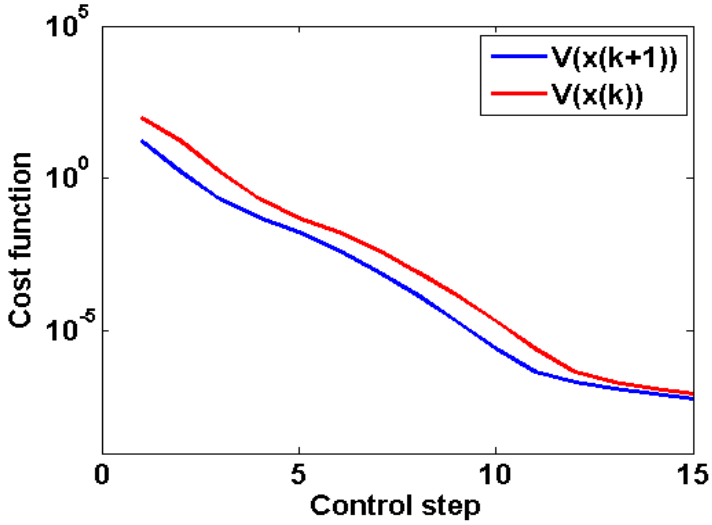

Figure 4.7: Cost function variation in nominal case 2

any differences in control performance among the unblocked nominal base case, and cases 1 and 2, which use different blocking strategies. Note that blocking strategies A and B show negligible differences. From these results, stability constraints are monitored in every iteration and we observe no control performance degeneration or instability with nonuniform grids.

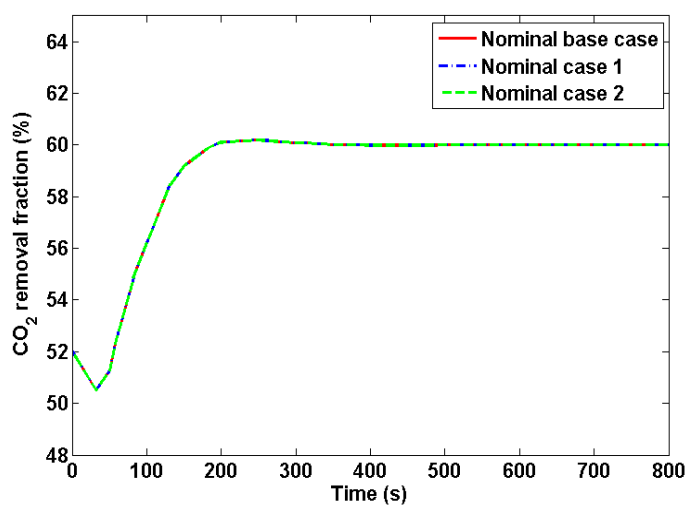

Figure 4.8: Comparison of control performances in nominal cases

Computational results for the nominal cases are listed in Table 5.2. In comparing

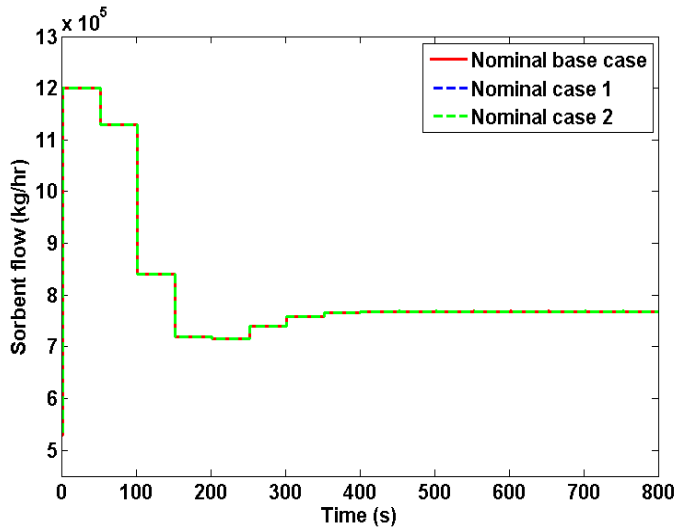

Figure 4.9: Comparison of control moves in nominal cases

Table 4.1: Computational results for nominal cases

	Number of NLP Variables	Average CPU sec	Max. CPU sec
Nominal base case	479704	507.1	1031.7
Nominal case 1	198723	45.0	74.6
Nominal case 2	238860	60.9	100.7

Nominal base case - no blocking
Nominal case 1 - blocking strategy A
Nominal case 2 - blocking strategy B

the unblocked nominal base case, nominal case 1 and 2, we see that the blocking strategy reduces the size of the NMPC problem by at least 50% and average computational cost is reduced by an order of magnitude for NMPC problems.

Next, we consider robust cases, where measurement noise and step change in the setpoint are introduced as additional disturbances. To account for these disturbances, an additional disturbance bound term is introduced and the corresponding stability constraint (4.1.13) is enforced. The disturbance bound term is defined as $\epsilon_w = L_V \|x(k+1) - f(x(k), u(k))\|$. L_V is a measure of sensitivity of cost function with respect to disturbances. In this case, we determine $L_V = 5$ by solving problem (4.1.4) offline after perturbation of input disturbances.

In robust case 1, we discretize the BFB model using blocking strategy A. The cost function variations in every NMPC iteration are shown in Figure 4.10. ϵ_w is intro-

duced to compensate for the effect of disturbances. From Figure 4.10, $V(x(k+1))$ is smaller than $V(x(k)) + \epsilon_w$ in all iterations, which means stability constraint (4.1.13) is always satisfied. In this scenario, in addition to measurement noises, setpoint changes are introduced as disturbances. When a setpoint change occurs, we assume that it is known one sampling time ahead, and thus we can determine the true state at the next sampling time in a feedforward manner. With this formulation, we calculate the error bound and find that the stability constraint (4.1.13) is still satisfied when the setpoint change is introduced. Otherwise, it may be violated when setpoint change is introduced. However, as discussed in the previous section, stability constraint (4.1.13) can be violated for a finite number of times and we can check it after some settling time. As shown in Figure 4.11, variations of value functions for robust case 2 are similar to robust case 1. Moreover, for all of the nominal and robust cases, the shifted blocking strategy was not needed by the blocked NMPC controller.

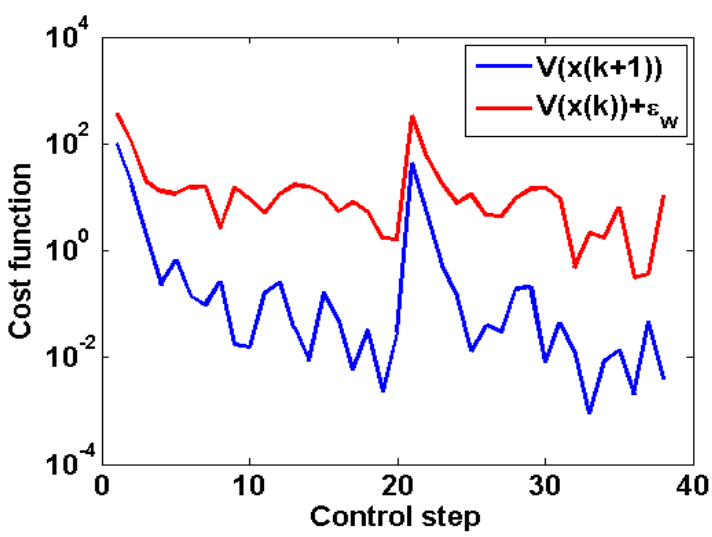

Figure 4.10: Cost function variation in robust case 1

We also compare the control performance of NMPC, using nonuniform grids, with a base case using the BFB model without any blocking. From Figure 4.12 and 4.13, we can see that the control performance of NMPC using nonuniform grids is nearly

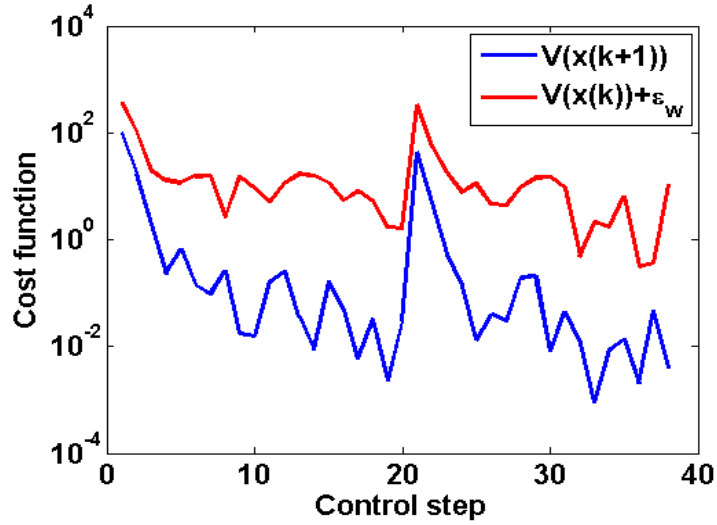

Figure 4.11: Cost function variation in robust case 2

the same as the base case. On the other hand, NMPC problem size and the computational cost is greatly reduced by using the blocking strategy, which is shown in Table 4.2.

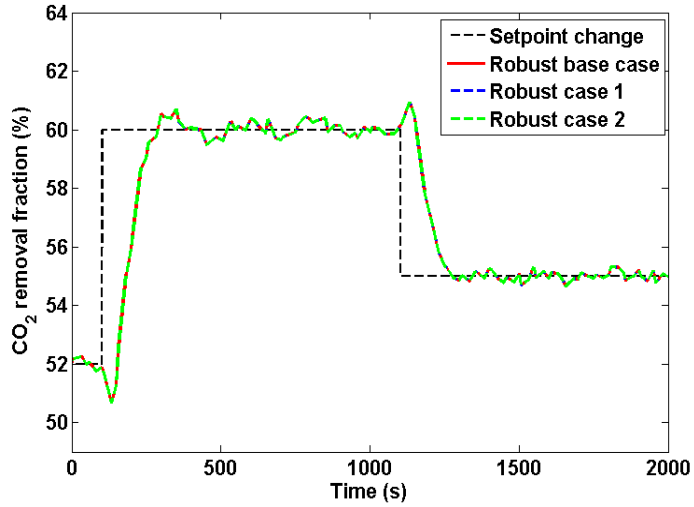

Figure 4.12: Comparison of control performances in robust cases

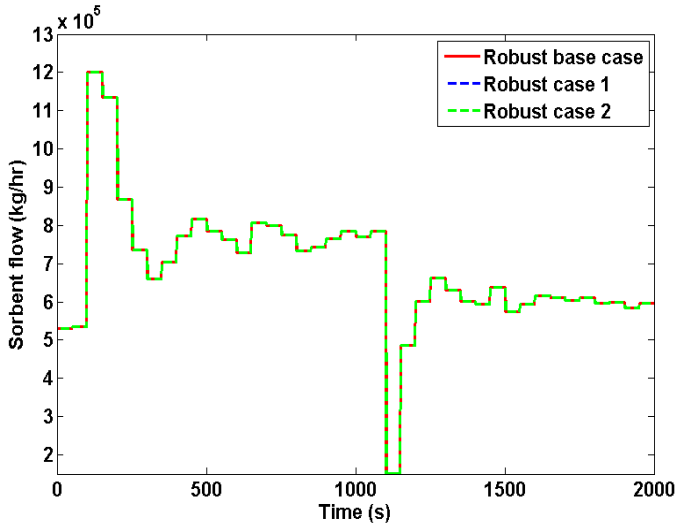

Figure 4.13: Comparison of control moves in robust cases

Table 4.2: Computational results for robust cases

	Number of NLP variables	Average CPU sec	Max. CPU sec
Nominal base case	479704	428.5	1212.6
Nominal case 1	198723	46.1	75.7
Nominal case 2	238860	62.6	94.1

Robust base case - no blocking
Robust case 1 - blocking strategy A
Robust case 2 - blocking strategy B

4.2 NMPC Case Study: Online Control of the BFB Adsorber

In the previous section, we introduced the input and state blocking strategy for NMPC and analyzed stability property of the blocked NMPC. From the case study, we demonstrated that with input and state blocking strategy, the computational cost can be reduced by an order of magnitude while maintaining nearly the same control performance.

In this section, we will present a comprehensive case study for online control of the BFB adsorber. Firstly we will compare the control performance of ideal nonlinear MPC and linear MPC. Then we will integrate model reduction and the blocking strategy to reduce the computational cost of nonlinear MPC. Lastly, a sensitivity based fast NMPC algorithm is applied to reduce the online computational cost of

NMPC.

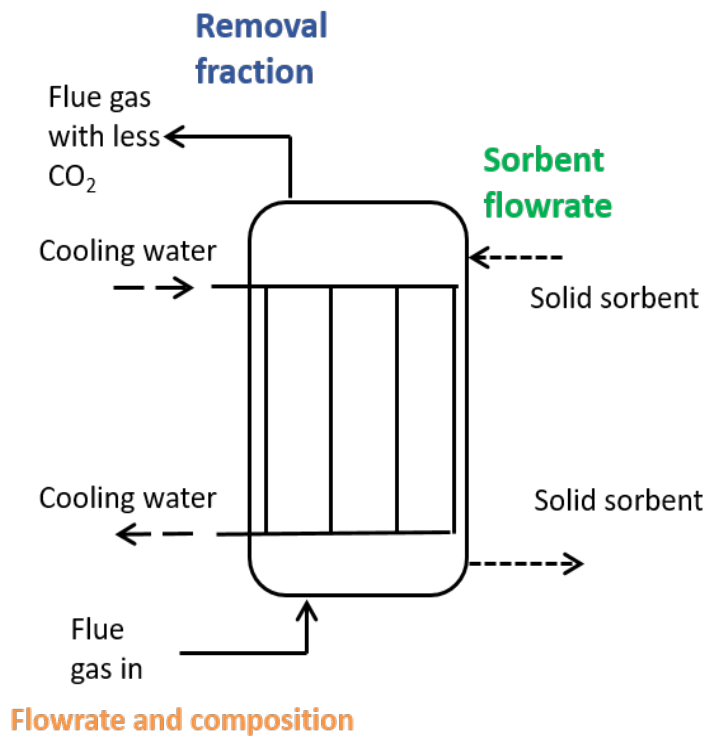

Figure 4.14: BFB adsorber

Figure 4.14 shows a sketch of the BFB adsorber. For this reactor, the controlled variable is the removal fraction of CO_2 from the fluegas and manipulated variable is the flowrate of the solid sorbent. In the case study, the BFB adsorber reactor is subject to disturbances of flue gas flowrate and composition. These disturbances could occur due to operational load changes in the power plant or variations in fuel quality. Thus one major goal of the NMPC controller is to maintain the setpoint for CO_2 removal fraction and reject these disturbances by manipulating the flowrate of solid sorbent. In addition, setpoint of CO_2 removal fraction usually comes from the upper RTO layer, which could get updated frequently due to economic or environmental concerns. For example, as electricity prices change, the operation of BFB adsorber may be switching between different operational modes with different capture rates to satisfy CO_2 removal requirement over a specified period of

time. This requires the controller to exhibit good performance for setpoint tracking, in addition to disturbance rejection. Therefore, in the following NMPC case study, we study the control performance in both setpoint tracking and disturbance rejection.

4.2.1 Comparison of Ideal Nonlinear MPC and Linear MPC

In the control case study, we introduce several disturbances in the fluegas flowrate and composition, which are shown in Figure 4.15. In addition, we introduce a setpoint change for CO_2 removal fraction from 52% to 60% at 2500 seconds and compare the setpoint tracking performance of different controllers. For MPC controller setting, the prediction horizon is 400 seconds and the sampling time is 50 seconds. In the following case study, the simulation time is 4500 seconds. The discretized BFB models are implemented in AMPL [31] and the NMPC problem is solved using IPOPT [85]. The computational tests are conducted on an Intel i7-930 2.80 GHz PC.

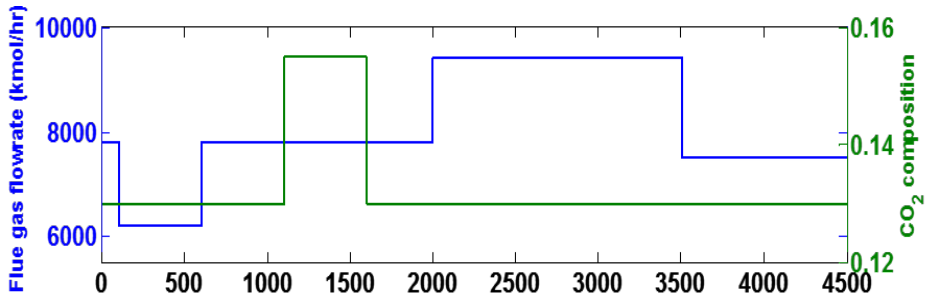

Figure 4.15: Disturbances introduced in the case study

Firstly, we compare the performance of ideal nonlinear MPC and linear MPC. For ideal NMPC, we assume that we will get the optimal control moves once the states are obtained. With this assumption, potential computational delay by solving dynamic optimization problem is neglected. It should be noted that ideal NMPC gives better performance than real implementation of NMPC with significant computational cost that cannot be ignored. For linear MPC, linear models are obtained

through system identification are used as the control model. Detailed implementation can be found in [66]. For ideal nonlinear MPC, we use the rigorous BFB model as the control model. The control performance is shown in the following figures.

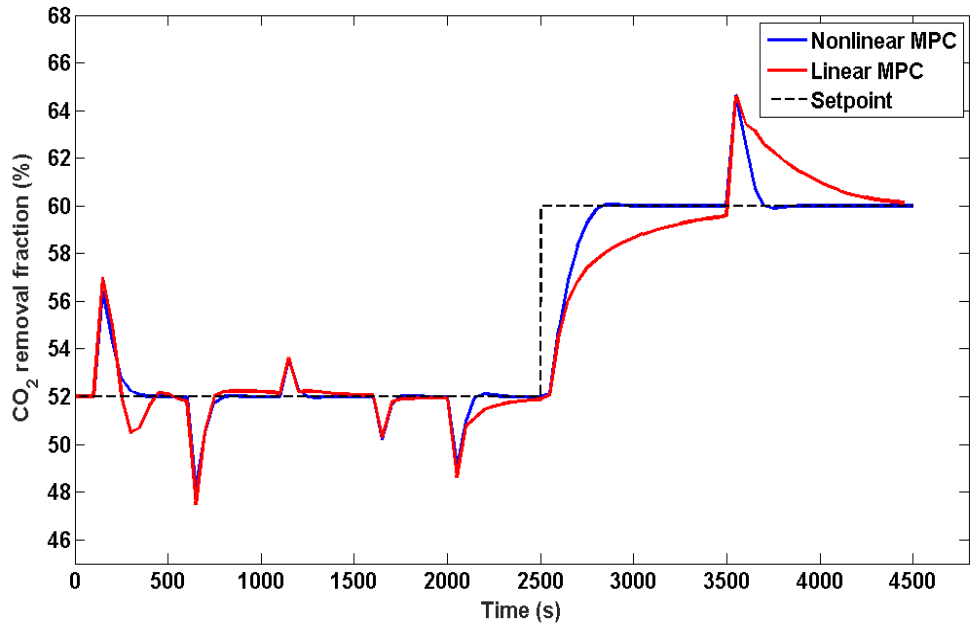

Figure 4.16: Closed-loop performance of BFB adsorber

As shown in Figure 4.16, from $t = 0$ to $t = 2500$, we can see that nonlinear MPC has better performance in disturbance rejection with fewer oscillations than linear MPC. At $t = 2500$, a setpoint change in CO_2 removal fraction is introduced. From Figure 4.16, we can see that nonlinear MPC drives the process to track the setpoint much faster than linear MPC. We can also see that NMPC shows much better performance in rejecting the disturbance introduced at $t = 3500$. This is mainly due to the fact that rigorous nonlinear model gives more accurate predictions than identified linear models, in a larger operational range. The performance of each control configuration is compared using the control performance metric mean integral square error (MISE), with the following definition:

$$MISE = \frac{1}{N}\sum_{k=1}^{N-1}\left(\frac{(r_k - y_k)^T(r_k - y_k)}{2} + \frac{(r_k - y_{k+1})^T(r_k - y_{k+1})}{2}\right) \tag{4.2.1}$$

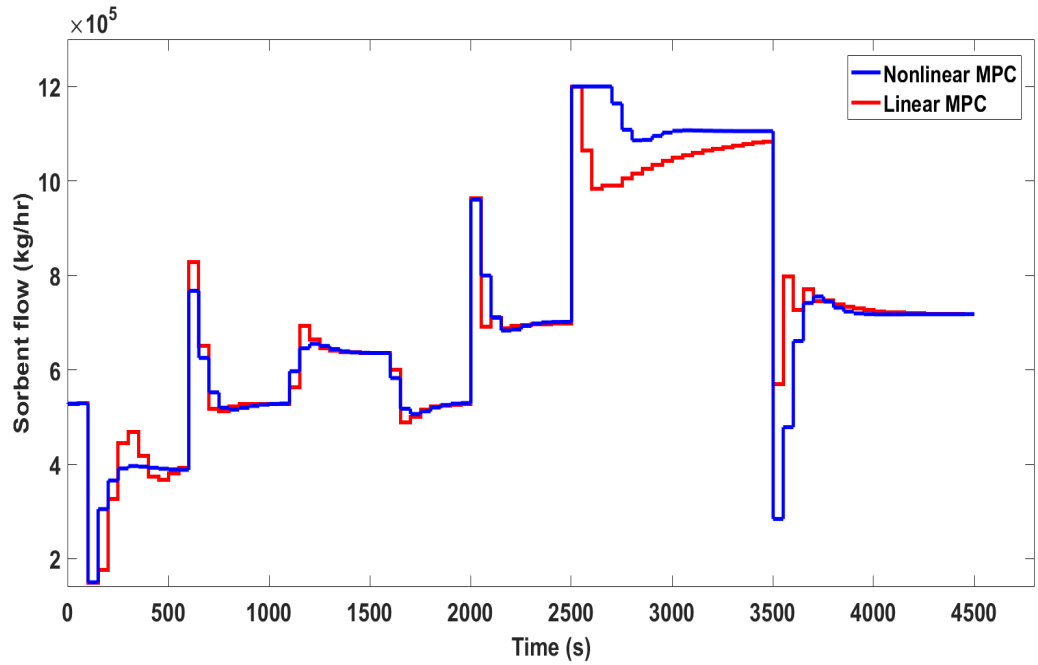

Figure 4.17: Control profiles of nonlinear MPC and linear MPC

where r_k are the reference values and y_k are the process outputs.

In this case study, the MISE for linear MPC is 3.68; while for nonlinear MPC, the MISE is 2.49. Therefore, ideal nonlinear MPC demonstrates a better control performance than linear MPC. As for computational cost , linear MPC takes less than 1 second to solve; however, the computational time for nonlinear MPC is much larger. And we will discuss this issue in the following sections.

4.2.2 NMPC Using Reduced Model and Blocking Strategy

In this section, we compare the control performance and computational results of the following 3 controllers:

- Controller 1: NMPC using rigorous BFB model, no state and input blocking
- Controller 2: NMPC using rigorous BFB model, with state and input blocking
- Controller 3: NMPC using reduced BFB model, with state and input blocking

For controller 1, we use rigorous BFB model as control model and apply uniform temporal grids. For controller 2, rigorous BFB model is also used as the control model. In addition, we introduce state and input blocking formulation proposed in previous section, with 3 small finite elements with length equal to 50 and 1 large finite element with length equal to 250. For controller 3, we integrate the reduced BFB model developed in the previous chapter as the control model. However, this formulation leads to the model mismatch between the control model and process model, which is simulated using the rigorous BFB model. To account for the model mismatch, we introduce a simple output additive correction term for the reduced model using the feedback measurements from the rigorous model. With this formulation, it can handle the model mismatch and achieve an offset-free control performance [40]. The same blocking strategy as controller 2 is also applied for controller 3.

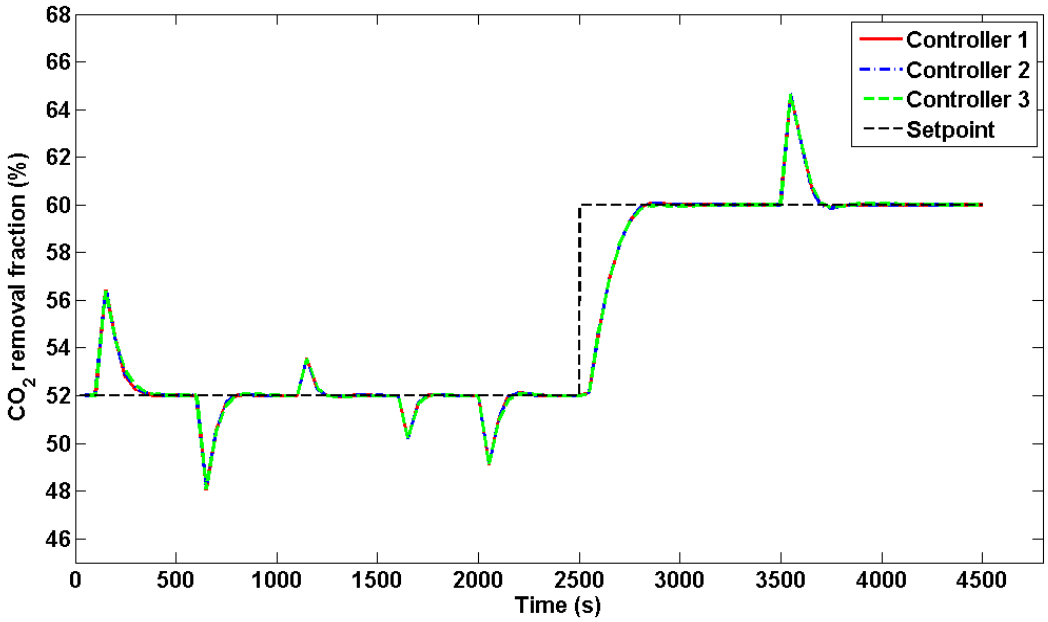

Figure 4.18: Closed-loop performance of BFB adsorber

The closed loop performance of these controllers are shown in the following figures and the computational results including computational time and MISE are listed in

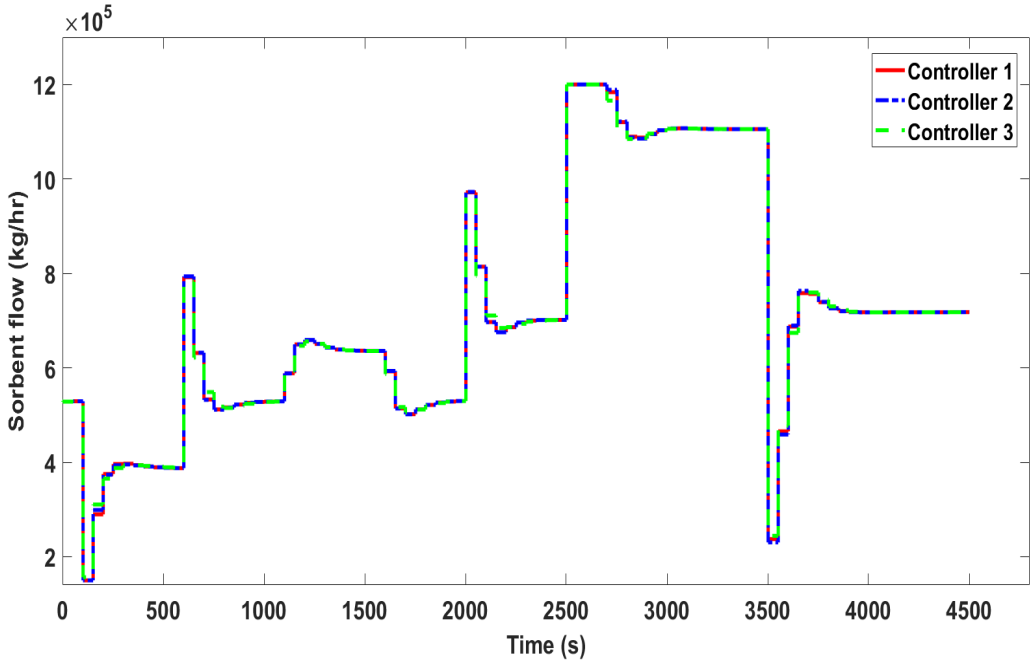

Figure 4.19: Control profiles of different NMPC formulation

Table 4.3. Firstly we compare the control performance. From Figure 4.18 and 4.19, we can see that control moves and closed loop performances of controllers 2 and 3 are nearly the same as controller 1. By comparing the MISE for controllers 1-3 shown in Table 4.3, we can find that the blocking strategy and reduced model introduce almost no compromise in the control performance. The reason is that the dynamics of the rigorous model are well captured by the reduced model, as we demonstrated in the previous chapter. The other reason is that we use the feedback from the process measurements to account for the model mismatch properly and achieve an offset-free performance.

As for computational time, controller 1 takes more than 4 CPU minutes to solve a single NMPC problem and the maximum time is about 15 CPU minutes. In this case, if we directly implement controller 1 online, it may lead to computational delay as long as 15 minutes while the sampling time is only 50 seconds. Such computational delay could greatly degenerate the control performance.

Table 4.3: Computational results for Controller 1-3

	Number of NLP Variables	Average CPU sec	Max. CPU sec	MISE
Controller 1	319136	260.67	906.34	2.487
Controller 2	166745	56.74	256.09	2.489
Controller 3	64229	23.86	39.36	2.501

Controller 1 - rigorous model, no blocking
Controller 2 - rigorous model, input and state blocking
Controller 3 - reduced model, input and state blocking

After we apply the blocking strategy and integrate reduced model into NMPC, we observe a significant reduction in the size of optimization problem compared with controller 1. That leads to a similar percentage of reduction in the average solution time of the optimization problem. We can observe even more significant reduction for maximum solution time. By comparing these 3 cases, both strategies can significantly reduce the size of the optimization problem and they lead to an order of magnitude reduction for NMPC solution time. Also it should be noted that, with the combined strategy, the computational time for every optimization problem is less than one sampling time, which is 50 seconds. With that, we will apply advanced step NMPC to enable online control of the reactor in the following section.

4.2.3 Online Control Using Advanced Step NMPC

Advanced step NMPC (asNMPC) is a fast online NMPC algorithm proposed in [95]. As discussed in chapter 2.4, the essential idea of asNMPC is to solve the NMPC problem one sampling time ahead using the predicted state as initial conditions. At the next sampling time when true states are obtained, an online update is conducted to approximate the optimal control move based on NLP sensitivity. As we showed in the previous section, after introducing blocking strategy and reduced model, the NMPC solution time is under a sampling time. Therefore we can move the calculation of NMPC in background within a sampling interval and online computational cost can be reduced through asNMPC.

In the following case study, we apply the advanced step NMPC algorithm to control the BFB adsorber, which we denote as controller 4. Controller 4 has the same configuration as controller 3, except that an NLP sensitivity based online update is performed. In this case study, we only consider parametric uncertainties brought by the disturbances shown in Figure 4.15. sIPOPT [67] is used to provide NLP sensitivity to approximate the optimal control moves when disturbances occur.

The following figures compare the simulation results of controllers 3 and 4.

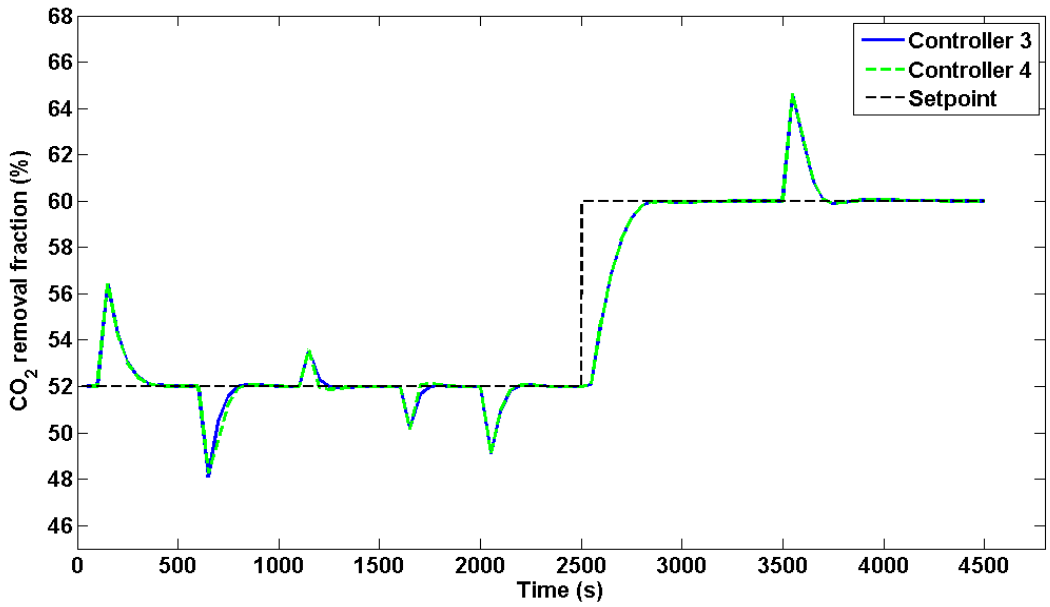

Figure 4.20: Closed-loop performance of BFB adsorber

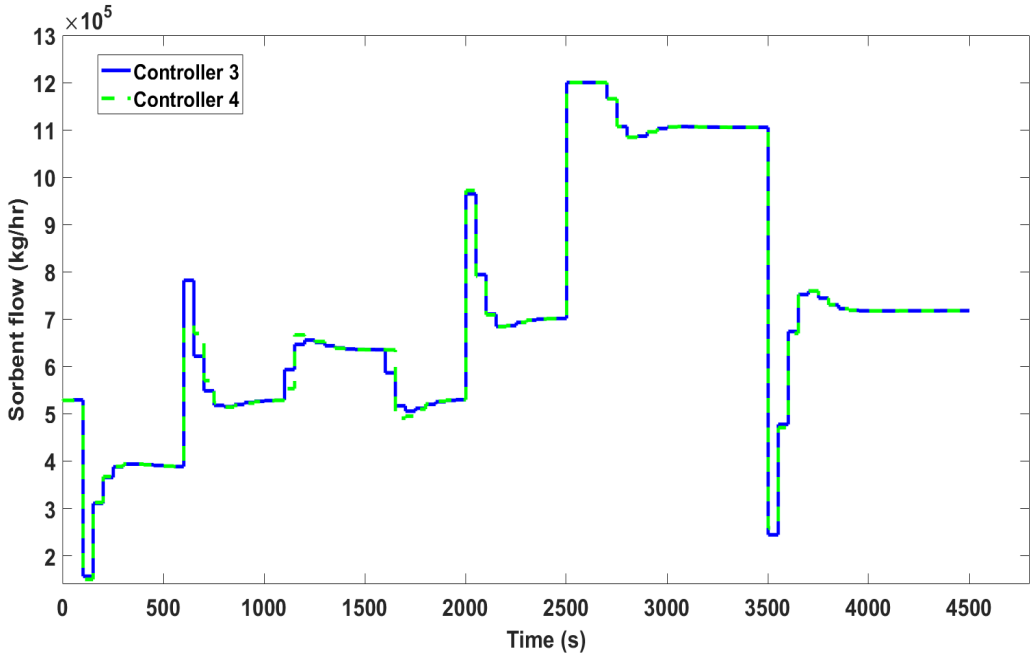

Figure 4.21: Control profiles of different NMPC formulation

From Figure 4.21, we observe that slightly different control moves occur after the disturbances are introduced, due to the approximation error given by the sensitivity update. But as shown in Figure 4.20, the closed-loop performance of asNMPC is very similar to the ideal NMPC case. The MISE for controller 4 is 2.529, which is just slightly larger than the controller 3 (2.501).

As for the computational result, the average online cost for sensitivity update is 1.04 second, which is much smaller than the solution time of NMPC problems. This online cost is comparable to linear MPC and the computational delay by controller 4 can be neglected in this case.

In this section, we demonstrate that by integrating reduced model and blocking strategy, significant reduction in computational time of NMPC can be achieved. Advanced step NMPC has been applied to reduce the online computational cost for NMPC. For online control purposes, advanced multiple step NMPC may be needed to handle the case where NMPC solution time is larger than a sampling

time. In addition, it should be noted that no measurement noises are considered in the case study. When measurement noises are introduced, there may be changes in active sets in the NMPC problem. In these cases, instead of directly implementing the control update by NLP sensitivity, a different strategy proposed in [44] may be needed to account for the active set changes to give more accurate updates.

4.3 Concluding Remarks

In this chapter, we demonstrate the application of nonuniform temporal discretization in dynamic, collocation-based models for NMPC formulations. With appropriate input and state blocking strategies, computational cost for NMPC problems can be greatly reduced without significant sacrifice of control performance. To address the stability concerns raised by general input and state blocking strategies, we analyze nominal and ISS stability for blocked NMPC and show that these properties can be enforced through treatment of model mismatch, quasi-infinite horizons and additional stability constraints. Our analysis leads to an efficient NMPC strategy that guarantees ISS stability for any blocking pattern, if recourse to the shifted blocking strategy is allowed.

In the NMPC case study, the proposed blocked NMPC strategy is applied to control a large-scale BFB adsorber simulated by first-principles models. By using reduced model with input and state blocking strategy, we observe significant reductions in computing effort for NMPC with almost no compromise in control performance. Finally, a sensitivity based fast NMPC algorithm is also applied to reduce the online computational cost of NMPC.

Chapter 5

Economic NMPC

In the previous chapter, we study the setpoint tracking NMPC problem of the BFB adsorber to improve the control performance in tracking setpoints, rejecting disturbances while enhancing computational efficiency for NMPC. In this chapter, we will study economic NMPC which directly optimizes the economics of the process operations subject to the process models and constraints.

5.1 Introduction

For the process industries, improving economic performance is a major goal in process operations. As discussed in chapter 1, in addition to the traditional RTO-APC two-layer structure, economic (nonlinear) model predictive control has been studied recently and it seems to be a promising solution to address the challenges for the two-layered structure, i.e. inconsistencies between the operation time scales and models used for different layers. Compared with setpoint tracking NMPC which minimizes the deviations of process states and outputs to setpoints, economic NMPC directly optimizes an economic function which represents the profit or cost information for process operation. With this formulation, optimization-

based controllers can explicitly optimize the economic performance of transient process operations and handle the constraints on states and inputs easily.

Though stability properties are well established for setpoint tracking NMPC, additional work is required to extend these results for economic NMPC. Since the economic stage cost could have an arbitrary form, it may violate some key assumptions used for Lyapunov stability analysis established for setpoint tracking NMPC. In recent years, considerable research work has been carried out in this area. For linear systems with convex stage costs, the stability proof for economic MPC can be found in [73]. In [6], it has been shown that economic MPC can achieve at least the same asymptotic average cost as the cost at optimal steady state. Stability results have been extended to nonlinear systems in [6, 26], based on properties such as dissipativity and strong duality. For a specific type of nonlinear system with periodic cycles, theoretical analysis and computational studies can be found in [39, 41]. For more general nonlinear systems, as shown in [44], regularization terms can be added to guarantee such properties and thus stability results can be maintained. In addition, an additional stabilizing constraint is introduced in [94] to stabilize economic NMPC for non-dissipative systems. Also design of economic NMPC with Lyapunov-based constraint is presented in [37]. Most stability analysis results for economic NMPC consider terminal constraints or terminal costs; although a study on stability and performance of economic NMPC without terminal constraints is given in [34]. More detailed reviews on economic NMPC can be found in [27, 72].

With increasing needs to improve process operation, rigorous first-principles models have been developed and corresponding model-based controllers can be designed. To handle these nonlinear first-principles models, fast (economic) model predictive control algorithms are proposed and applied for various complex systems. In addition to the computational burden, for complex systems with a large number of states, there are also challenges for analysis and design of stable economic NMPC controllers. For economic NMPC, standard regularization strategies

require analysis of the full system state space, and regularization terms are usually required for most system states. When dealing with large-scale detailed process models with significant number of states, the standard analysis becomes very tedious and may also lead to conservative economic performance. In this chapter, we aim to extend stability results for economic NMPC with a focus on only a subset of system states and propose a systematic approach to determine sufficient regularization weights for economic NMPC.

In the following sections, we will discuss the stability properties and full state regularization of economic NMPC. Then we will analyze the stability property for economic NMPC with reduced sets of regularization. A systematic approach to calculate the sufficient regularization weights for economic NMPC will be discussed later. Lastly, we apply the proposed strategy to economic NMPC of a nonlinear CSTR and a large-scale CO_2 capture system to demonstrate its performance through comprehensive case studies.

5.2 Stability Properties of Economic NMPC

We consider the following steady state optimization problem for economic NMPC with x_s and u_s as optimal steady state solutions.

$$\begin{aligned} &\min_{x,u} \psi^{ec}(x,u) \\ &\text{s.t.} \quad x = f(x,u) \\ &u \in \mathbb{U}, x \in \mathbb{X}. \end{aligned} \tag{5.2.1}$$

The dynamic optimization problem for economic NMPC is defined as follows:

$$V(x(k)) := \min_{v_l, z_l} \sum_{l=0}^{N-1} \psi^{ec}(z_l, v_l) \tag{5.2.2}$$

$$\text{s.t.} \quad z_{l+1} = f(z_l, v_l), l = 0, \ldots N-1$$

$$z_0 = x(k), z_N = x_s$$

$$v_l \in \mathbb{U}, z_l \in \mathbb{X}.$$

Here we assume that the states and controls are restricted to the domains $\mathbb{X}$ and $\mathbb{U}$, respectively. The set $\mathbb{U}$ is compact and contains the origin; the set $\mathbb{X}$ is closed and contains the origin in its interior. We consider a stage cost given by $\psi^{ec}(\cdot,\cdot) : \Re^{n_x+n_u} \rightarrow \Re.$, which is assumed to be Lipschitz continuous. For simplicity, here we use the NMPC formulation with terminal equality constraints. Compared with tracking NMPC, the major difference of economic NMPC is that the economic stage cost $\psi^{ec}(\cdot,\cdot)$ can have arbitrary forms which represent process economics.

Regarding the stability analysis for economic NMPC, we follow the Lyapunov stability framework and we can derive a similar inequality as shown in equation (2.2.5) with the same assumptions for setpoint tracking NMPC:

$$V(x(k+1)) - V(x(k)) \leq -(\psi^{ec}(x(k), u(k)) - \psi^{ec}(x_s, u_s)) \tag{5.2.3}$$

For setpoint tracking NMPC, the stage cost $\psi^{tr}(x, u)$ is usually in a quadratic form, which satisfies Assumption 2.2.2. With this inequality, the tracking objective is decreasing monotonically and thus it can be shown to be a Lyapunov function. For economic NMPC, however, the economic stage cost $\psi^{ec}(x, u)$ can have any arbitrary form which represents the economic information for process operation. For an arbitrary economic objective, the right hand side of inequality (5.2.3) may not be always negative since the optimal solution (x_s, u_s) may not be the global minimum of $\psi^{ec}(x, u)$ for all x and u. In addition, Assumption 2.2.2 is not fulfilled for

a general $\psi^{ec}(x,u)$. Thus the value function of economic NMPC may not be directly used as a Lyapunov function to demonstrate the stability of the closed-loop systems using economic NMPC.

To guarantee the stability for economic NMPC, additional properties are needed. Firstly, as shown in [6], dissipativity can be used to establish the stability for economic NMPC, which is defined as follows:

Definition 5.2.1. *[6] A control system $x^+ = f(x,u)$ is dissipative with respect to a supply rate $s : \mathbb{X} \times \mathbb{U} \to \mathbb{R}$ if there exists a function $\lambda : \mathbb{X} \to \mathbb{R}$, such that*

$$\lambda(f(x,u)) - \lambda(x) \leq s(x,u) \tag{5.2.4}$$

for all feasible control-input pairs. If in addition $\rho : \mathbb{X} \to \mathbb{R}_{\geq 0}$ positive definite ($\rho(x_s) = 0$ and $\rho(x) > 0$ for all $x \neq x_s$) exists such that

$$\lambda(f(x,u)) - \lambda(x) \leq -\rho(x) + s(x,u) \tag{5.2.5}$$

then the system is said to be strictly dissipative.

From Theorem 2 in [6], if the closed-loop system by economic NMPC (5.2.2) is strictly dissipative with respect to the supply rate:

$$s(x,u) = \psi^{ec}(x,u) - \psi^{ec}(x_s,u_s) \tag{5.2.6}$$

Then x_s is an asymptotically stable equilibrium point of the closed-loop system. Therefore, with the dissipativity of the stage cost and dynamic model, the economic NMPC is asymptotically stable.

By choosing $\lambda(x) = \bar{\lambda}^T x$ for some $\bar{\lambda} \in \mathbb{R}^n$, the dissipativity assumption is equivalent to the following:

$$min \quad \psi^{ec}(x,u) + \bar{\lambda}^T(x - f(x,u)) \geq \psi^{ec}(x_s,u_s) \tag{5.2.7}$$

As pointed out in [6], the dissipativity assumption can be fulfilled if the economic stage cost and dynamic model form a strongly dual problem. More importantly, this leads to the idea of rotated stage cost [6, 26] defined as follows:

$$\phi(x,u) = \psi^{ec}(x,u) + \lambda^T(x - f(x,u)) \tag{5.2.8}$$

where λ are the multipliers form the equality constraints in the steady state optimization problem (5.2.1). Moreover, it has been shown in [41, 44] that if the rotated stage cost $\phi(x,u)$ is strongly convex, then strong duality property together with the stability of the corresponding economic NMPC can be guaranteed. These results provide sufficient conditions to establish stability for economic NMPC. Note that these conditions can be satisfied by adding quadratic regularization terms to the economic stage cost, which will be discussed in the following section.

5.2.1 Regularization of Non-convex Economic Stage Costs

For a general economic stage cost $\psi^{ec}(x,u)$ and process dynamic model $f(x,u)$, properties like dissipativity, strong duality or strong convexity are not fulfilled in general. To guarantee such properties, an easy remedy is to add quadratic regularization terms to the original economic stage cost.

After introducing the regularization terms, the modified steady state problem and the corresponding regularized rotated stage cost is defined as follows:

$$\begin{aligned} \min_{x,u} \psi^{ec}(x,u) + \frac{1}{2}\|(x,u) - (x_s,u_s)\|_Q^2 \\ \text{s.t.} \quad x = f(x,u) \\ u \in \mathbb{U}, x \in \mathbb{X}. \end{aligned} \tag{5.2.9}$$

$$\phi_{reg}(x,u) = \psi^{ec}(x,u) + \lambda^T(x - f(x,u)) + \frac{1}{2}\|(x,u) - (x_s,u_s)\|_Q^2 \tag{5.2.10}$$

where (x_s, u_s) are the optimal solutions to the original optimization problem (5.2.1). Q is a diagonal regularization weighting matrix.

As shown in [26, 44] , there are two major steps to show the stability of the economic NMPC controller after adding quadratic regularization terms. Firstly we consider a pseudo controller using the rotated stage cost $\phi(x,u)$ as objective function. With a sufficiently large regularization matrix Q, the regularized rotated stage cost $\phi_{reg}(x,u)$ can be strongly convex. Then, as shown in [44], a local optimal solution from problem (5.2.9) is a global minimum for the regularized rotated stage cost. With this result, the value function of this pseudo controller is monotonically decreasing based on inequality (5.2.3). Also it can be proved that regularized rotated stage cost satisfies Assumption 2.2.2. Therefore the pseudo economic NMPC controller using the rotated stage cost as objective is asymptotically stable. The next step is to extend the stability result to economic NMPC controller by showing that it has the same solution as the pseudo controller. Then the stability of economic NMPC can be guaranteed after adding sufficiently large regularization.

In addition to stabilizing the controller, these quadratic regularization terms provide guidance for economic NMPC to drive the process to optimal steady state, which is desired in most practical applications.

Though adding regularization terms is easy, finding appropriate regularization weights which guarantee the stability of economic NMPC could be a challenging task. In [44], a systematic approach to find the sufficient regularization weights has been proposed. The key idea is to apply the Gershgorin theorem to find "minimal" regularization matrix Q, which makes the regularized rotated stage cost $\phi_{reg}(x,u)$ strongly convex.

The proposed condition for Gershgorin weights is shown as follows:

$$q_i > \sum_{i \neq j} |a_{i,j}| - a_{i,j} \tag{5.2.11}$$

where q_i are the diagonal elements of the regularization weighting matrix Q and $a_{i,j}$ are the elements of matrix A, the Hessian matrix of the rotated stage cost $\phi(x, u)$ in (5.2.8), which is defined as follows.

$$A = \nabla^2 \phi(x, u) \tag{5.2.12}$$

With condition (5.2.11) satisfied, the Hessian of the regularized rotated stage cost $\phi_{reg}(x, u)$ is positive definite and thus it's strongly convex. Based on this simple criterion, we can determine the "minimal" regularization weights that guarantees stability of economic NMPC.

On the other hand, it should be noted that this condition (5.2.11) must be satisfied for all $u \in \mathbb{U}, x \in \mathbb{X}$. In other words, we need to check this criterion over the entire space of (x, u) so that the regularized rotated stage cost is guaranteed to be strongly convex. In practice, we can sample a sufficient number of possible combinations of states and controls in order to check this criterion. In [89], the author divides the feasible regions of every variable, including differential states, algebraic variables and controls, into N grid points and calculates the Hessian matrix of the rotated stage cost at each grid point. Though all calculations are done offline, it could be cumbersome especially for large-scale systems with a significant number of variables. The number of calculations needed to determine sufficient regularization weights could be exponentially increasing with increased dimension of system variables. Moreover, based on this criterion, regularization may be required for most system variables including dynamic states, algebraic variables and controls, which could lead to very conservative economic performance.

To overcome this issue, we propose the economic NMPC formulation with reduced sets of regularization. The key idea is that we only focus on a set of critical states, which are a subset of full system states, for stability analysis and regularization. Then we further introduce strategies to determine regularization weights for these critical states. If this is possible, we can achieve much easier control implementation and less conservative performance. In the next section, we will discuss the proposed regularization strategy for economic NMPC of differential and algebraic equation (DAE) systems. Firstly we will demonstrate that the algebraic variables can be removed for regularization analysis and economic NMPC can maintain asymptotic stability. Then we will study the stability property of economic NMPC with regularization of subsets of system states. A comprehensive case study will be presented to demonstrate the proposed regularization strategy.

5.3 Regularization Strategy for Economic NMPC of DAE systems

As we mentioned before, first-principles process models have been developed for complex processes, which are usually modeled as differential and algebraic equations. In addition to simulation and offline optimization, these first-principles models can also be used in NMPC framework to improve the control and economic performance for process operations.

Next we want to improve the regularization strategy for economic NMPC of DAE systems firstly by removing the algebraic variables.

The steady state optimization problem for economic NMPC of a DAE system is

defined as follows:

$$\begin{aligned} &\min_{x,y,u} \psi^{ec}(x,y,u) \\ \text{s.t.} \quad & x = f(x,y,u) \\ & y = g(x,y,u) \\ & u \in \mathbb{U}, x \in \mathbb{X}, y \in \mathbb{Y}. \end{aligned} \tag{5.3.1}$$

where x and y are the differential and algebraic variables existed in the first-principles process models; f and g are the corresponding differential and algebraic equations.

By introducing extended variables for control $\tilde{v}_{l+1} = v_l$, we can write the dynamic optimization problem for economic NMPC controller of a DAE system as follows:

$$\begin{aligned} V(x(k)) = &\min_{v_l, y_l, z_l} \sum_{l=0}^{N-1} \psi^{ec}(z_l, y_l, v_l) \\ \text{s.t.} \quad & z_{l+1} = f(z_l, y_l, v_l), l = 0, \ldots N-1 \\ & y_l = g(z_l, y_l, \tilde{v}_l), l = 1, \ldots, N \\ & y_0 = g(z_0, y_0, u(k-1)) \\ & z_0 = x(k), z_N = x_s \\ & v_l, \tilde{v}_l \in \mathbb{U}, z_l \in \mathbb{X}, y_l \in \mathbb{Y}. \end{aligned} \tag{5.3.2}$$

We can define the following rotated stage cost:

$$\phi(x,y,u) = \psi^{ec}(x,y,u) + \lambda_f^T(x - f(x,y,u)) + \lambda_g^T(y - g(x,y,u)) \tag{5.3.3}$$

After adding regularization terms, we obtain the following regularized rotated

stage cost:

$$\begin{aligned}\phi_{reg}(x,y,u) = \psi^{ec}(x,y,u) + \lambda_f^T(x - f(x,y,u)) + \lambda_g^T(y - g(x,y,u)) \\ + \frac{1}{2}\|(x,y,u) - (x_s,y_s,u_s)\|_Q^2\end{aligned} \tag{5.3.4}$$

Then the previous results can be easily extended to the above rotated stage cost. By adding additional regularization terms, if the regularized rotated stage cost (5.3.4) is strongly convex, then a local optimal solution to problem (5.3.1) using the regularized rotated stage cost (5.3.4) as objective function is the global minimum for (5.3.4) [44]. Therefore we can establish the stability for NMPC (5.3.2) using the regularized rotated stage cost (5.3.4) as the objective. Then it's straightforward to show that the NMPC problem (5.3.2) using the regularized rotated stage cost (5.3.4) as objective has the same solution as the NMPC problem (5.3.2) using the original economic stage cost and same regularization. Thus the stability for the regularized economic NMPC of DAE systems can be established.

However, if we directly apply this result, then the Hessian matrix of the regularized rotated state cost should be positive definite for all feasible (x, y, u). In many applications, there could be many more algebraic variables than differential variables. So this could significantly increase the work to find the sufficient regularization weights and make control performance very conservative.

To cope with this issue, we propose a strategy to determine regularization weights only for these differential variables and controls, which could be easily applied to designing stable economic NMPC controllers for processes modeled by general DAE systems.

5.3.1 Reduction of Algebraic Variables

Assumption 5.3.1. *The semi-explicit DAE system in economic NMPC problem* (5.3.2) *is*

index-1.

With this assumption, the algebraic variables can be determined by differential variables via solving the square algebraic equations systems. High-index DAE systems can be transformed into index-1 system through index reduction strategies. Under Assumption 5.3.1, we can find the following function $g_y(.,.)$ to determine algebraic variables y in terms of states x and controls u:

$$y = g_y(x, u) \tag{5.3.5}$$

Substituting $y = g_y(x, u)$ into the original optimization problem (5.3.1), which leads to the following reformulated steady state optimization problem:

$$\begin{aligned} \min_{x,u} \; & \psi^{ec}(x, g_y(x, u), u) \\ \text{s.t.} \quad & x = f(x, g_y(x, u), u) \\ & u \in \mathbb{U}, x \in \mathbb{X}. \end{aligned} \tag{5.3.6}$$

Here we introduce a robust formulation similar to [91] to remove constraints on y by ℓ_1 penalty terms in the objective function. With a sufficiently large penalty weight, at optimal solutions, these penalty terms will be zero and the original constraints on y will be satisfied. With this reformulation, algebraic variables and equations are removed from the reformulated optimization problem.

The corresponding dynamic optimization problem for NMPC can be defined as

follows:

$$
\begin{aligned}
V(x(k)) = \min_{v_l, z_l} \sum_{l=0}^{N-1} \psi^{ec}(z_l, g_y(z_l, \tilde{v}_l), v_l) \qquad (5.3.7)\\
\text{s.t.} \quad z_{l+1} = f(z_l, g_y(z_l, \tilde{v}_l), v_l), l = 0, \ldots N-1\\
z_0 = x(k), z_N = x_s\\
v_l, \tilde{v}_l \in \mathbb{U}, z_l \in \mathbb{X}.
\end{aligned}
$$

Theorem 5.3.1. *Under Assumption 5.3.1, economic NMPC controller described by (5.3.7) can be made asymptotically stable, by adding a sufficiently large regularization on dynamic states z and controls v.*

Proof: After removing algebraic variables, economic NMPC controller described by (5.3.7) is equivalent to the economic NMPC (5.2.2). Then we can directly use the proof in [44] to establish the stability property. □

After removing the algebraic variables, we can guarantee the stability of economic NMPC controller by only regularizing states x and controls u. While there may not exist an explicit form for function $g_y(\cdot, \cdot)$, but we can at least determine this steady state relationship implicitly based on the implicit function theorem. A systematic approach to determine the sufficient weights for x and u based on the original DAE model will be discussed in the following sections.

5.3.2 Economic NMPC with Regularization of Reduced States

In previous section, we showed that algebraic variables can be removed from the regularization analysis. Based on that, we redefine the steady state optimization (5.3.6) into the following problem S1 where all algebraic variables and equations

are removed:

$$
\begin{aligned}
S1: \quad & \min_{\bar{x},\hat{x},u} \psi^{ec}(x,u) \\
\text{s.t.} \quad & \bar{x} = f_1(\bar{x},\hat{x},u) \\
& \hat{x} = f_2(\bar{x},\hat{x},u) \\
& \bar{x},\hat{x} \in \mathbb{X}, u \in \mathbb{U}.
\end{aligned}
\tag{5.3.8}
$$

In the steady state problem S1, system states x are divided into two subsets $\bar{x}, \hat{x} \in \mathbb{X}$. Here $\bar{x}$ represent some critical states of the system, which will be considered for systematic analysis and may require regularization to stabilize economic NMPC controller; while $\hat{x}$ represent the rest of the system states. These subsets of states can be located through structural analysis of the original optimization problem given by (5.2.1). For example, the states that are directly involved in the economic stage cost could be treated as critical states since they directly affect the optimal solutions to the economic NMPC controller. More guidelines will be discussed in the following section.

For NMPC problem, we apply the robust problem formulation in [91] by relaxing $\mathbb{X}$ with ℓ_1 penalty terms. Without loss of generality, we assume that $\mathbb{X}$ and $\mathbb{U}$ can be represented by simple upper and lower bounds. Then we can write $\mathbb{X}$ as inequalities $g(z_l) \leq 0$, and redefine $g_+^{(j)}(z_l) = max(0, g^{(j)}(z_l))$, $\psi(z_l, v_l) := \psi(z_l, v_l) + \rho\|g_+(z_l)\|$. Note that the redefined objective function is no longer differentiable everywhere, but still Lipschitz continuous, which is sufficient for the stability analysis. With constraint qualifications and second order conditions (e.g. MFCQ, CRCQ and GSSOSC) satisfied, if we select a sufficiently large penalty weight ρ, the optimal solution of the reformulated problem is the same as the original optimization problem and the penalty terms equal zero. Similarly, terminal equality constraints can also be removed with ℓ_1 penalty terms. Here we choose a penalty parameter ρ_t which is large enough so that $z_N = x_s$ at the optimal solution.

After this reformulation, we define the dynamic optimization problem for economic NMPC controller D1 as follows:

$$
\begin{aligned}
D1 : V_{D1}(x(k)) = \min_{\bar{z}_l, \hat{z}_l, v_l} & \sum_{l=0}^{N-1} \psi^{ec}(z_l, v_l) + \rho_t ||z_N - x_s|| \\
\text{s.t.} \quad \bar{z}_{l+1} &= f_1(\bar{z}_l, \hat{z}_l, v_l) \\
\hat{z}_{l+1} &= f_2(\bar{z}_l, \hat{z}_l, v_l) \\
\bar{z}_0 &= \bar{x}(k) \\
\hat{z}_0 &= \hat{x}(k) \\
v_l &\in \mathbb{U}, \qquad l = 0, \ldots N-1.
\end{aligned}
\tag{5.3.9}
$$

To separate two subsets of system states for analysis, we firstly introduce the following assumption.

Assumption 5.3.2.

- *For steady state economic problem S1, $\hat{x}$ can be uniquely determined by $(\bar{x}, u)$.*

With assumption 5.3.2, $\hat{x}$ can be uniquely calculated via the square equation system $f_2(.,.)$ with fixed values of $\bar{x}$ and u. Under Assumption 5.3.2, the rest of system states $\hat{x}$ can be expressed as a function of critical states $\bar{x}$ and controls u, which leads to the following reformulated steady state optimization problem S2:

$$
\begin{aligned}
S2 : \min_{\bar{x}, \hat{x}, u} & \ \psi^{ec}(x, u) \\
\text{s.t.} \quad \bar{x} &= f_1(\bar{x}, \hat{x}, u) \\
\hat{x} &= h(\bar{x}, u) \\
\bar{x}, \hat{x} &\in \mathbb{X}, u \in \mathbb{U}.
\end{aligned}
\tag{5.3.10}
$$

Note that there may not exist an explicit form for function $h(\cdot, \cdot)$, but we can at least determine this steady state relationship implicitly based on implicit function

theorem under Assumption 5.3.2.

Next we introduce a *pseudo* DAE system, where critical states $\bar{x}$ are determined by the original dynamic model, but unimportant states $\hat{x}$ are treated as algebraic variables. Assume that this pseudo system is an index 1 DAE system, and define extended states $\tilde{v}_{l+1} = v_l$, then we apply the same robust reformulation and have the following *pseudo* economic NMPC controller D2:

$$
\begin{aligned}
D2 : V_{D2}(\bar{x}(k)) = \min_{z_l, \hat{z}_l, v_l} & \sum_{l=0}^{N-1} \psi^{ec}(z_l, v_l) + \rho_t ||z_N - x_s|| \qquad (5.3.11) \\
\text{s.t.} \quad \bar{z}_{l+1} &= f_1(\bar{z}_l, \hat{z}_l, v_l), \quad l = 0, \dots N-1 \\
\hat{z}_l &= h(\bar{z}_l, \tilde{v}_l), \quad l = 1, \dots N \\
\bar{z}_0 &= \bar{x}(k) \\
\hat{z}_0 &= h(\bar{x}(k), u(k-1)) \\
v_l, \tilde{v}_l &\in \mathbb{U}.
\end{aligned}
$$

Next we are going to analyze the stability property of economic NMPC with regularization of reduced states. As mentioned before, to design a stable economic NMPC controller, an offline analysis step is usually required to determine sufficient regularization weights. To simplify this process and avoid over-regularization, we want to perform analysis only in a reduced space of states. Such analysis will lead to regularization on only a subset of states, which will be added to the unregularized economic NMPC controller D1 (5.3.9) .

To analyze the stability property of this strategy, we firstly study the stability of *pseudo* economic NMPC controller D2 (5.3.11), where unimportant states are treated as algebraic variables and a much simpler and less conservative regularization can be obtained. Then we analyze the stability of economic NMPC D1 with reduced regularization obtained from D2, by considering the effect of errors in such approximations in the analysis step. Similar to the previous analysis, the main stability

analysis is conducted for economic NMPC using the rotated stage cost as objective. To begin, we will demonstrate the equivalence of NMPC using two objectives with the following Lemmas.

Here we define the rotated stage cost for the steady state problem S2 as follows:

$$\phi(x,u) = \psi^{ec}(x,u) + \lambda^T(\bar{x} - f_1(\bar{x},\hat{x},u)) \tag{5.3.12}$$

It should be noted that only a subset of model equations are rotated. λ are the multipliers for the equality constraints in the optimization problem S2 that have been rotated.

Lemma 5.3.1. *Economic NMPC controller D1 has the same solution when using $\phi(x,u)$ given by* (5.3.12) *as the stage cost.*

Proof: Using $\phi(x,u)$ given by (5.3.12) as the stage cost, we obtain a new objective for problem D1:

$$V_{D1,ro} = \sum_{l=0}^{N-1} (\psi^{ec}(z_l,v_l) + \lambda^T(\bar{z}_l - f_1(\bar{z}_l,\hat{z}_l,v_l)) \tag{5.3.13}$$

Note that from the dynamic model for controller D1, we have $\bar{z}_{l+1} = f_1(\bar{z}_l,\hat{z}_l,v_l)$. Then we derive the relationship of the new objective $V_{D1,ro}$ for controller D1 and original objective V_{D1}:

$$\begin{aligned} V_{D1,ro}(\bar{x}(k)) &= \sum_{l=0}^{N-1} (\psi^{ec}(z_l,v_l) + \lambda^T(\bar{z}_l - f_1(\bar{z}_l,\hat{z}_l,v_l)) \\ &= \sum_{l=0}^{N-1} \psi^{ec}(z_l,v_l) + \sum_{l=0}^{N-1} \lambda^T(\bar{z}_l - \bar{z}_{l+1}) \\ &= \sum_{l=0}^{N-1} \psi^{ec}(z_l,v_l) + \lambda^T\bar{x}(k) \\ &= V_{D1}(\bar{x}(k)) + \lambda^T\bar{x}(k) \end{aligned} \tag{5.3.14}$$

From the above equation, we find that $V_{D1,ro}$ and V_{D1} differ by only a constant term.

Therefore economic NMPC controller D1 has the same solution as using the rotated stage cost (5.3.13) as objective. □

Lemma 5.3.2. *Economic NMPC controller D2 has the same solution as using* $\phi(x,u)$ *given by* (5.3.12) *as the stage cost.*

Proof: Similar to the proof for Lemma 5.3.1, the new objective for D2 is defined as

$$V_{D2,ro} = \sum_{l=0}^{N-1} (\psi^{ec}(z_l, v_l) + \lambda^T(\bar{z}_l - f_1(\bar{z}_l, \hat{z}_l, v_l)) \tag{5.3.15}$$

and the relationship of the new objective $V_{D2,ro}$ for controller D2 and original objective V_{D2} is as follows:

$$\begin{aligned} V_{D2,ro}(\bar{x}(k)) &= \sum_{l=0}^{N-1} (\psi^{ec}(z_l, v_l) + \lambda^T(\bar{z}_l - f_1(\bar{z}_l, \hat{z}_l, v_l)) \\ &= \sum_{l=0}^{N-1} \psi^{ec}(z_l, v_l) + \sum_{l=0}^{N-1} \lambda^T(\bar{z}_l - \bar{z}_{l+1}) \\ &= \sum_{l=0}^{N-1} \psi^{ec}(z_l, v_l) + \lambda^T \bar{x}(k) \\ &= V_{D2}(\bar{x}(k)) + \lambda^T \bar{x}(k) \end{aligned} \tag{5.3.16}$$

From the above equation, we find that $V_{D2,ro}$ and V_{D2} differ by only a constant term. Therefore economic NMPC controller D2 has the same solution as using the rotated stage cost as objective. □

From equations (5.3.14) and (5.3.16) in the above Lemmas, we can also find that $V_{D1,ro}(\bar{x}(k)) - V_{D2,ro}(\bar{x}(k)) = V_{D1}(\bar{x}(k)) - V_{D2}(\bar{x}(k))$.

Moreover, problems D1 and D2 can be linked with the following parametric NLP

formulation pNLP(t), with a parameter t:

$$\min_{\bar{z}_l,\hat{z}_l,v_l} \sum_{l=0}^{N-1} \psi^{ec}(z_l, v_l) + \rho_t||z_N - x_s|| \tag{5.3.17}$$

$$\begin{aligned}
\text{s.t.} \quad & \bar{z}_{l+1} = f_1(\bar{z}_l, \hat{z}_l, v_l), \quad l = 0, \dots N-1 \\
& \hat{z}_l = h(\bar{z}_l, \tilde{v}_1) + t(f_2(\bar{z}_{l-1}, \hat{z}_{l-1}, v_{l-1}) - h(\bar{z}_l, \tilde{v}_l)), \quad l = 1, \dots N \\
& \bar{z}_0 = \bar{x}(k) \\
& \hat{z}_0 = h(\bar{x}(k), u(k-1)) + t(\hat{x}(k) - h(\bar{x}(k), u(k-1))) \\
& v_l, \tilde{v}_l \in \mathbb{U}.
\end{aligned}$$

Here we introduce a noise vector $w(k) = [w_0 \dots w_N]^T$ with entries defined as follows:

$$w_0 = \hat{x}(k) - h(\bar{x}(k), u(k-1)) \tag{5.3.18}$$

$$w_l = f_2(\bar{z}_{l-1}, \hat{z}_{l-1}, v_{l-1}) - h(\bar{z}_l, \tilde{v}_l) \quad l = 1 \dots N \tag{5.3.19}$$

The noise vector $w(k)$ represents the differences in the values of $\hat{z}_l$ given by the dynamic function and steady state relationship. For the above parametric NLP problem, when $t = 0$, it corresponds to problem D2. On the other hand, when $t = 1$, it corresponds problem D1.

Next we will show that, in the *pseudo nominal* case where $w(k) = 0$, stability property can be guaranteed for economic NMPC by adding regularization terms only for critical states $\bar{x}$ and u.

Theorem 5.3.2. *In the pseudo nominal case where $w(k) = 0$, under Assumption 5.3.2, economic NMPC controller D1 can be made asymptotically stable, by adding a sufficiently large regularization on reduced sets of states $\bar{z}$ and v.*

Proof: In this *pseudo nominal* case, we assume that $w(k) = 0$; so that NMPC problem D1 is equivalent to NMPC problem D2, where all unimportant states $\hat{x}$ are

algebraic variables. Then we can perform the similar analysis as reducing the algebraic variables as discussed in chapter 5.3.1.

Substituting the steady state relationship $\hat{z}_l = h(\bar{z}_l, \tilde{v}_l)$, D2 can be rewritten as:

$$\begin{aligned} \min_{\bar{z}_l, \tilde{v}_l, v_l} & \sum_{l=0}^{N-1} \psi^{ec}(\bar{z}_l, h(\bar{z}_l, \tilde{v}_l), v_l) \\ \text{s.t.} \quad & \bar{z}_{l+1} = f_1(\bar{z}_l, h(\bar{z}_l, \tilde{v}_l), v_l) \\ & \bar{z}_0 = \bar{x}(k) \\ & v_l, \tilde{v}_l \in \mathbb{U}, l = 0, \dots N-1. \end{aligned} \tag{5.3.20}$$

Similarly, we can rewrite the steady state problem S2 as follows:

$$\begin{aligned} \min_{\bar{x}, u} \quad & \psi^{ec}(\bar{x}, h(\bar{x}, u), u) \\ \text{s.t.} \quad & \bar{x} = f_1(\bar{x}, h(\bar{x}, u), u) \\ & \bar{x} \in \mathbb{X}, u \in \mathbb{U}. \end{aligned} \tag{5.3.21}$$

Here we also introduce a robust formulation similar to [91] to remove constraints on $\hat{z}$ by ℓ_1 penalty terms in the objective function. With sufficiently large penalty weight, at optimal solutions, these penalty terms will be zero and the original constraints on $\hat{z}$ will be satisfied.

Now this problem is equivalent to economic NMPC described by (5.2.2) and we can follow the proof in [44] to establish stability results. For this reduced system, if the regularized rotated stage cost $\phi_{reg}(\bar{x}, u) = \psi^{ec}(\bar{x}, h(\bar{x}, u), u) + \lambda^T(\bar{x} - f_1(\bar{x}, h(\bar{x}, u), u)) + \frac{1}{2}\|(\bar{x}, u) - (\bar{x}_s, u_s)\|_Q^2$ is strongly convex, as shown in [44], the monotonic decrease of the value function can be guaranteed and the regularized stage cost is bounded by $\mathcal{K}_\infty$ functions. Therefore, the asymptotic stability for regularized economic NMPC controller using rotated stage cost as objective can be established. Based on Lemma 5.3.2, in the *pseudo nominal* case where $w(k) = 0$,

economic NMPC controller D1 is asymptotically stable. □

Next we will consider the stability property for economic NMPC controller D1 for cases where $w(k) \neq 0$. In these cases, the economic NMPC controller D1 can be treated as the controller D2 corrupted with non-zero noise terms $w(k)$.

The *pseudo* process model for controller D2 is defined as follows:

$$\bar{x}(k+1) = f_1(\bar{x}(k), u(k), h(\bar{x}(k), u(k-1))) \tag{5.3.22}$$

while the process model is defined as follows:

$$\bar{x}(k+1) = f_1(\bar{x}(k), u(k), h(\bar{x}(k), u(k-1)) + w(k, 0)) \tag{5.3.23}$$

Here $w(k, 0)$ is the first element of the noise vector $w(k)$ and it's defined as $\hat{x}(k) - h(\bar{x}(k), u(k-1))$, which represents the difference in the values for $\hat{x}$ at initial time in D1 and D2.

Firstly we will analyze the stability property for controller D2 when the process model is given by equation (5.3.23), which is the nominal process model. However, model mismatch exists between the nominal process model and the control model (5.3.22) for controller D2. Then we introduce an assumption on $w(k)$ that it's always bounded. With additional standard assumptions for robust stability, we can establish Input-to-State Stability (ISS) property for controller D2.

Assumption 5.3.3.

- *The noise vector $w(k) = [w_0 \dots w_N]^T$ is drawn from a bounded set $\mathcal{W}$ with an upper bound $\bar{w}$.*

Assumption (5.3.3) is a key assumption for the following stability analysis, which assumes that the deviations of dynamic states $\hat{x}$ from their algebraic predictions are bounded, i.e. dynamic states $\hat{x}$ have a similar behavior as algebraic variables.

For example, the states that have very fast dynamics and quickly converge to their algebraic counterparts may satisfy this assumption.

Assumption 5.3.4. *Robust stability assumptions*

- *The optimal solution to problem D1 and D2 is continuous with respect to $x(k)$ and w.*
- *$V(x(k))$ is Lipschitz with respect to $x(k)$, with a positive Lipschitz constant L_v.*
- *Model equations f and steady state relationship h are Lipschitz with its arguments with corresponding Lipschitz constants.*

Theorem 5.3.3. *Under Assumption 5.3.2, 5.3.3 and 5.3.4, the controller D2 can be made ISS stable when process model is given by equation (5.3.23) and $w(k) \neq 0$.*

Proof: Here we consider the controller D2 using rotated stage cost $V_{D2,ro}$ (5.3.15) as objective, which is equivalent to D2 using the original stage cost, as shown in Lemma 5.3.2.

Then we compare the differences between value functions at two consecutive sampling times. Similar to the robust stability proof shown in [45, 59], we can derive the following inequality, with Assumption 5.3.4.

$$\begin{aligned}
&V_{D2,ro}(\bar{x}(k+1)) - V_{D2,ro}(\bar{x}(k)) \qquad (5.3.24)\\
&= V_{D2,ro}(\bar{x}(k+1)) - V_{D2,ro}(f_1(\bar{x}(k), u(k), h(\bar{x}(k), u(k-1))))\\
&\quad + V_{D2,ro}(f_1(\bar{x}(k), u(k), h(\bar{x}(k), u(k-1)))) - V_{D2,ro}(\bar{x}(k))\\
&\leq L_v|\bar{x}(k+1) - f_1(\bar{x}(k), u(k), h(\bar{x}(k), u(k-1)))| - \psi_{ro}(\bar{x}(k), u(k))\\
&\leq L_v L_f |w(k,0)| - \psi_{ro}(\bar{x}(k), u(k))\\
&\leq -\alpha_l(|\bar{x}(k) - \bar{x}_s|) + L_V|w(k,0)|
\end{aligned}$$

The last line of derivation follows the fact that the rotated stage cost $\psi_{ro}(\bar{x}(k), u(k))$ can be bounded by a $\mathcal{K}_\infty$ function $\alpha_l(\cdot)$ after adding sufficient regularization on $\bar{z}$ and v based on Theorem 5.3.2. $w(k,0)$ is the first element of the noise vector $w(k)$

at sampling time t_k, which causes the differences in the states predictions given by and *pseudo* process model (5.3.22) and process model (5.3.23). Under Assumption 5.3.3, $w(k,0)$ is drawn from the bounded set $\mathcal{W}$. Therefore, ISS property can be established for controller D2. □

Next we analyze the stability property for economic NMPC D1 with reduced sets of regularization by linking the solutions to problems D1 and D2.

By introducing a notation $v = [v_l, \tilde{v}_l]$, we can rewrite the pNLP(t) defined by (5.3.17) as follows:

$$\begin{aligned} pNLP(t) = & \min_{z,v} F(z,v) \\ \text{s.t.} \quad & c_1(z,v) = 0 \\ & c_2(z,v) + tc_3(z,v) = 0 \end{aligned} \tag{5.3.25}$$

The new notations c_1, c_2, c_3 are defined as follows, which is derived from pNLP(t) by (5.3.17):

$$c_1(z,v) = \begin{bmatrix} \bar{z}_{l+1} - f_1(\bar{z}_l, \hat{z}_l, v_l) \\ \bar{z}_0 - \bar{x}(k) \end{bmatrix} \tag{5.3.26}$$

$$c_2(z,v) = \begin{bmatrix} \hat{z}_l - h(\bar{z}_l, \tilde{v}_1) \\ \hat{z}_0 - h(\bar{x}(k), u(k-1)) \end{bmatrix} \tag{5.3.27}$$

$$c_3(z,v) = \begin{bmatrix} -(f_2(\bar{z}_{l-1}, \hat{z}_{l-1}, v_{l-1}) - h(\bar{z}_l, \tilde{v}_l)) \\ -(\hat{x}(k) - h(\bar{x}(k), u(k-1))) \end{bmatrix} \tag{5.3.28}$$

The above NLP is equivalent to D2 when $t = 0$ and is the same as D1 when $t = 1$. The difference in the solutions of D2 and D1 *with the same control inputs* v can be bounded with the following Lemma.

Lemma 5.3.3. *Assume that solutions* $(z^*(t), v^*(t))$ *exist for pNLP(t) given by* (5.3.25),

for all $t \in [0,1]$. *Then with* $v^*(t)$ *specified, and* z *calculated from the equality constraints in* (5.3.25), *the difference of value functions and state profiles at* $t = 0$ *and* $t = 1$ *is* $O(\bar{w})$, *i.e.* $|F(z(0), v^*(t)) - F(z(1), v^*(t))| \leq L_F \bar{w}$, $|z(0) - z(1)| \leq L_z \bar{w}$.

Proof: The equation systems for pNLP(t) are shown as follows:

$$P(t): \quad \begin{aligned} & c_1(z, v) = 0 \\ & c_2(z, v) + t c_3(z, v) = 0 \end{aligned} \tag{5.3.29}$$

With fixed inputs $v^*(t)$, the equation systems for pNLP(t) becomes a square system. Then solving pNLP(t) is equivalent to solving a dynamic simulation problem and the equation systems P(t) can be solved by marching step by step from $l = 0$ to $l = N$. Here we assume that the square systems are non-singular for all $t \in [0,1]$. Then we can apply the implicit function theorem to find the parametric sensitivity of state variables z with respect to t:

$$\begin{bmatrix} \nabla c_1(z, v^*(t)) \\ \nabla c_2(z, v^*(t)) + t \nabla c_3(z, v^*(t)) \end{bmatrix} \dot{z} = - \begin{bmatrix} 0 \\ c_3(z, v^*(t)) \end{bmatrix} \tag{5.3.30}$$

and the differences in the state variables z can be bounded by:

$$\begin{aligned} |z(1) - z(0)| &= \left| \int_0^1 \begin{bmatrix} \nabla c_1(z, v^*(t)) \\ \nabla c_2(z, v^*(t)) + t \nabla c_3(z, v^*(t)) \end{bmatrix}^{-1} \begin{bmatrix} 0 \\ c_3(z, v^*(t)) \end{bmatrix} dt \right| \\ &\leq L_K |c_3(z, v^*(t))| \leq L_K |\bar{w}| \end{aligned} \tag{5.3.31}$$

Note that $c_3(z, v^*(t))$ is the same as $w(k)$, which is bounded by $\bar{w}$ based on Assumption 5.3.3. In addition, under the assumption that F is lipschitz in x, the difference

in value functions can be bounded by:

$$|F(z(0), v^*(t)) - F(z(1), v^*(t))| \leq L_F|\bar{w}| \tag{5.3.32}$$

Theorem 5.3.4. *Under Assumption 5.3.2, 5.3.3 and 5.3.4, economic NMPC controller D1 can be made Input-to-State Practical Stable (ISpS), by adding a sufficiently large regularization on reduced sets of states $\bar{z}$ and v.*

Proof: Firstly, we solve problem D2 and obtain optimal control sequences v_l^{D2}. Then we apply v_l^{D2} to solving the square systems for controller D1:

$$\begin{aligned} P1: \quad & c_1(z_l, v_l^{D2}) = 0 \\ & c_2(z_l, v_l^{D2}) + c_3(z_l, v_l^{D2}) = 0 \end{aligned} \tag{5.3.33}$$

Injecting v_l^{D2} and solving P1 may lead to violations of state inequality constraints and terminal equality constraints used in D1. For example, the solution z_N from P1 may not equal to x_s. However, the difference $||z_N - x_s||$ is bounded by a constant $c(\bar{w})$ based on Lemma 5.3.3. After using the robust reformulation, these constraints are replaced with ℓ_1 penalty terms and these additional penalty terms in the objective functions are also bounded by a constant $c(\bar{w})$. With the robust reformulation, P1 can be solved and we denote the value function associated with P1 as V_{D1}^f. Based on Lemma 5.3.3, the difference of value functions of P1 and D2 can be bounded by:

$$|V_{D1}^f - V_{D2}| \leq L_{V1}\bar{w} \tag{5.3.34}$$

On the other hand, it should be noted that the solution of P1 provides a feasible solution to D1. Based on the principle of optimality, we have the following inequality:

$$V_{D1}^f \geq V_{D1} \tag{5.3.35}$$

Similarly, we solve problem D1 and obtain optimal control sequences v_l^{D1}. Then we apply v_l^{D1} to solving the square systems for controller D2:

$$P2: \qquad c_1(z_l, v_l^{D2}) = 0 \qquad (5.3.36)$$
$$c_2(z_l, v_l^{D2}) = 0$$

Here we denote the value function associated with P2 as V_{D2}^f. Also based on Lemma 5.3.3, the difference of value functions of P2 and D1 can be bounded by:

$$|V_{D1} - V_{D2}^f| \leq L_{V2}\bar{w} \qquad (5.3.37)$$

Since the solution of P2 provides a feasible solution to D2, based on the principle of optimality, we have:

$$V_{D2}^f \geq V_{D2} \qquad (5.3.38)$$

To establish the stability property, we consider the controller D1 using rotated stage cost $V_{D1,ro}$ as objective, which is equivalent to D1 using the original stage cost, as shown in Lemma 5.3.1. Also based on Lemma 5.3.1 and Lemma 5.3.2, we have $V_{D1,ro}(\bar{x}(k)) - V_{D2,ro}(\bar{x}(k)) = V_{D1}(\bar{x}(k)) - V_{D2}(\bar{x}(k))$.

Then the difference of rotated stage cost at two consecutive sampling times is

shown as follows:

$$
\begin{aligned}
& V_{D1,ro}(\bar{x}(k+1)) - V_{D1,ro}(\bar{x}(k)) \qquad (5.3.39)\\
&= V_{D1,ro}(\bar{x}(k+1)) - V_{D2,ro}(\bar{x}(k+1)) + V_{D2,ro}(\bar{x}(k+1)) - V_{D2,ro}(\bar{x}(k))\\
&\quad + V_{D2,ro}(\bar{x}(k)) - V_{D1,ro}(\bar{x}(k))\\
&= V_{D1}(\bar{x}(k+1)) - V_{D2}(\bar{x}(k+1)) + V_{D2,ro}(\bar{x}(k+1)) - V_{D2,ro}(\bar{x}(k))\\
&\quad + V_{D2}(\bar{x}(k)) - V_{D1}(\bar{x}(k))\\
&\leq V_{D1}^{f}(\bar{x}(k+1)) - V_{D2}(\bar{x}(k+1)) + V_{D2,ro}(\bar{x}(k+1)) - V_{D2,ro}(\bar{x}(k))\\
&\quad + V_{D2}^{f}(\bar{x}(k)) - V_{D1}(\bar{x}(k))\\
&\leq L_{V1}\bar{w} + (-\alpha_l(|x(k) - \bar{x}_s|) + L_V|w(k,0)|) + L_{V2}\bar{w}\\
&\leq -\alpha_l(|\bar{x}(k) - \bar{x}_s|) + L_V|w(k,0)| + L_{V3}\bar{w}
\end{aligned}
$$

The inequality for the pair $V_{D2,ro}(\bar{x}(k+1)) - V_{D2,ro}(\bar{x}(k))$ comes from equation (5.3.24) in the proof for Theorem 5.3.3, where $\alpha_l(\cdot)$ is a $\mathcal{K}_\infty$ function. As for the other two pairs, the inequalities can be derived with the previous analysis. Therefore the ISpS property can be established for D1. It should be noted that the constant is related with the upper bound $\bar{w}$ for $w(k)$. □

From the above results, we can guarantee ISpS stability of the economic NMPC controller by regularizing important states $\bar{x}$, under the assumption that the derivations of unimportant dynamic states $\hat{x}$ from their algebraic predictions are bounded. Though the *pseudo* controller D2 has a stronger stability result than controller D1, we only use the *pseudo* process model to determine reduced regularization weight but still use the full model for the controller which gives accurate predictions in terms of the dynamic behavior of both states $\bar{x}$ and $\hat{x}$.

Unlike exogenous process disturbances which exist all the time and are independent of process states, the noise vector $w(k)$ in our analysis may have some different properties that could lead to stronger stability results. Next we will study the

stability results if a stronger assumption is made for $w(k)$.

Assumption 5.3.5. *The noise vector* $|w(k)| \leq \frac{\rho}{L_w}(|\bar{x}(k) - \bar{x}_s|)$, *where* $\frac{\rho}{L_w}(|\bar{x}(k) - \bar{x}_s|) \leq \bar{w}, L_w = L_{V3} + L_V, \rho \in [0, 1)$, *after a finite number of iterations K.*

In Assumption 5.3.5, we assume that as critical states $\bar{x}$ approach to steady state, the noise vector $w(k)$ can be bounded by the distance of $\bar{x}$ to the optimal steady state, which is stronger than Assumption 5.3.3. However, this assumption may hold for cases where $\bar{x}(k)$ and $\hat{x}(k)$ are close to steady state; the deviations of dynamic states $\hat{x}(k)$ and their algebraic predictions are bounded by a decaying bound and $w(k)$ will go to 0 as $\bar{x}$ converge to steady state $\bar{x}_s$.

Theorem 5.3.5. *Under Assumption 5.3.5, NMPC controller D1 can be made asymptotically stable, by adding a sufficiently large regularization on reduced sets of states* $\bar{z}$ *and* v.

Proof: The Assumption 5.3.5 assumes that $|w(k)| \leq \frac{\rho}{L_w}(|\bar{x}(k) - \bar{x}_s|) \leq \bar{w}$ after a finite number (e.g. K) iterations. With this assumption, we can define a new upper bound $\bar{w}_n$ for $w(k)$, with $\bar{w}_n = \frac{\rho}{L_w}(|\bar{x}(k) - \bar{x}_s|), L_w = L_{V3} + L_V, \rho \in [0, 1)$.

From (5.3.39) in Theorem 5.3.4, we can derive a similar inequality, for $k \geq K$:

$$\begin{aligned} & V_{D1,ro}(\bar{x}(k+1)) - V_{D1,ro}(\bar{x}(k)) \\ & \leq -\alpha_l(|\bar{x}(k) - \bar{x}_s|) + L_{V3}\bar{w}_n + L_V\bar{w}_n \\ & \leq -(1-\rho)\alpha_l(|\bar{x}(k) - \bar{x}_s|) \end{aligned} \tag{5.3.40}$$

where $\alpha_l(\cdot)$ is a $\mathcal{K}_\infty$ function.

This theorem can be proved by summing inequalities (5.3.39) and (5.3.40) over k

from 0 to ∞, and it leads:

$$\begin{aligned} V_{D1,ro}(\bar{x}(0)) - V_{D1,ro}(\bar{x}(\infty)) &\geq \sum_{k=0}^{\infty}(V_{D3,ro}(\bar{x}(k)) - V_{D3,ro}(\bar{x}(k+1)) \\ &\geq \sum_{k=0}^{K}\alpha_l(|\bar{x}(k) - \bar{x}_s|) - \sum_{k=0}^{K} L_{V3}|w(k,0)| - \sum_{k=0}^{K} L_V\bar{w} \\ &\quad + \sum_{k=K+1}^{\infty}(1-\rho)\alpha_l(|\bar{x}(k) - \bar{x}_s|) \end{aligned} \tag{5.3.41}$$

Since $V_{D1,ro}$ is bounded above and below, the above inequality can be valid only if $\lim_{k\to\infty}\alpha_l(|\bar{x}(k) - \bar{x}_s|) \to 0$ and $\lim_{k\to\infty}\bar{x}(k) \to \bar{x}_s$. □

Remark: Note that it's not necessary to derive the steady state relationship $h(\cdot,\cdot)$ to reduce the state space for economic NMPC implementation or to use problem D2 as the controller. This reduction is only used to facilitate the stability analysis.

In this section, we have shown that, with a sufficiently large regularization on a reduced set of system states, the stability of economic NMPC controller can still be maintained. Next we will briefly discuss the guidelines for critical states selection and introduce a systematic approach to determine the sufficient weights for the reduced regularization that guarantees the stability of economic NMPC controller.

5.3.3 Selection of Critical States

In the previous section, we analyze the stability property of economic NMPC using reduced regularization on critical states. Moreover, it's crucial to identify the critical states that need to be considered for regularization analysis. Though the selection of critical states may be application-dependent and there is no unifying criterion, we will discuss some general guidelines in this section.

Based on the previous stability results, we can see that dynamic states that have similar performance as their algebraic counterparts may be removed from regularization analysis by treating them as algebraic variables. These states can be lo-

cated via time scale analysis of the original system. For example, the fast states in the standard singularly perturbed system (3.3.1) may be removed for the regularization analysis if ϵ is small. For these states, Assumption 5.3.3 may be satisfied implicitly and no regularization is required for these states.

In addition to time scale analysis, sensitivity analysis of the optimization problem may provide insights to locate the critical states. When considering the steady state optimization problem (5.2.1), only a subset of the full system states affects its optimal solution. Therefore, when solving the corresponding NLP problem for economic NMPC, the optimal control moves of economic NMPC controller are affected by only a subset of system states. By doing a sensitivity analysis of the optimization problem, we can find the states that significantly affect the optimization objective function. The states that have little impact on the objective functions may not need regularization and can be removed from the regularization analysis.

Moreover, to select appropriate critical states for regularization, it also requires a good understanding of dynamic process model structure. For example, we can conduct a structural analysis of the dynamic model to see if there are inherently unstable states. If so, we need to treat these unstable states as critical states as well. In addition, the coupling of states may provide hints to remove unnecessary states for regularization analysis. For instance, if there exist strong dependency of some states on the rest of states, like the slaving relationship for algebraic variables, then these dependent states may be neglected for regularization analysis.

5.3.4 Regularization Weight Calculation

After removing algebraic variables and unimportant differential variables, we end up with the following rotated stage cost consisting of $\bar{x}$ and u at steady state:

$$\phi_{red}(\bar{x}, u) = \psi^{ec}(\bar{x}, h(\bar{x}, u), u) + \lambda^T(\bar{x} - f_1(\bar{x}, u, h(\bar{x}, u))) \tag{5.3.42}$$

Next we need to find sufficient regularization to make the regularized rotated stage cost $\phi_{red}(\bar{x}, u) + \frac{1}{2}\|(\bar{x}, u) - (\bar{x}_s, u_s)\|^2_{\bar{Q}}$ to be strongly convex. This is equivalent to finding a regularization matrix to make the Hessian matrix of the rotated stage cost positive definite, which is defined as follows:

$$\bar{A}_r = \nabla^2 \phi_{red}(\bar{x}, u) \tag{5.3.43}$$

Compared with the strategy proposed in [44], one major difference is that we only need to calculate the Hessian of the reduced system given by (5.3.43), rather than the Hessian of the full system (5.2.12). Also it should be noted that the rotated stage cost has been simplified since equations $f_2(\cdot, \cdot)$ are not included.

To make the reduced Hessian $\bar{A}_r$ positive definite, we can apply the same criterion based on the Gershgorin theorem to find sufficient weights, as shown in [44].

$$\bar{q}_i > \sum_{i \neq j} |\bar{a}_{i,j}| - \bar{a}_{i,j} \tag{5.3.44}$$

where $\bar{q}_i$ are the diagonal elements of the weighting matrix $\bar{Q}$ for regularization of critical states $\frac{1}{2}\|(\bar{x}, u) - (\bar{x}_s, u_s)\|^2_{\bar{Q}}$; $\bar{a}_{i,j}$ are the elements of matrix $\bar{A}_r$.

With the inequality (5.3.44) being satisfied for all $u \in \mathbb{U}, \bar{x} \in \mathbb{X}$, the regularized rotated stage cost $\phi_{red}(\bar{x}, u) + \frac{1}{2}\|(\bar{x}, u) - (\bar{x}_s, u_s)\|^2_{\bar{Q}}$ is strongly convex. Then the stability results shown in the previous sections hold for economic NMPC controller after adding this regularization. As we mentioned before, the inequality (5.3.44) needs to be satisfied for all values in the space of critical states, which is much smaller than the original full state space.

In addition, other strategies can be used to find the minimum regularization weight which makes the reduced Hessian $\bar{A}_r$ positive definite. For example, we can introduce a diagonal regularization matrix $\bar{Q} = qI$, where I is a identity matrix of the

dimension of $\bar{x}$ and u. The scalar regularization weight q can be determined by:

$$q > max(0, -\lambda_i) \tag{5.3.45}$$

where λ_i is the negative eigenvalue of the reduced Hessian without any regularization. After adding regularization matrix $\bar{Q} = qI$, the regularized reduced Hessian can be positive definite since all of its eigenvalues are positive.

Prior to regularization, we need to calculate the reduced Hessian matrix $\bar{A}_r$. Since the explicit form of $h(\cdot,\cdot)$ may not be available, we need to start with the rotated stage cost with $(\bar{x}, \hat{x}, u)$. To simplify the notation, we define $\tilde{x} = [\bar{x}, u] \in \Re^{n_{\tilde{x}}}$ and $x = [\tilde{x}, \hat{x}] \in \Re^{n_x}$. Then the rotated stage cost can be defined as follows:

$$\phi(x) = \psi^{ec}(x) + \lambda^T(\bar{x} - f_1(x)) \tag{5.3.46}$$

Based on the chain rule, we can derive the Jacobian and Hessian of $\phi(x)$ with respect to $\tilde{x}$ as follows:

$$\frac{\partial \phi(x)}{\partial \tilde{x}} = \frac{\partial \phi(x)}{\partial x}\frac{\partial x}{\partial \tilde{x}} \tag{5.3.47}$$

$$\frac{\partial^2 \phi(x)}{\partial \tilde{x}^2} = \frac{\partial x}{\partial \tilde{x}}^T \frac{\partial^2 \phi(x)}{\partial x^2}\frac{\partial x}{\partial \tilde{x}} + \sum_{i=1}^{n_x} \frac{\partial \phi(x)}{\partial x_i}\frac{\partial^2 x_i}{\partial \tilde{x}^2} \tag{5.3.48}$$

In the above equations, we have:

$$\frac{\partial x}{\partial \tilde{x}}^T = \begin{bmatrix} I & \frac{\partial \hat{x}}{\partial \tilde{x}}^T \end{bmatrix} \tag{5.3.49}$$

where I is an identity matrix with the dimension of $\tilde{x}$.

As discussed earlier, we can derive the implicit steady state relationship $\hat{x} = h(\tilde{x})$

from the following square equation system from problem S1:

$$F_2(\tilde{x}, \hat{x}) = f_2(\tilde{x}, \hat{x}) - \hat{x} = 0 \tag{5.3.50}$$

Based on chain rule, the dependent sensitivity and Hessian can be determined by:

$$J_1 \frac{\partial \hat{x}}{\partial \tilde{x}} + J_2 = 0 \tag{5.3.51}$$

$$\frac{\partial J_1}{\partial \tilde{x}_i} \frac{\partial \hat{x}}{\partial \tilde{x}} + J_1 \frac{\partial^2 \hat{x}}{\partial \tilde{x} \partial \tilde{x}_i} + \frac{\partial J_2}{\partial \tilde{x}_i} = 0 \qquad i = 1 \cdots n_{\tilde{x}} \tag{5.3.52}$$

where $J_1 = \dfrac{\partial F_2}{\partial \hat{x}}$ and $J_2 = \dfrac{\partial F_2}{\partial \tilde{x}}$.

With (5.3.51) and (5.3.52) plus the Jacobian and Hessian information of rotated stage cost $\phi(x)$, we can calculate $\dfrac{\partial^2 \phi(x)}{\partial \tilde{x}^2}$ given by (5.3.48), which is equivalent to the reduced Hessian $\bar{A}_r$. Note that all these calculations are based on the original full space model, which means we can find the reduced Hessian implicitly without the need to find an explicit form for $h(\cdot, \cdot)$ or to reformulate the original model equations. Also it should be noted that all information required to perform the above calculation is the Jacobian and Hessian matrix of the original model. So we can directly apply these equations to check criterion (5.3.44) or (5.3.45) if we have access to analytic Jacobian and Hessian which is available in modeling platform such as AMPL. Another practical alternative is to approximate the dependent derivatives and the reduced Hessian numerically using the perturbation method.

5.4 Case Studies

5.4.1 Economic NMPC of a CSTR

To illustrate the reduced regularization strategy proposed in the previous section, we firstly study the economic NMPC problem of a well-mixed, continuous stirred

tank reactor (CSTR). The CSTR model is taken from [26], with a first order irreversible reaction $A \rightarrow B$. The mass balances for reactant A and product B are shown as follows:

$$\frac{dc_A}{dt} = \frac{F}{V}(c_{A0} - c_A) - kc_A \tag{5.4.1}$$

$$\frac{dc_B}{dt} = \frac{F}{V}(-c_B) + kc_A \tag{5.4.2}$$

Here c_A and c_B represent the concentrations of A and B, in mol/l. The reactor volume V = 10 l, and the rate constant k = 1.2 l/(mol·min). The manipulated variable is F, the flowrate of feed A, in l/min, and c_{A0} = 1 mol/l is the feed concentration. Here we consider a similar economic stage cost as used in [26]:

$$\psi^{ec}(F, c_A, c_B) = -(3Fc_B - 0.5F) \tag{5.4.3}$$

where the first term represents the profit of product B and the second term represents the cost for raw material A.

In addition, we set the variable bounds as:

$$10 \leq F \leq 20 \tag{5.4.4}$$

$$0.45 \leq c_B \leq 1 \tag{5.4.5}$$

Then we apply the robust reformulation to constraints on c_B which softens the variable bounds with ℓ_1 norm penalty in the objective function. The penalty weight ρ is chosen as 10^6. For economic NMPC problem, we discretize the CSTR model using a three-point Radau collocation with a finite element length of 0.5 min. The prediction horizon $N = 200$. The initial conditions $c_{A,0}$ = 0.1 mol/l, $c_{B,0}$ = 1 mol/l. In addition, the steady state optimum of the above problem are $c_A^* = 0.55, c_B^* = 0.45, F^* = 14.67$.

Next we need to find sufficient regularization weights to stabilize economic NMPC

controller. Firstly we apply the full regularization strategy proposed in [44]. The rotated stage cost of the original system is defined as:

$$\phi(F, c_A, c_B) = -3Fc_B + 0.5F + \lambda_1^*[\frac{F}{V}(c_{A0} - c_A) - kc_A] + \lambda_2^*[\frac{F}{V}(-c_B) + kc_A] \tag{5.4.6}$$

To make the rotated stage cost strongly convex, we introduce regularization terms $\frac{1}{2}[q_A(c_A - c_A^*)^2 + q_B(c_B - c_B^*)^2 + q_F(F - F^*)^2]$ for all 3 variables. After adding the regularization terms, the Hessian of the rotated stage cost is:

$$A = \nabla^2\phi = \begin{bmatrix} q_F & 1.54 & 0.43 \\ 1.54 & q_A & 0 \\ 0.43 & 0 & q_B \end{bmatrix} \tag{5.4.7}$$

It should be noted that, for CSTR example, the elements of Hessian matrix A remain constant for all (z, v) since there are only linear and bilinear terms in the CSTR model. Based on the Gershgorin theorem, A can be made strongly convex with regularization weights that satisfy the following inequality:

$$q_F > 1.97, \quad q_A > 1.54, \quad q_B > 0.43 \tag{5.4.8}$$

Next we demonstrate the reduced regularization strategy proposed in the previous section. Here we choose c_B as $\hat{x}$ and thus equation (5.4.2) is $f_2(\cdot)$. By setting the left hand side of equation (5.4.2) to zero, we can easily find a steady state function $h(\cdot)$ for c_B:

$$c_B = h(F, c_A) = kV\frac{c_A}{F} \tag{5.4.9}$$

Then we substitute $c_B = h(F, c_A)$ into the economic stage cost. After that, we obtain a rotated stage cost for the reduced system:

$$\phi_{red}(F, c_A) = -3kVc_A + 0.5F + \lambda_1^*[\frac{F}{V}(c_{A0} - c_A) - kc_A] \tag{5.4.10}$$

Compared with the original rotated stage cost $\phi(F, c_A, c_B)$, the above reduced rotated stage cost $\phi_{red}(F, c_A)$ only involves 2 variables. To make the reduced rotated stage cost strongly convex, we introduce regularization terms $\frac{1}{2}[q_F(F - F^*)^2 + q_A(c_A - c_A^*)^2]$ for the reduced states. After adding the regularization term, the Hessian of the reduced rotated stage cost is:

$$A_r = \nabla^2\phi_{red} = \begin{bmatrix} q_F & 1.54 \\ 1.54 & q_A \end{bmatrix} \tag{5.4.11}$$

Then we can obtain the following Gershgorin bounds for F and c_A to make A_r positive definite:

$$q_F > 1.54, \quad q_A > 1.54 \tag{5.4.12}$$

The CSTR example illustrates how the reduced regularization procedure works. In the CSTR example, the explicit form of $h(\cdot)$ can be found based on the steady state model equation. In the dynamic case where the explicit form of $h(\cdot)$ may be difficult to obtain, we can still find the Hessian of the reduced system by implicit function theorem or numerical perturbations, as discussed in the previous section, since only Jacobian and Hessian information of the original model is needed.

In the CSTR example, we obtain less conservative Gershgorin bounds using the reduced regularization strategy. In addition, we only need to check the inequality condition by Gershgorin theorem in a reduced space. Though the Hessian is constant for all states values in CSTR example, the efforts to find sufficient weights can be reduced for other general cases.

Next, we will compare the control performances of the following 3 controllers:

- Controller 1: pure economic NMPC, with no regularization
- Controller 2: economic NMPC, with full regularization
- Controller 3: economic NMPC, with reduced regularization

It should be noted that CSTR models given by (5.4.1) and(5.4.2) are used for all controllers. The above reduction procedure is only required to determine the regularization weight. For controller 2, we choose regularization weights $q_F = 1.98, q_A = 1.55, q_B = 0.44$, and for controller 3, we choose $q_F = 1.55, q_A = 1.55, q_B = 0$.

The control performances of the above 3 controllers are shown in the following figures. For pure economic NMPC controller 1, we observe oscillatory profiles for both controls and states. After adding regularization terms, both controllers 2 and 3 are able to drive the process to the optimal steady state.

As for the economic performance, the accumulated cost $\sum_{k=0}^{K} \psi^{ec}(x(k), u(k))$ for controllers 1-3 are shown in Table 5.1. Since controllers 2 and 3 approach steady states quickly, we firstly compare the economic performance in the transient process by choosing $K = 10$ NMPC cycles. From Table 5.1, we can see that pure economic NMPC controller has the best economic performance, though it leads to cyclic operations. After adding regularization terms, both controllers 2 and 3 have worse economic performance than pure economic NMPC. However, we can see that by using the reduced regularization strategy, we obtain a slightly better economic performance than using the full space regularization strategy. Since economic NMPC

keeps oscillating in this case study, we also compare the accumulated economic stage cost for $K = 50$ NMPC cycles. From Table 5.1, we find that pure economic NMPC achieves better economic performance by not converging to the optimal steady state. However, such cyclic operations may not be favored for practical process operations.

Table 5.1: Accumulated economic stage cost for CSTR example

	K = 10	K = 50
Controller 1	-164.14	- 666.56
Controller 2	-160.90	- 659.57
Controller 3	-161.15	- 659.81

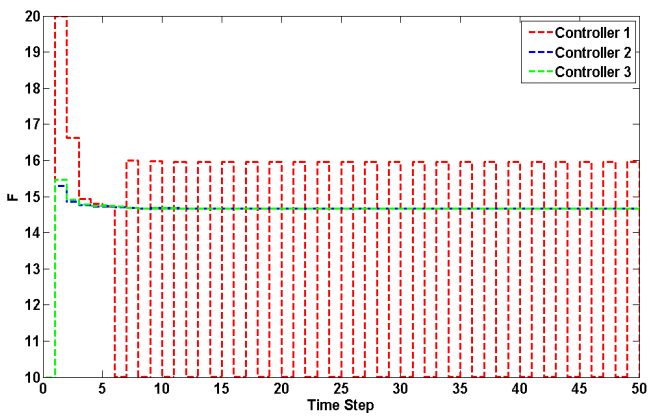

Figure 5.1: Comparison of control profiles in CSTR example

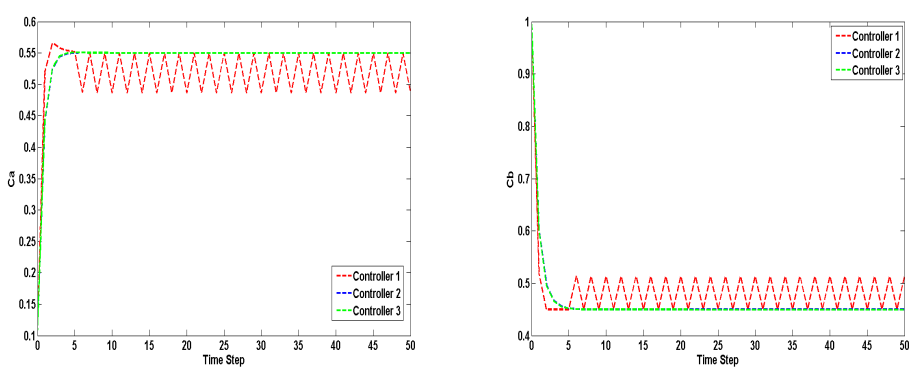

Figure 5.2: Comparison of states profiles in CSTR example

In this section, we demonstrate the idea of the reduced regularization strategy by studying the economic NMPC problem for a nonlinear CSTR. In this example, to drive the process to the optimal steady state, regularization terms need to be added to the economic NMPC controller. From the case study, we can see that economic NMPC can achieve a less conservative economic performance by using the proposed reduced regularization strategy than the full regularization.

5.4.2 Economic NMPC of a Solid Sorbent-Based CO_2 Capture System

In the previous NMPC case for BFB reactors, we study setpoint tracking NMPC to control the plant at certain setpoints and reject process disturbances, which are the traditional goals for NMPC. As we know, the operation of CO_2 capture process for power plants is energy intensive, which requires more sophisticated strategies to reduce the energy consumption of the process. To handle this problem, we want to consider economic NMPC to minimize the operational cost of the CO_2 capture system.

In this section, we present an economic NMPC case study of an integrated CO_2 capture system. In the case study, we will compare the economic performance of economic NMPC and setpoint tracking NMPC. We will also apply the proposed regularization strategy and demonstrate its performance. An illustration of the solid sorbent-based post-combustion CO_2 capture system studied in the case study is shown in Figure 5.3. BFB reactors are the key components of this system and are used to remove CO_2 from fluegas and regenerate the solid sorbents. For the operation of the system, flue gas from the power plant is fed into the BFB adsorber at the bottom. In the adsorber, CO_2 is adsorbed via gas-solid reactions and the clean gas exists at the top. Since these reactions are exothermic reactions, cooling water is used to remove the reaction heat and enhance the adsorption of CO_2. The loaded solid sorbent is fed into the regenerator, which operates at higher temperature range to release the CO_2 captured by the solid sorbent. In the regenerator,

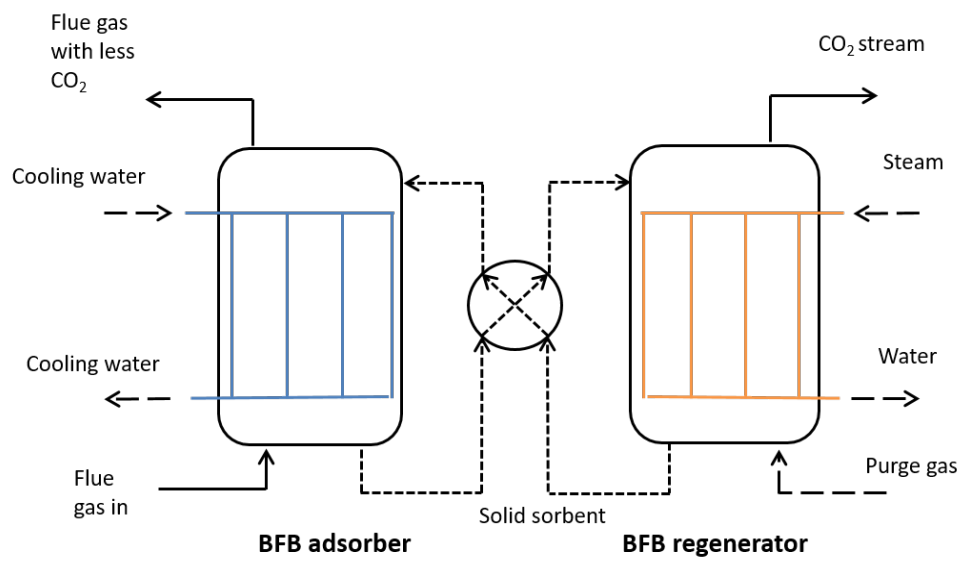

Figure 5.3: Schematic of the integrated carbon capture system

steam and purge stream is used to maintain high temperature which favors the desorption process. Then fresh solid sorbent is cooled down through the heat exchanger and recycled back to the adsorber. Similarly, pre-heating is also provided to loaded sorbent before it is transported into the regenerator.

The economic NMPC problem formulation for the integrated carbon capture system is written as follows:

$$\min_{z_l, v_l} \Psi(z_N) + \sum_{l=0}^{N-1} \psi^{ec}(z_l, v_l) \tag{5.4.13}$$

$$\text{s.t.} \quad z_{l+1} = f(z_l, v_l), \quad l = 0, \ldots N-1$$

$$z_0 = x(k)$$

$$z_l \in \mathbb{X}, v_l \in \mathbb{U}.$$

The model used in the NMPC controller is two interconnected BFB models, with over 1000 states after spatial discretization using orthogonal collocation on finite element. For state constraints, bounds on regenerator temperature and pressure are considered for safety reasons. In addition, bounds on control inputs and limits

on maximum moves are also added in this problem. In this case study, we use the NMPC formulation with quadratic terminal cost with large weights. The sampling time is 50 seconds and the prediction horizon is 1500 seconds which is long enough to satisfy the terminal constraint implicitly. The dynamic optimization problem in NMPC controller is discretized in time using a 3-point Radau collocation on finite elements. To reduce the NLP size, we apply the input and state blocking strategy using 5 finite elements with lengths equal $[50 \quad 50 \quad 200 \quad 600 \quad 600]$. The discretized model is implemented in AMPL [31] and the NMPC problem is solved using IPOPT [85]. The computational tests are conducted on an Intel i7-3770 3.40 GHz PC.

For the economic NMPC case study, we want to minimize the operational cost of the integrated carbon capture system while satisfying the environmental constraint on the CO_2 removal fraction. The economic stage cost $\psi^{ec}(x, u) = p_1 u_1 + p_2 u_2$, where u_1 and u_2 are two manipulated variables of the system; while p_1 and p_2 are the corresponding unit prices. Two manipulated variables of this system are the flowrate of cooling water used to cool down the fresh solid sorbent and the flowrate of purge gas fed into the regenerator. To satisfy the environmental requirement on CO_2 capture, we also add a lower bound for CO_2 removal fraction in the economic NMPC problem. In this case study, the economic stage cost only involves two manipulated variables.

Next we discuss the regularization weight calculation for economic NMPC. The steady state problem for economic NMPC of the CO_2 capture system has over 1000 differential variables and over 7000 algebraic variables. Firstly, we can find the sufficient regularization weights for all the variables using using the strategy outlined in [44]. But here we consider only the regularization weights that satisfy the inequality condition (5.2.11) only at the optimal steady states. The regularization weights for all variables (larger than 1) are shown in Figure 5.4. It should be noted that the y axis is in the log scale and we can see that very large regularization

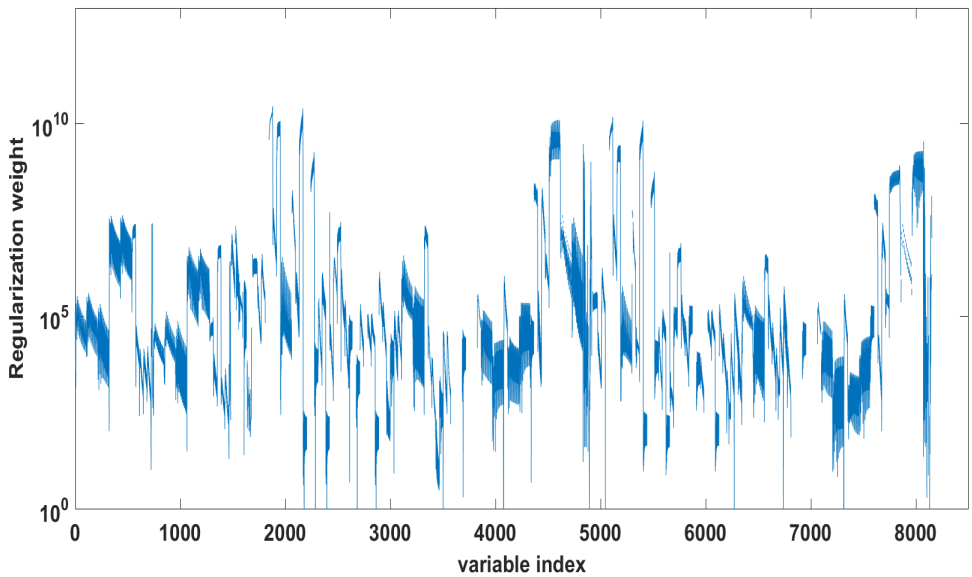

Figure 5.4: Regularization weight for all variables in economic NMPC

weights are required for some variables. In addition, we only check the inequality condition (5.2.11) at optimal steady states to obtain this result, even though it must be checked for all feasible values of all variables; this can be an intractable task for the problem with this size. Therefore it is difficult to directly apply the strategy outlined in [44] and the regularization weights calculated in this way can be very large.

To handle this issue, we apply the proposed strategy to find sufficient regularization for a subset of system states. By studying the steady state optimization problem, we find that only CO_2 removal fraction is active at its lower bound for the optimal solution. Since the removal fraction is directly determined by the gas concentrations at the top of the BFB adsorber, we choose the concentrations of three gas species as critical states. In addition, we also choose a temperature state as a critical state since it involves safety constraints. Besides that, we want to consider two manipulated variables for regularization analysis, because they are directly involved in the economic stage cost. In the following case study, these 6 variables are considered for regularization analysis.

To determine sufficient regularization weights for these critical states, we calculate the reduced Hessian given by (5.3.43) using numerical perturbations. The reduced Hessian is calculated at different sampling points within the feasible regions of 6 variables, and we determine the minimum regularization weight that make the reduced Hessian positive definite at all these sampling points. Compared with full regularization, the calculation process is greatly simplified since we only sample values for 6 variables rather than the complete set of over 8000 variables.

Instead of using the Gershgorin theorem to determine the minimum regularization weight, we also consider finding the minimum weight by eigenvalue decomposition using a diagonal regularization matrix $\bar{Q} = qI$, where q can be determined by (5.3.45). In the case study, we find that the reduced Hessian matrix has small negative eigenvalues, thus we can obtain much smaller regularization weights by (5.3.45) than using condition (5.3.44) given by Gershgorin theorem. From the test results, we find that $q = 60$ such that the regularized reduced Hessian matrix is positive definite at all sample points of the 6 variables. It should be noted that the regularization weight is the same for all the regularized variables, which is different from regularization weight calculated based on Gershgorin theorem.

Next we compare the performances of the following controllers in the case study.

- Controller 1: setpoint-tracking NMPC
- Controller 2: pure economic NMPC, with no regularization
- Controller 3: economic NMPC, with reduced regularization

For Controller 1, the objective includes quadratic tracking terms $x^T Q_x x + u^T Q_u u$. The weighting matrix Q_x for scaled states is an identity matrix while Q_u is a diagonal matrix with diagonal elements p_1 and p_2. For Controller 2, the economic stage cost $p_1 u_1 + p_2 u_2$ is used as objective; while for Controller 3, in addition to the economic stage cost, a regularization term $\frac{1}{2}\bar{x}^T \bar{Q} \bar{x}$ with diagonal element $q_r = 60$ is also added to the objective. In the case study, these controllers are initialized

with the same initial states and we will compare the control performance during the transient response.

Firstly we look at the nominal case. The simulation profiles are shown in the following figures.

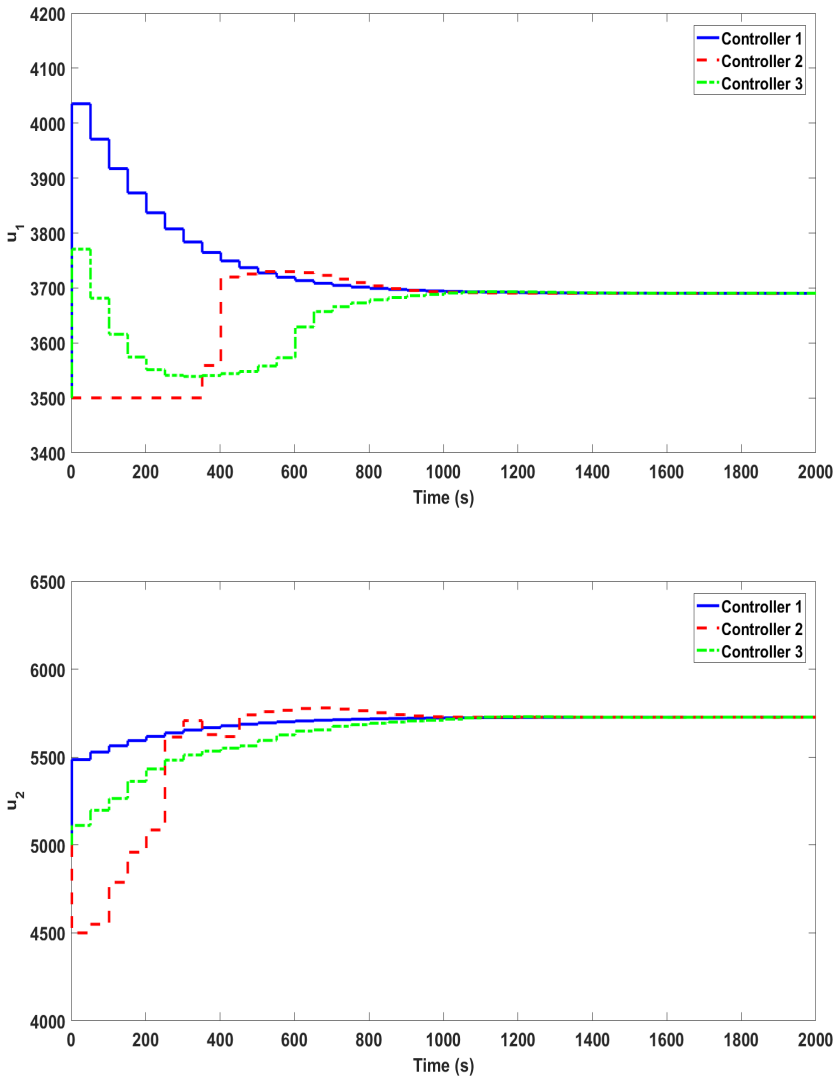

Figure 5.5: Comparison of control profiles in the nominal case

In Figure 5.5, control profiles of controllers 1-3 are plotted. Selected state profiles of controllers 1-3 are shown in Figure 5.6. x_1 - x_3 represent the concentrations of

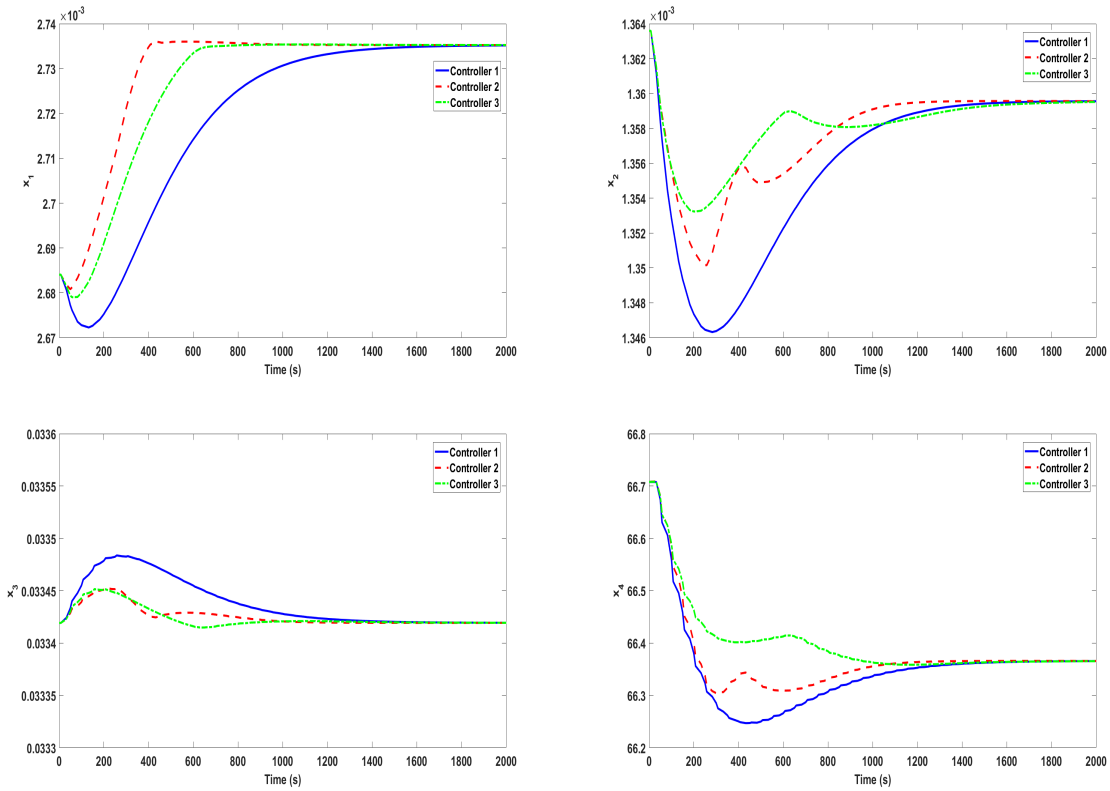

Figure 5.6: Comparison of states profiles in the nominal case

CO_2, H_2O and N_2 at the top of BFB adsorber and x_4 represents the gas temperature state at the top of the BFB adsorber. From these figures we can see that all three controllers converge to the optimal steady state, including pure economic NMPC. However, it should be noted that unregularized economic NMPC is not guaranteed to converge to optimal steady state, since economic NMPC may achieve a lower economic objective by not going to steady state. In addition, it should be noted that, for this case study, if the terminal constraints are removed, then pure economic NMPC may drive the process to suboptimal steady state, though the open-loop solution of each NMPC iteration is not steady. Similar phenomena are reported in [34]. With special turnpike property and controllability properties, the controller without terminal constraints may converge to a neighborhood of the optimal steady state. But even here regularization terms and terminal constraints may still be needed for economic NMPC to drive the process to the optimal steady state.

Table 5.2: Accumulated economic stage cost for the nominal case

	K = 20
Controller 1	4152321.69
Controller 2	4019062.41
Controller 3	4044969.02

In Figure 5.5, compared with setpoint tracking NMPC, Controller 2 penalizes the usage of u_1 and u_2 in the initial stages because the economic stage cost is directly minimized in pure economic NMPC. On the other hand, it leads to more oscillatory control profiles. Regularized NMPC has a similar trend as pure economic NMPC, but it has smoother control profiles due to the regularization terms added.

Next we study the economic performances by comparing the accumulated economic stage cost $\sum_{k=0}^{K} \psi^{ec}(x(k), u(k))$ during the transient process. Since the control moves become almost steady after 20 NMPC cycles, we choose $K = 20$. For pure economic NMPC, it achieves 3.21% reduction in the accumulated economic stage compared tracking NMPC. For regularized economic NMPC, the economic performance is sacrificed slightly due to the regularization terms, but it is still 2.59% less than setpoint tracking NMPC.

Next we consider the performance of controllers 1-3 in the robust case with additive measurement noises. In the case study, we add the measurement noises with standard deviations of 1% of optimal steady state values. For robust case, the control profiles are plotted in Figure 5.7 and selected states profiles are shown in Figure 5.8.

Firstly, from Figure 5.7, we observe that pure economic NMPC controller has the most oscillatory control profiles, especially for u_2, the flowrate of the purge gas fed into the regenerator. By adding the regularization terms, the regularized economic NMPC has less oscillatory control profiles in the robust case. It should be noted that the performance of regularized economic NMPC is also different from the setpoint tracking NMPC, since only regularization for 6 variables is added to controller 3.

Table 5.3: Accumulated economic stage cost for the robust case

	K = 20
Controller 1	4180053.94
Controller 2	4017700.93
Controller 3	4051150.66

The oscillatory control profiles also lead to the oscillations in the state profiles, which is shown in Figure 5.8. In addition to the states on the adsorber side ($x_1 - x_4$), 4 selected states from the regenerator side are also plotted in Figure 5.8. $x_5 - x_8$ represent the loading of 3 species in the solid sorbent and gas temperature respectively. From Figure 5.8, we can see that pure economic NMPC leads to the most oscillatory state profiles, especially for 4 states on the regenerator side. By adding regularization terms, we observe that state profiles are less oscillatory and closer to optimal steady state.

As for the economic performances in the robust case, the accumulated economic stage cost $\sum_{k=0}^{K} \psi^{ec}(x(k), u(k))$ in the first 20 time steps are listed in Table 5.3. In this case, we can observe a similar improvement in the economic performance by economic NMPC over setpoint tracking NMPC as in the nominal case.

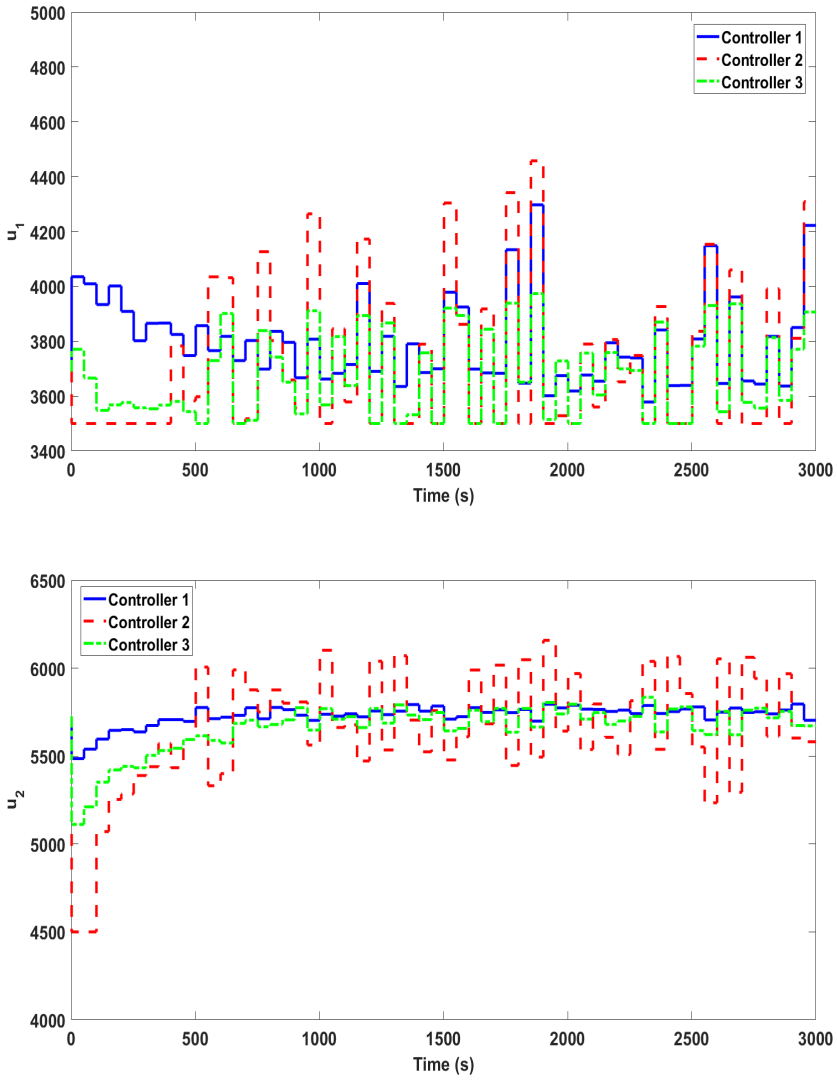

Figure 5.7: Comparison of control profiles in the robust case

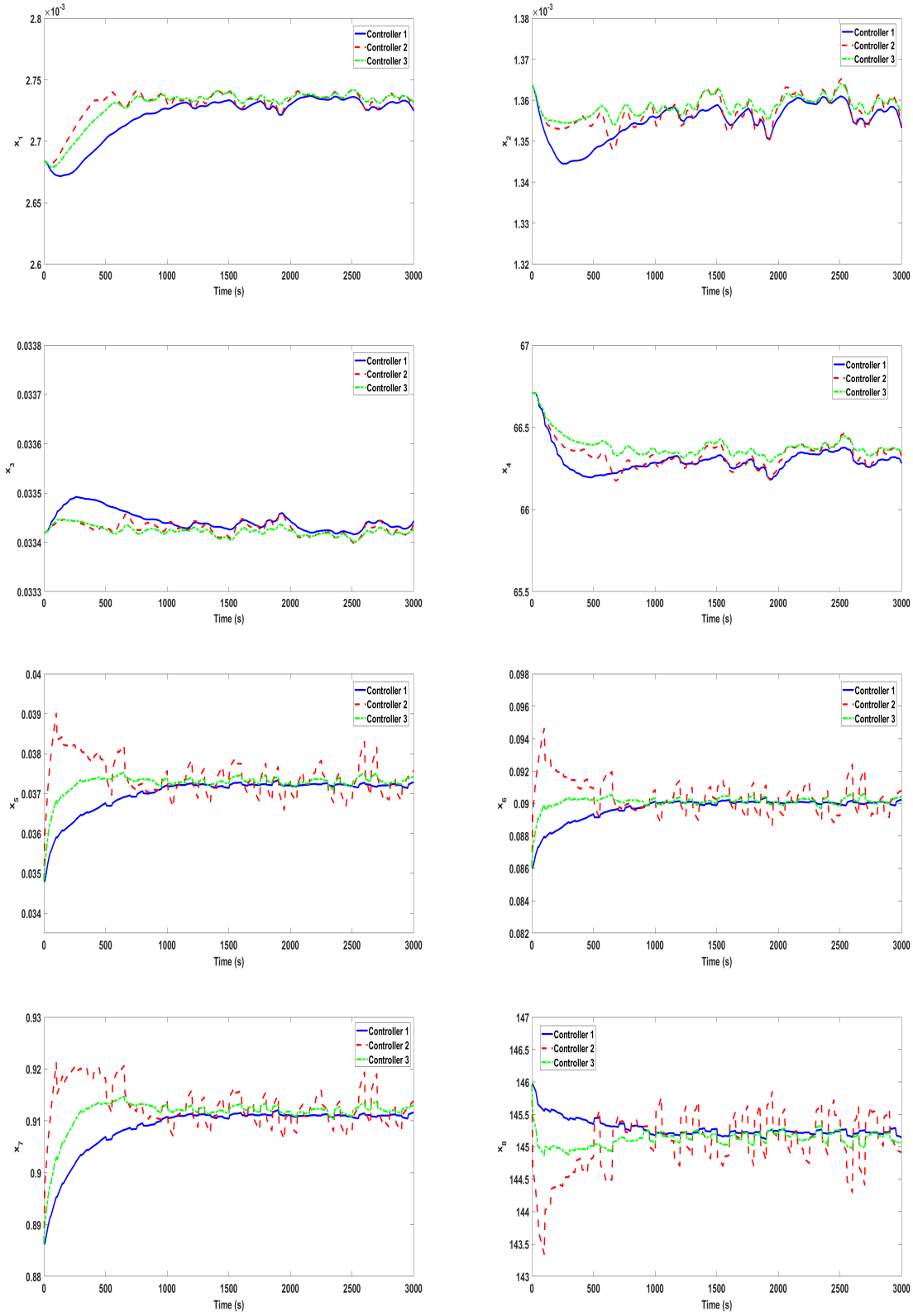

Figure 5.8: Comparison of states profiles in the robust case

5.5 Concluding Remarks

In this chapter, we focus on the economic NMPC problem for large-scale DAE systems. The stability of economic NMPC controller can be guaranteed if specific properties, such as dissipativity and strong duality, hold true for the economic stage cost and process model. In general cases, regularization terms are needed to enforce such properties. In this chapter, we propose an economic NMPC formulation with reduced sets of regularization. Compared with full regularization, the regularization strategy with a reduced set of states is much simpler to implement and may lead to less conservative economic performance. To determine the regularization weight, we show that algebraic variables can be removed without affecting the stability results. Moreover, a subset of system states can be removed from the regularization analysis. By adding a reduced regularization, the economic NMPC has the ISpS property, with the assumption that derivations of unregulated states from their algebraic predictions are bounded. With stronger assumptions, asymptotic stability can be achieved by reduced regularization. The proposed strategy has been applied to a case study on an integrated CO_2 capture system. In the case study, we demonstrate that adding reduced regularization improves the economic NMPC controller performance especially in robust cases while still getting improved economic performance over setpoint tracking NMPC. In addition, the procedures to determine sufficient regularization weights are greatly simplified and can be applied to economic NMPC of large-scale DAE systems.

For future work, one important task is to develop systematic approaches to determine the critical states for general applications, which are crucial to the performance of regularized economic NMPC. In terms of regularization weight calculations, other strategies like semidefinite programming may be considered to find less conservative regularization weights that can guarantee the stability of the economic NMPC.

Chapter 6

Conclusions

6.1 Thesis Summary and Contributions

For dynamic process operations, first-principles process models provide accurate predictions of process dynamics and they are crucial for dynamic simulation, offline optimization and nonlinear model predictive control (NMPC). In addition, the integration of RTO and APC layers via economic NMPC is a promising solution to improve the overall economic performance for complex integrated process systems. However, it should be noted that successful applications of these strategies always require efficient solutions, which could be challenging with tighter integration of separate layers and increasing applications of more detailed first-principles models.

This dissertation studies some computational and analytic challenges for dynamic process operations brought by large-scale spatially distributed first-principles process models. Specifically, in this thesis, we study the operation problems of a solid sorbent-based CO_2 capture system with bubbling fluidized bed (BFB) reactors as key components. The BFB model is described by a large-scale nonlinear system of partial-differential algebraic equations. Specific tasks for this thesis include dy-

namic model reduction, input and state blocking formulation for NMPC and regularization strategies for economic NMPC. These proposed strategies are demonstrated on the setpoint tracking NMPC and economic NMPC of the BFB reactors with applications in CO_2 capture.

This thesis can be summarized as follows:

Chapter 1 reviews the process operation regime and provides an overview for the research work in this thesis.

Chapter 2 provides background and literature reviews for the tasks in the dissertation, including MPC stability, computational strategies and model reduction techniques, which provides a basis for the discussions in Chapter 3 to 5.

Chapter 3 deals with the model reduction for the dynamic first-principles BFB reactor, which is described by a large-scale partial differential and algebraic equations system. To handle the computational challenges, we utilize temporal and spatial model reduction techniques to develop computationally efficient dynamic reduced models that are suitable for time-critical applications, such as NMPC. The major contributions of this chapter are:

- Develop temporally dynamic reduced models for the BFB reactor with 40% simulation time reduction, by utilizing nullspace projection and eigenvalue analysis methods to reduce the stiffness of the DAE system.
- Develop a spatially dynamic reduced model for the BFB reactor with 60% time reduction and good prediction accuracy using orthogonal collocation on non-uniformly distributed finite elements to reduce the number of model equations after spatial discretization.
- Combine the temporal and spatial model reduction to generate a computationally efficient dynamic reduced model with accurate prediction capacity; and compare the advantage and disadvantages of various model reduction

techniques using the BFB example.

Chapter 4 focuses on improving computational efficiency for NMPC of large-scale first-principles models. For processes with strong nonlinearities, NMPC provides superior performance over linear MPC in terms of setpoint tracking and disturbance rejection. However, directly incorporating detailed first-principles models into NMPC may lead to significant computational delay which can degenerate the control performance. To handle this issue, we propose to use non-uniform grids in the direct transcription of process models for NMPC and incorporate dynamic reduced models developed in the previous chapter to reduce the computational burden for NMPC of the BFB adsorber. In this chapter, our contributions are:

- Propose an input and state blocking strategy to reduce NLP problem size for NMPC and apply it in a moving horizon blocking scheme for NMPC.
- Analyze the stability property for moving horizon blocking NMPC and show that nominal and robust stability can be maintained with potential recourse to the cyclic shifted blocking scheme.
- Incorporate the dynamic reduced BFB model developed in Chapter 3 into the NMPC framework and introduce additive correction terms to handle the model mismatch, which guarantees an offset-free control performance.
- Integration of dynamic reduced models and blocking strategies lead to an order of magnitude reduction of NMPC computational time, with almost no sacrifice in control performance.
- Apply advanced step NMPC to reduce the online computational delay and enable online control of the BFB reactor.

Chapter 5 studies the economic NMPC of large-scale DAE systems. Economic NMPC directly optimizes the process economics based on first-principles process models. To guarantee the stability of economic NMPC, quadratic regularization

terms are usually required. In this chapter, we study the regularization strategy with focuses on reduced sets of states, which is much simpler to implement and lead to less conservative economic performance than full regularization. The proposed strategy has been tested in the economic NMPC of an integrated carbon capture system aiming at reducing its operational costs. In this chapter, our specific contributions are:

- Propose a regularization strategy for reduced sets of states to stabilize economic NMPC controller of large-scale DAE systems, with simpler analysis process and potentially less conservative regularization weights than full regularization strategy.
- Analyze the stability property of reduced regularization for economic NMPC of DAE systems. To determine the regularization weight, we show that algebraic variables can be removed without affecting the stability results. Moreover, a subset of system states can be removed as well and the stability property of economic NMPC can be guaranteed under additional assumptions.
- Apply the proposed reduced regularization strategy to the economic NMPC case study of an integrated carbon capture system. In the case study, reduced regularization strategy generates much smaller regularization weights than full regularization and the reduced regularization can still maintain the stability of the economic NMPC controller in the nominal and robust cases.

6.2 Recommendations for Future Work

In this section, we provide some recommendations for future work.

6.2.1 Model Reduction

In chapter 3, we develop computationally efficient dynamic reduced models using temporally and spatially model reduction techniques. These techniques are generally applicable to other nonlinear dynamic systems and we compare the advantages and disadvantages of various methods using the BFB example [93]. In the case study, we identify the limitations of POD methods and find that though it may lead to significant reduction in the model size, the computational cost may not be reduced due to the sparsity is destroyed with POD method with Galerkin projection. To handle this issue, POD with collocation formulation [83] may be considered. In addition, improved strategies like missing point estimation [10] and discrete empirical interpolation method [21] can be applied to improve the effectiveness of the POD method.

Note that in this thesis, we focus on physics-based model reduction techniques. However, it would be interesting to study data-driven techniques and compare the performances of reduced models generated by both physics-based and data-driven methodologies in the dynamic simulation, optimization and control applications.

6.2.2 Blocking Strategy for NMPC

In chapter 4, we introduce an input and state blocking strategy for NMPC and apply it online as moving horizon blocking NMPC. This strategy can be applied to general NMPC formulations, and leads to significant reduction of the NLP size of each NMPC problem [92]. As discussed in chapter 4, the choices of blocking scheme directly affect the performance of moving horizon blocking NMPC and they depends on the dynamic characteristics of specific processes. Therefore, it's worthwhile to develop a systematic scheme to determine optimal blocking strategy for NMPC. This work can be done offline via studying the representative dynamic trajectories from process simulation/plant data. Optimal blocking scheme can be

determined by balancing the state approximation errors and block numbers.

6.2.3 Regularization Strategy for Economic NMPC

In chapter 5, we study the regularization strategy to design stable economic NMPC controller and propose the reduced regularization strategy. The key idea is that we only focus on a set of critical states for stability analysis and regularization, which could reduce efforts in finding sufficient regularization weights and lead to less conservative economic performance. It should be noted that the selection of critical states will affect the regularization weights and the control performance. Right now there is no unifying criterion to determine critical states. Therefore it's important to develop a systematic approach to select critical states. Based on the previous stability results, we can see that dynamic states that have similar performance as their algebraic counterparts may be removed from regularization analysis by treating them as algebraic variables. These states can be located via time scale analysis of the original system. In addition, we can apply sensitivity analysis of the optimization problem and structural analysis of the dynamic model to provide insights for critical state selection.

6.2.4 Other Areas

To implement NMPC online in real plants, additional tasks should also be considered. For example, fast state estimation is required to enable NMPC and sensitivity based fast NMPC algorithms. In addition to some commonly used state estimators such as extended Kalman filter, moving horizon estimation (MHE) [70] provides an attractive alternative to constrained state estimation for nonlinear systems. Similar to NMPC, MHE solves a dynamic optimization strategy based on first-principles models in a rolling horizon manner. Therefore the blocking strategy and model reduction work can be extended to MHE as well. In addition, to handle the com-

putational burden for MHE, the advanced step strategy has also been applied in [40] to reduce the online cost. Another important topic is handling the uncertainty for optimization and control. For NMPC, there may exist model mismatch between the first-principles model and real process, and model reduction can introduce additional errors in the states predictions. To account for this, strategies like back-off constraints [80] and multi-scenario formulations [42] can be considered to avoid violations of critical constraints under model uncertainties.

Bibliography

[1] Anshul Agarwal, Lorenz T Biegler, and Stephen E Zitney. Simulation and optimization of pressure swing adsorption systems using reduced-order modeling. *Industrial & Engineering Chemistry Research*, 48(5):2327–2343, 2008.

[2] Johan Åkesson, Carl D Laird, Geoffry Lavedan, Katrin Prölss, Hubertus Tummescheit, Stéphane Velut, and Yu Zhu. Nonlinear model predictive control of a co2 post-combustion absorption unit. *Chemical Engineering & Technology*, 35(3):445–454, 2012.

[3] Henk Aling, Suman Banerjee, Anil K Bangia, Vernon Cole, Jon Ebert, Abbas Emami-Naeini, Klavs F Jensen, Ioannis G Kevrekidis, and Stanislav Shvartsman. Nonlinear model reduction for simulation and control of rapid thermal processing. In *American Control Conference*, volume 4, pages 2233–2238. IEEE, 1997.

[4] Leonard R Anderson. Pole placement and order reduction in two-time-scale control systems through riccati iteration. *Mathematical Modelling*, 3(1):93–101, 1982.

[5] David Angeli, Rishi Amrit, and James B Rawlings. Receding horizon cost optimization for overly constrained nonlinear plants. In *Proceedings of the 48th IEEE Conference on Decision and Control and 28th Chinese Control Conference*, pages 7972–7977. IEEE, 2009.

[6] David Angeli, Rishi Amrit, and James B Rawlings. On average performance and stability of economic model predictive control. *IEEE transactions on automatic control*, 57(7):1615–1626, 2012.

[7] Athanasios C Antoulas and Dan C Sorensen. Approximation of large-scale dynamical systems: An overview. *Applied Mathematics and Computer Science*, 11(5):1093–1122, 2001.

[8] Antonios Armaou and Panagiotis D Christofides. Finite-dimensional control of nonlinear parabolic pde systems with time-dependent spatial domains using empirical eigenfunctions. *Applied Mathematics and Computer Science*, 11(2):287–318, 2001.

[9] Uri M Ascher and Linda R Petzold. *Computer methods for ordinary differential equations and differential-algebraic equations*, volume 61. Siam, 1998.

[10] Patricia Astrid, Siep Weiland, Karen Willcox, and Ton Backx. Missing point estimation in models described by proper orthogonal decomposition. *IEEE Transactions on Automatic Control*, 53(10):2237–2251, 2008.

[11] Michael Baldea and Prodromos Daoutidis. *Dynamics and nonlinear control of integrated process systems*. Cambridge University Press, 2012.

[12] Eugene Bendersky and Panagiotis D Christofides. Optimization of transport-reaction processes using nonlinear model reduction. *Chemical Engineering Science*, 55(19):4349–4366, 2000.

[13] Gal Berkooz, Philip Holmes, and John L Lumley. The proper orthogonal decomposition in the analysis of turbulent flows. *Annual review of fluid mechanics*, 25(1):539–575, 1993.

[14] Lorenz T Biegler. *Nonlinear programming: concepts, algorithms, and applications to chemical processes*. SIAM, 2010.

[15] Lorenz T Biegler and Victor M Zavala. Large-scale nonlinear programming using ipopt: An integrating framework for enterprise-wide dynamic optimization. *Computers & Chemical Engineering*, 33(3):575–582, 2009.

[16] Mai Bui, Indra Gunawan, Vincent Verheyen, Paul Feron, Erik Meuleman, and Sam Adeloju. Dynamic modelling and optimisation of flexible operation in post-combustion co 2 capture plants—a review. *Computers & Chemical Engineering*, 61:245–265, 2014.

[17] Raphael Cagienard, Pascal Grieder, Eric C Kerrigan, and Manfred Morari. Move blocking strategies in receding horizon control. *Journal of Process Control*, 17(6):563–570, 2007.

[18] Long Cai and Ralph E White. Reduction of model order based on proper orthogonal decomposition for lithium-ion battery simulations. *Journal of The Electrochemical Society*, 156(3):A154–A161, 2009.

[19] Ian T Cameron and Ashley M Walsh. *The Integration of Process Design and Control*, volume 17, chapter A5 Unravelling Complex System Dynamics Using Spectral Association Methods, pages 126–145. Elsevier, 2004.

[20] GF Carey and Bruce A Finlayson. Orthogonal collocation on finite elements. *Chemical Engineering Science*, 30(5-6):587–596, 1975.

[21] Saifon Chaturantabut and Danny C Sorensen. Nonlinear model reduction via discrete empirical interpolation. *SIAM Journal on Scientific Computing*, 32(5):2737–2764, 2010.

[22] Yang Chen, John Eslick, Ignacio Grossmann, and David Miller. Simultaneous optimization and heat integration based on rigorous process simulations. In *8th International Conference on Foundations of Computer-Aided Process Design*, 2014.

[23] Panagiotis Christofides and Prodromos Daoutidis. Feedback control of two-time-scale nonlinear systems. *International Journal of Control*, 63(5):965–994, 1996.

[24] Alison Cozad, Nikolaos V Sahinidis, and David C Miller. Learning surrogate models for simulation-based optimization. *AIChE Journal*, 60(6):2211–2227, 2014.

[25] Charles R Cutler and Brian L Ramaker. Dynamic matrix control - a computer control algorithm. In *Joint automatic control conference*, number 17, page 72, 1980.

[26] Moritz Diehl, Rishi Amrit, and James B Rawlings. A lyapunov function for economic optimizing model predictive control. *IEEE Transactions on Automatic Control*, 56(3):703–707, 2011.

[27] Matthew Ellis, Helen Durand, and Panagiotis D Christofides. A tutorial review of economic model predictive control methods. *Journal of Process Control*, 24(8):1156–1178, 2014.

[28] José D Figueroa, Timothy Fout, Sean Plasynski, Howard McIlvried, and Rameshwar D Srivastava. Advances in co2 capture technology—the us department of energy's carbon sequestration program. *International journal of greenhouse gas control*, 2(1):9–20, 2008.

[29] Rolf Findeisen, Lars Imsland, Frank Allgöwer, and Bjarne A Foss. Output feedback stabilization of constrained systems with nonlinear predictive control. *International Journal of robust and nonlinear control*, 13(3-4):211–227, 2003.

[30] BA Finlayson and LE Scriven. The method of weighted residuals—a review. *Appl. Mech. Rev*, 19(9):735–748, 1966.

[31] Robert Fourer, David Gay, and Brian Kernighan. *Ampl*, volume 117. Boyd & Fraser, 1993.

[32] Carlos E Garcia and AM Morshedi. Quadratic programming solution of dynamic matrix control (qdmc). *Chemical Engineering Communications*, 46(1-3):73–87, 1986.

[33] Ravi Gondhalekar and Jun-ichi Imura. Least-restrictive move-blocking model predictive control. *Automatica*, 46(7):1234–1240, 2010.

[34] Lars Grüne. Economic receding horizon control without terminal constraints. *Automatica*, 49(3):725–734, 2013.

[35] Juergen Hahn and Thomas F Edgar. An improved method for nonlinear model reduction using balancing of empirical gramians. *Computers & chemical engineering*, 26(10):1379–1397, 2002.

[36] William E Hart, Carl Laird, Jean-Paul Watson, and David L Woodruff. *Pyomo–optimization modeling in python*, volume 67. Springer Science & Business Media, 2012.

[37] Mohsen Heidarinejad, Jinfeng Liu, and Panagiotis D Christofides. Economic model predictive control of nonlinear process systems using lyapunov techniques. *AIChE Journal*, 58(3):855–870, 2012.

[38] Achim Helbig, Olaf Abel, and Wolfgang Marquardt. Structural concepts for optimization based control of transient processes. In *Nonlinear Model Predictive Control*, pages 295–311. Springer, 2000.

[39] Rui Huang, Lorenz T Biegler, and Eranda Harinath. Robust stability of economically oriented infinite horizon nmpc that include cyclic processes. 2012.

[40] Rui Huang, Lorenz T Biegler, and Sachin C Patwardhan. Fast offset-free nonlinear model predictive control based on moving horizon estimation. *Industrial & Engineering Chemistry Research*, 49(17):7882–7890, 2010.

[41] Rui Huang, Eranda Harinath, and Lorenz T Biegler. Lyapunov stability of economically oriented nmpc for cyclic processes. *Journal of Process Control*, 21(4):501–509, 2011.

[42] Rui Huang, Sachin C Patwardhan, and Lorenz T Biegler. Multi-scenario-based robust nonlinear model predictive control with first principle models. *Computer Aided Chemical Engineering*, 27:1293–1298, 2009.

[43] Rui Huang, Victor M Zavala, and Lorenz T Biegler. Advanced step nonlinear model predictive control for air separation units. *Journal of Process Control*, 19(4):678–685, 2009.

[44] Johannes Jäschke, Xue Yang, and Lorenz T Biegler. Fast economic model predictive control based on nlp-sensitivities. *Journal of Process Control*, 24(8):1260–1272, 2014.

[45] Zhong-Ping Jiang and Yuan Wang. Input-to-state stability for discrete-time nonlinear systems. *Automatica*, 37(6):857–869, 2001.

[46] Sathiya Keerthi and Elmer Gilbert. Optimal infinite-horizon feedback laws for a general class of constrained discrete-time systems: Stability and moving-horizon approximations. *Journal of optimization theory and applications*, 57(2):265–293, 1988.

[47] Petar Kokotović, Hassan K Khalil, and John O'reilly. *Singular perturbation methods in control: analysis and design*. SIAM, 1999.

[48] Aditya Kumar and Prodromos Daoutidis. Nonlinear dynamics and control of process systems with recycle. *Journal of Process Control*, 12(4):475–484, 2002.

[49] Daizo Kunii and Octave Levenspiel. *Fluidization Engineering*. John Wiley & Sons Inc., 1969.

[50] Daizo Kunii and Octave Levenspiel. Fluidized reactor models. i: For bubbling beds of fine, intermediate, and large particles. ii: For the lean phase: Freeboard and fast fluidization. *Industrial & Engineering Chemistry Research*, 29(7):1226–1234, 1990.

[51] Sanjay Lall, Jerrold E Marsden, and Sonja Glavaški. Empirical model reduction of controlled nonlinear systems. International Federation of Automatic Control, 1999.

[52] Andrew Lee, D Mebane, DJ Fauth, and DC Miller. A model for the adsorption kinetics of co2 on amine-impregnated mesoporous sorbents in the presence of water. In *28th International Pittsburgh Coal Conference*, 2011.

[53] Andrew Lee and David C Miller. A one-dimensional (1-d) three-region model for a bubbling fluidized-bed adsorber. *Industrial & Engineering Chemistry Research*, 52(1):469–484, 2012.

[54] Grégoire Léonard, Bruno Cabeza Mogador, Ségolène Belletante, and Georges Heyen. Dynamic modelling and control of a pilot plant for post-combustion co_2 capture. *Comput.-Aided Chem. Eng.*, 31:451–456, 2013.

[55] Han-Xiong Li and Chenkun Qi. Modeling of distributed parameter systems for applications—a synthesized review from time–space separation. *Journal of Process Control*, 20(8):891–901, 2010.

[56] D Limon, T Alamo, DM Raimondo, D Muñoz De La Peña, JM Bravo, A Ferramosca, and EF Camacho. Input-to-state stability: a unifying framework for robust model predictive control. In *Nonlinear model predictive control*, pages 1–26. Springer, 2009.

[57] Dennis Y Lu, Robin W Hughes, and Edward J Anthony. Ca-based sorbent looping combustion for co 2 capture in pilot-scale dual fluidized beds. *Fuel Processing Technology*, 89(12):1386–1395, 2008.

[58] Jinliang Ma, Priyadarshi Mahapatra, Stephen E Zitney, Lorenz T Biegler, and David C Miller. D-rm builder: A software tool for generating fast and accurate nonlinear dynamic reduced models from high-fidelity models. *Computers & Chemical Engineering*, 94:60–74, 2016.

[59] Lalo Magni and Riccardo Scattolini. Robustness and robust design of mpc for nonlinear discrete-time systems. In *Assessment and future directions of nonlinear model predictive control*, pages 239–254. Springer, 2007.

[60] Wolfgang Marquardt. Nonlinear model reduction for optimization based control of transient chemical processes. In *AIChE Symposium Series*, pages 12–42. New York; American Institute of Chemical Engineers; 1998, 2002.

[61] David Q Mayne, James B Rawlings, Christopher V Rao, and Pierre OM Scokaert. Constrained model predictive control: Stability and optimality. *Automatica*, 36(6):789–814, 2000.

[62] David C Miller, Madhava Syamlal, David S Mebane, Curt Storlie, Debangsu Bhattacharyya, Nikolaos V Sahinidis, Deb Agarwal, Charles Tong, Stephen E Zitney, Avik Sarkar, et al. Carbon capture simulation initiative: a case study in multiscale modeling and new challenges. *Annual review of chemical and biomolecular engineering*, 5:301–323, 2014.

[63] Srinivasarao Modekurti, Debangsu Bhattacharyya, and Stephen E Zitney. Dynamic modeling and control studies of a two-stage bubbling fluidized bed adsorber-reactor for solid–sorbent co2 capture. *Industrial & Engineering Chemistry Research*, 52(30):10250–10260, 2013.

[64] Zoltan K Nagy, Bernd Mahn, Rüdiger Franke, and Frank Allgöwer. Real-time implementation of nonlinear model predictive control of batch processes in an industrial framework. In *Assessment and Future Directions of Nonlinear Model Predictive Control*, pages 465–472. Springer, 2007.

[65] Yisu Nie, Lorenz T Biegler, Carlos M Villa, and John M Wassick. Reactor modeling and recipe optimization of polyether polyol processes: Polypropylene glycol. *AIChE Journal*, 59(7):2515–2529, 2013.

[66] Benjamin P Omell, Jinliang Ma, Priyadarshi Mahapatra, Mingzhao Yu, Andrew Lee, Debangsu Bhattacharyya, Stephen E Zitney, Lorenz T Biegler, and David C Miller. Advanced modeling and control of a solid sorbent-based co2 capture process. *IFAC-PapersOnLine*, 49(7):633–638, 2016.

[67] Hans Pirnay, Rodrigo López-Negrete, and Lorenz T Biegler. Optimal sensitivity based on ipopt. *Mathematical Programming Computation*, 4(4):307–331, 2012.

[68] David M Prett and Carlos E García. *Fundamental Process Control*. Butterworths, Boston, MA, 1988.

[69] S Joe Qin and Thomas A Badgwell. A survey of industrial model predictive control technology. *Control engineering practice*, 11(7):733–764, 2003.

[70] Christopher V Rao, James B Rawlings, and David Q Mayne. Constrained state estimation for nonlinear discrete-time systems: Stability and moving horizon approximations. *IEEE transactions on automatic control*, 48(2):246–258, 2003.

[71] James B Rawlings and Rishi Amrit. Optimizing process economic performance using model predictive control. In *Nonlinear model predictive control*, pages 119–138. Springer, 2009.

[72] James B Rawlings, David Angeli, and Cuyler N Bates. Fundamentals of economic model predictive control. In *2012 IEEE 51st IEEE Conference on Decision and Control (CDC)*, pages 3851–3861. IEEE, 2012.

[73] James B Rawlings, Dennis Bonné, John B Jorgensen, Aswin N Venkat, and Sten Bay Jorgensen. Unreachable setpoints in model predictive control. *IEEE Transactions on Automatic Control*, 53(9):2209–2215, 2008.

[74] James B Rawlings and David Q Mayne. *Model predictive control: Theory and design*. Nob Hill Pub., 2009.

[75] GA Robertson and IT Cameron. Analysis of dynamic process models for structural insight and model reduction—part 1. structural identification measures. *Computers & chemical engineering*, 21(5):455–473, 1997.

[76] Jacquelien MA Scherpen. Balancing for nonlinear systems. *Systems & Control Letters*, 21(2):143–153, 1993.

[77] Ahmad Shamiri, Mohamed Azlan Hussain, Farouq Sabri Mjalli, Navid Mostoufi, and Mohammad Saleh Shafeeyan. Dynamic modeling of gas phase propylene homopolymerization in fluidized bed reactors. *Chemical Engineering Science*, 66(6):1189–1199, 2011.

[78] Rohan C Shekhar and Jan M Maciejowski. Robust variable horizon mpc with move blocking. *Systems & Control Letters*, 61(4):587–594, 2012.

[79] Jun Shi, Lorenz T Biegler, and Intan Hamdan. Optimization of grade transitions in polyethylene solution polymerization processes. *AIChE Journal*, 2015.

[80] Jun Shi, Lorenz T Biegler, Intan Hamdan, and John Wassick. Optimization of grade transitions in polyethylene solution polymerization process under uncertainty. *Computers & Chemical Engineering*, 95:260–279, 2016.

[81] Lawrence Sirovich. Turbulence and the dynamics of coherent structures. i. coherent structures. *Quarterly of applied mathematics*, 45(3):561–571, 1987.

[82] Bolesław Tabiś and Abdelilah Essekkat. Three-phase multi-compartment model for fluidized-bed catalytic reactors: autothermicity and multiplicity of steady states. *Chemical engineering science*, 47(2):407–419, 1992.

[83] Artemis Theodoropoulou, Raymond A Adomaitis, and Evanghelos Zafiriou. Model reduction for optimization of rapid thermal chemical vapor deposition systems. *IEEE Transactions on Semiconductor Manufacturing*, 11(1):85–98, 1998.

[84] Nishith Vora and Prodromos Daoutidis. Nonlinear model reduction of chemical reaction systems. *AIChE Journal*, 47(10):2320–2332, 2001.

[85] Andreas Wächter and Lorenz T Biegler. On the implementation of an interior-point filter line-search algorithm for large-scale nonlinear programming. *Mathematical programming*, 106(1):25–57, 2006.

[86] Dianne E Wiley, Minh T Ho, and Lindsay Donde. Technical and economic opportunities for flexible co2 capture at australian black coal fired power plants. *Energy Procedia*, 4:1893–1900, 2011.

[87] Inga J Wolf and Wolfgang Marquardt. Fast nmpc schemes for regulatory and economic nmpc–a review. *Journal of Process Control*, 44:162–183, 2016.

[88] Lynn Würth and Wolfgang Marquardt. Infinite-horizon continuous-time nmpc via time transformation. *IEEE Transactions on Automatic Control*, 59(9):2543–2548, 2014.

[89] Xue Yang. *Advanced-Multi-Step and Economically Oriented Nonlinear Model Predictive Control*. PhD thesis, Carnegie Mellon University, 2015.

[90] Xue Yang and Lorenz T Biegler. Advanced-multi-step nonlinear model predictive control. *Journal of process control*, 23(8):1116–1128, 2013.

[91] Xue Yang, Devin W Griffith, and Lorenz T Biegler. Nonlinear programming properties for stable and robust nmpc. *IFAC-PapersOnLine*, 48(23):388–397, 2015.

[92] Mingzhao Yu and Lorenz T Biegler. A stable and robust nmpc strategy with reduced models and nonuniform grids. *IFAC-PapersOnLine*, 49(7):31–36, 2016.

[93] Mingzhao Yu, David C Miller, and Lorenz T Biegler. Dynamic reduced order models for simulating bubbling fluidized bed adsorbers. *Industrial & Engineering Chemistry Research*, 54(27):6959–6974, 2015.

[94] Victor M Zavala. A multiobjective optimization perspective on the stability of economic mpc. *IFAC-PapersOnLine*, 48(8):974–980, 2015.

[95] Victor M Zavala and Lorenz T Biegler. The advanced-step nmpc controller: Optimality, stability and robustness. *Automatica*, 45(1):86–93, 2009.

[96] Victor M Zavala and Lorenz T Biegler. Optimization-based strategies for the operation of low-density polyethylene tubular reactors: nonlinear model predictive control. *Computers & Chemical Engineering*, 33(10):1735–1746, 2009.

Appendix A

BFB Model Equations

This section gives a brief summary of the BFB model equations [52, 53, 63]. In the BFB model, mass and energy balances have been written for all the chemical components in all three regions for both gas and solid phases. Three regions including a bubble region, cloud-wake region and emulsion region are shown in Figure 3.2(a). The differential equations are shown in the following section.

A.1 Differential Equations

Bubble region

- Gas phase component balance

$$\frac{\partial c_{b,j}}{\partial t}\delta A_x = -\frac{\partial G_b y_{b,j}}{\partial x} - A_x \delta K_{bc,j}(c_{b,j} - c_{c,j}) + K_{g,bulk,j} \tag{A.1}$$

- Gas phase energy balance

$$\frac{\partial T_{g,b}}{\partial t} c_{p,g} c_{b,t} A_x \delta = -c_{p,g}\frac{\partial G_b T_{g,b}}{\partial x} - A_x \delta H_{bc}(T_{g,b} - T_{g,c}) + H_{g,bulk} \tag{A.2}$$

Cloud-wake region

- Gas phase component balance

$$\frac{\partial c_{c,j}}{\partial t} f_{cw}\delta\varepsilon_d = \delta K_{bc,j}(c_{b,j} - c_{c,j}) - \delta K_{ce,j}(c_{c,j} - c_{e,j}) - f_{cw}\delta(1-\varepsilon_d) r_{g,c,j} \tag{A.3}$$

- Gas phase energy balance

$$\begin{aligned}\frac{\partial T_{g,c}}{\partial t} A_x c_{p,g} c_{c,t} f_{cw}\delta\varepsilon_d &= A_x\delta H_{bc}(T_{g,b} - T_{g,c}) - A_x\delta H_{ce}(T_{g,c} - T_{g,e}) \\ &- A_x f_{cw}\delta(1-\varepsilon_d)\rho_s a_p h_p (T_{g,c} - T_{s,c}) - A_x f_{cw}\delta(1-\varepsilon_d)\Sigma r_{g,c,j} c_{p,g,c,j}(T_{g,c} - T_{ref})\end{aligned} \tag{A.4}$$

- Solid phase adsorbed species balance

$$\begin{aligned}\frac{\partial n_{c,i}}{\partial t} A_x f_{cw}\delta(1-\varepsilon_d)\rho_s &= -A_x \frac{\partial J_c n_{c,i}}{\partial x} - K_{s,bulk,i} - A_x\delta\rho_s K_{ce,bs}(n_{c,i} - n_{e,i}) \\ &+ A_x f_{cw}\delta(1-\varepsilon_d) r_{s,c,i}\end{aligned} \tag{A.5}$$

- Solid phase energy balance

$$\begin{aligned}\frac{\partial T_{s,c}}{\partial t} c_{p,s}\rho_s A_x f_{cw}\delta(1-\varepsilon_d) &= -\frac{\partial J_c h_{s,c}}{\partial x} A_x - H_{s,bulk} - A_x\delta\rho_s K_{ce,bs}(h_{s,c} - h_{s,e}) \\ &+ A_x f_{cw}\delta(1-\varepsilon_d)\Sigma(r_{g,c,j} c_{p,g,c,j})(T_{g,c} - T_{ref}) + A_x f_{cw}\delta(1-\varepsilon_d)\rho_s a_p h_p (T_{g,c} - T_{s,c})\end{aligned} \tag{A.6}$$

Emulsion region

- Gas phase component balance

$$\frac{\partial c_{e,j}}{\partial t} A_x(1 - f_{cw}\delta - \delta)\varepsilon_d = A_x\delta K_{ce,j}(c_{c,j} - c_{e,j}) - A_x(1 - f_{cw}\delta - \delta)(1-\varepsilon_d) r_{g,e,j} - K_{g,bulk,j} \tag{A.7}$$

- Gas phase energy balance

$$\frac{\partial T_{g,e}}{\partial t} c_{p,g} c_{e,t} A_x (1 - f_{cw}\delta - \delta)\varepsilon_d = A_x \delta H_{ce}(T_{g,c} - T_{g,e}) - A_x(1 - f_{cw}\delta - \delta)(1 - \varepsilon_d)\rho_s a_p h_p (T_{g,e} - T_{s,e})$$
$$- H_{g,bulk} - A_x(1 - f_{cw}\delta - \delta)(1 - \varepsilon_d)\Sigma r_{g,e,j} c_{p,g,e,j}(T_{g,e} - T_{ref}) \tag{A.8}$$

- Solid phase adsorbed species balance

$$\frac{\partial n_{e,i}}{\partial t} A_x (1 - f_{cw}\delta - \delta)(1 - \varepsilon_d)\rho_s = A_x \frac{\partial J_e n_{e,i}}{\partial x} + K_{s,bulk,i} + A_x \delta \rho_s K_{ce,bs}(n_{c,i} - n_{e,i})$$
$$+ A_x(1 - f_{cw}\delta - \delta)(1 - \varepsilon_d) r_{s,e,i} \tag{A.9}$$

- Solid phase energy balance

$$\frac{\partial T_{s,e}}{\partial t} c_{p,s} \rho_s A_x (1 - f_{cw}\delta - \delta)(1 - \varepsilon_d) = A_x \frac{\partial J_e h_{s,e}}{\partial x} + H_{s,bulk} + A_x \delta \rho_s K_{ce,bs}(h_{s,c} - h_{s,e})$$
$$+ A_x(1 - f_{cw}\delta - \delta)(1 - \varepsilon_d)\Sigma r_{g,e,j} c_{p,g,e,j}(T_{g,e} - T_{ref}) + A_x(1 - f_{cw}\delta - \delta)(1 - \varepsilon_d)\rho_s a_p h_p (T_{g,e} - T_{s,e})$$
$$+ \pi d_x h_t \Delta T_{hx} N_x C_r \tag{A.10}$$

Boundary conditions

Flue gas is fed into the reactor at the bottom of the reactor ($x = 0$). equation (A.11) - equation (A.13) give the boundary condition for the upward gas flow.

$$y_{b,j,0} = z_{g,in,j} \tag{A.11}$$

$$G_{b,0} = F_{g,in} \tag{A.12}$$

$$T_{g,b,0} = T_{g,in} \tag{A.13}$$

The solid phase mass and energy balances at the top of the reactor ($x = L$) are given by equation (A.14) - equation (A.15). Since the reactor is in top-feed and over-flow configuration, the addition and removal of solid sorbent are also included.

$$J_{e,L} n_{e,i,L} A_x + F_{s,out} z_{s,out,i} = J_{c,L} n_{c,i,L} A_x + F_{s,in} z_{s,in,i} \tag{A.14}$$

$$J_{e,L} h_{s,e,L} A_x + F_{s,out} h_{s,out} = J_{c,L} h_{s,c,L} A_x + F_{s,in} h_{s,in} \tag{A.15}$$

Similarly, equation (A.16) - equation (A.17) give the solid phase mass and energy balances at the bottom of the reactor ($x = 0$).

$$J_{e,0} n_{e,i,0} A_x = J_{c,0} n_{c,i,0} A_x \tag{A.16}$$

$$J_{e,0} h_{s,e,0} A_x = J_{c,0} h_{s,c,0} A_x \tag{A.17}$$

A.2 Algebraic Equations

The mass and energy balance equations provide a description of gas and solid flow throughout different regions of the reactor. Solving these differential equations requires correlation equations for heat and mass transfer coefficients and hydrodynamic properties of the bed. These algebraic equations can be generally classified into the following categories:

1. Hydrodynamic correlations
2. Heat and mass transfer coefficients
3. Gas phase properties
4. Heat exchanger tube correlations
5. Reaction kinetics

All the algebraic equations are described by Lee and Miller [53]. Some representative equations are briefly discussed below:

Hydrodynamic Correlations

The hydrodynamic model describes the behavior of the fluidized bed, and defines the variables used in other parts of the model. Hydrodynamic properties, such as the gas velocity, size of the rising bubbles, and the voidage of the fluidized bed, can be calculated by correlations derived from experimental studies. For example, the following equation calculates an approximate value for the minimum fluidization velocity v_{mf}:

$$\frac{1.75Re_{mf}^2}{\phi_s \varepsilon_{mf}^3} + \frac{150(1-\varepsilon_{mf})Re_{mf}}{\phi_s^2 \varepsilon_{mf}^3} = Ar \tag{A.1}$$

where the particle Reynolds number Re and Archimedes number Ar are defined as follows:

$$Ar = \frac{d_p^3 \rho_g (\rho_s - \rho_g) g}{\mu_g^2} \tag{A.2}$$

$$Re = \frac{v_e d_p \rho_g}{\mu_g} \tag{A.3}$$

The gas velocity v_e through the emulsion region of the bed can be calculated by:

$$\frac{v_e}{v_{mf}} = \frac{188 \rho_g^{0.089} \mu_g^{0.371} e^{0.508F}}{d_p^{0.568} g^{0.663} (\rho_s - \rho_g)^{0.663} x^{0.244}} \tag{A.4}$$

The following equations are correlations describing the emulsion region voidage, ε_d, and cross-sectional average voidage ε:

$$\frac{1-\varepsilon_{mf}}{1-\varepsilon_d} = \frac{2.54 \rho_g^{0.016} \mu_g^{0.066} e^{0.090F}}{d_p^{0.1} g c^{0.118} (\rho_s - \rho_g)^{0.118} x^{0.043}} \tag{A.5}$$

$$(1-\varepsilon) = (1-\varepsilon_d)(1-\delta) \tag{A.6}$$

The following equations calculate the equilibrium size of a bubble $d_{b,e}$ and the di-

ameter of a bubble $d_{b,x}$ at a given height within the fluidized bed:

$$d_{b,e} = \frac{D_t}{4}(-g_1 + g_3)^2 \tag{A.7}$$

$$\left(\frac{\sqrt{d_{b,x}} - \sqrt{d_{b,e}}}{\sqrt{d_{b,0}} - \sqrt{d_{b,e}}}\right)^{1-\frac{g_1}{g_3}} \left(\frac{\sqrt{d_{b,x}} - \sqrt{g_2}}{\sqrt{d_{b,0}} - \sqrt{g_2}}\right)^{1+\frac{g_1}{g_3}} = e^{-0.3\frac{x}{D_t}} \tag{A.8}$$

where the initial diameter of the bubble $d_{b,0}$ and parameters g_1, g_2 and g_3 are defined as follows:

$$d_{b,0} = 1.38 g^{-0.2}((v_{g,0} - v_{e,0})A_0)^{0.4} \tag{A.9}$$

$$g_1 = 2.56 \times 10^{-2} \frac{\sqrt{\frac{D_t}{g}}}{v_{mf}} \tag{A.10}$$

$$g_2 = \frac{D_t(g_1 + g_3)^2}{4} \tag{A.11}$$

$$g_3 = \sqrt{g_1^2 + \frac{4d_{b,m}}{D_t}} \tag{A.12}$$

Heat and Mass Transfer Coefficients

The gas phase mass transfer between the bubble and cloud-wake regions for each component, and also the coefficient for mass transfer between cloud-wake and emulsion region, are given by the following equations:

$$K_{bc,j} = 5.94\frac{v_{mf}}{d_b} + 5.85\frac{D_j^{0.5} g^{0.25}}{d_b^{5/4}} \tag{A.13}$$

$$K_{ce,j} = 6.77\sqrt{\frac{\varepsilon_d^2 D_j v_b}{d_b^3}} \tag{A.14}$$

Heat transfer coefficients for the gas phase are developed by analogy to the mass transfer coefficients, resulting in the following equations:

$$H_{bc} = 5.94\frac{v_{mf}\rho_g c_{p,g}}{d_b} + 5.85\frac{\sqrt{k_g\rho_g c_{p,g}}g^{0.25}}{d_b^{5/4}} \tag{A.15}$$

$$H_{ce} = 6.78\sqrt{\frac{\varepsilon_d v_b k_g \rho_g c_{p,g}}{d_b^3}} \tag{A.16}$$

The following equation is used to calculate the mass transfer coefficient for the exchange of solids between the cloud-wake and emulsion regions.

$$K_{ce,bs} = \frac{3(1-\varepsilon_d)v_{mf}}{(1-\delta)\varepsilon_d d_b} \tag{A.17}$$

For gas-solid heat transfer, an empirical correlation is used to to relate the Nusselt number Nu_p and the gas-solids heat transfer coefficient h_p:

$$Nu_p = \frac{h_p d_p}{k_g} \tag{A.18}$$

Gas Phase Properties

A number of physical properties of the gas phase are used within the model, and they are calculated using Aspen Properties. As discussed previously, in the reference BFB model, surrogate models with explicit forms are developed using date generated by the Aspen property subroutines. The properties of the mixed gas are assumed to be a linear sum of those of the pure components. For example, the following linear regression equations calculate the gas thermal conductivity k_g, gas viscosity μ_g and gas molar heat capacity c_{pg}:

$$\begin{aligned} k_g &= y_{e,CO_2}(-7.7214\times10^{-7}\times P + 7.9571\times10^{-5}\times T_{g,e} + 0.01923) \\ &+ y_{e,H_2O}(-1.8623\times10^{-6}\times P + 8.7126\times10^{-5}\times T_{g,e} + 0.02078) \\ &+ y_{e,N_2}\times(9.0592\times10^{-7}\times P + 6.921\times10^{-5}\times T_{g,e} + 0.02794) \end{aligned} \tag{A.19}$$

$$\begin{aligned}\mu_g &= y_{e,CO_2}(8.512 \times 10^{-7} \times P + 4.6155 \times 10^{-5} \times T_{g,e} + 0.016614) \\ &+ y_{e,H_2O}(-2.282 \times 10^{-7} \times P + 3.7075 \times 10^{-5} \times T_{g,e} + 0.011082) \\ &+ y_{e,N_2}(9.6301 \times 10^{-7} \times P + 4.3339 \times 10^{-5} \times T_{g,e} + 0.019267))\end{aligned} \tag{A.20}$$

$$\begin{aligned}c_{p,g} &= y_{b,CO_2}(0.003054 \times P + 0.04579 \times T_{g,b} + 38.9499) \\ &+ y_{b,H_2O}(-0.0008426 \times P + 0.005919 \times T_{g,b} + 33.7558) \\ &+ y_{b,N_2} * (-0.0002627 \times P + 0.0009494 \times T_{g,b} + 29.1509)\end{aligned} \tag{A.21}$$

For properties such as gas concentration and gas density, the idea gas law is used to approximate these gas properties:

$$c_{b,t} = \frac{100P}{8.314 \times (T_{g,b} + 273.16)} \tag{A.22}$$

$$\rho_g = \frac{100P(y_{e,CO_2} \times 44.01 + y_{e,N_2} \times 28.01 + y_{e,H_2O} \times 18.02)}{8.314 \times (T_{g,e} + 273.16)} \tag{A.23}$$

Immersed Heat Exchanger Tube Correlations

For processes like CO_2 adsorption, there is a large amount of heat released during the process, so it's crucial to add heat exchanger tubes within the bed. Several correlation equations are used to calculate the key properties for the heat exchanger. Firstly the thermal conductivity of an emulsion packet is calculated by:

$$k_{p,a} = (3.58 - 2.5\varepsilon_d)k_g(\frac{k_p}{k_g})^{0.46-0.46\varepsilon_d} \tag{A.24}$$

Next, the residence time of emulsion packets at the heat exchanger surface τ, is calculated using the correlation equation:

$$\tau = 0.44(\frac{d_p g}{v_{mf}^2(f_n - a_h)^2})^{0.14}(\frac{d_p}{d_x})^{0.225} \tag{A.25}$$

where f_n is the fluidization number of the bed defined as:

$$f_n = \frac{v_g}{v_{mf}} \tag{A.26}$$

Next, the fraction of time that the heat exchanger surface is exposed to emulsion packets can be obtained by:

$$f_b = 0.33(\frac{v_{mf}^2(f_n - a_h)^2}{d_p g})^{0.14} \tag{A.27}$$

The following equation is used to calculate the heat transfer coefficient between the heat exchanger tubes and the emulsion packets:

$$h_d = 2\sqrt{\frac{k_{p,a}\rho_s c_{p,s}(1-\varepsilon_d)}{\Pi\tau}} \tag{A.28}$$

The heat transfer coefficient between the heat exchanger tubes and gas bubbles, h_l, and the overall heat transfer coefficient h_t are calculated using the following correlations with the Prandtl number Pr:

$$\frac{1000 h_l d_p}{k_g} = 0.009 Ar^{0.5} Pr^{0.33} \tag{A.29}$$

$$h_t = f_b h_d + (1 - f_b) h_l \tag{A.30}$$

Reaction Kinetics

The kinetic equations used in the model come from a simple kinetic model [52] built for a sorbent developed and tested at NETL (sorbent 32D). The model assumes that the adsorption of CO_2 and water occurs through a three-reaction scheme shown in equation (3.2.1) to equation (3.2.3). Each reaction is described by a kinetic expression involving a rate constant and an equilibrium constant. For each equation, the temperature dependence of these constants is described using the Arrhenius and

Gibbs equations respectively, and the temperature is in Kelvin.

$$k_j = A_j T exp(\frac{-E_j}{RT}) \tag{A.31}$$

$$10^5 K_j P = exp(\frac{-\Delta H_j}{RT} + \frac{\Delta S_j}{R}) \tag{A.32}$$

The reaction rates for each reaction are then described by the following equations:

$$r_{H_2O} = k_1(10^5 P y_{H_2O} - \frac{n_{H_2O}\rho_s}{K_1}) \tag{A.33}$$

$$r_{carb} = k_2((1 - \frac{2n_{carb}\rho_s + n_{bicarb}\rho_s}{nv})^2 (P y_{c,1} \times 10^5)^{m_1} - \frac{1}{K_2}\frac{n_{carb} + n_{bicarb}}{nv} n_{bicarb}\rho_s^2) \tag{A.34}$$

$$r_{bicarb} = k_3((1 - \frac{2n_{carb}\rho_s + n_{bicarb}\rho_s}{nv}) n_{H_2O}\rho_s P y_{CO_2} \times 10^5 - \frac{1}{K_3}\frac{n_{carb} + n_{bicarb}}{nv} n_{bicarb}\rho_s^2) \tag{A.35}$$

Nomenclature

a_h: empirical constant

a_p: particle specific surface area (m^2/kg)

A_o: area of distributor plate per orifice (m^2)

Ar: particle Archimedes number

A_x: cross-sectional area of fluidized bed (m^2)

C_r: average correction factor for heat exchanger tubes

c: gas phase concentration ($kmol/m^3$)

$c_{p,s}$: particle heat capacity (kJ/(kg K))

c_p: gas molar specific heat capacity (kJ/(kmol K))

D: diffusivity of species (m^2/s)

D_t: diameter of reactor vessel (m)

d_x: heat exchanger tube diameter (m)

d_p: particle diameter (m)

E: activation energy (J/mol)

$F_{g,in}$: input flue gas flow (kmol/s)

$F_{s,in}$: input solid sorbent flow (mol/s)

$F_{s,in}$: output solid sorbent flow (mol/s)

f_b: fraction of time heat exchanger surface is exposed to bubbles

f_{cw}: cloud-wake to bubble region volume ratio

f_n: fluidization number

g: gravity acceleration (m/s^2)

g_1, g_2, g_3: bubble growth coefficients

G_b: molar flowrate of gas in bubble region (kmol/s)

$H_{g,bulk}$: rate of heat transfer due to gas bulk flow (kJ/(s m))

$H_{s,bulk}$: rate of heat transfer due to solid bulk flow (kJ/(s m))

H_{bc}: bubble to cloud-wake gas heat transfer coefficient (kJ/(m^3 K s))

H_{ce}: cloud-wake to emulsion gas heat transfer coefficient (kJ/(m^3 K s))

h_s: sorbent specific enthalpy (kJ/kg)

h_t: overall heat transfer coefficient (kJ/(m^2 K s))

h_p: convective heat transfer coefficient (kJ/(m^2 K s))

h_d: heat transfer coefficient between heat exchanger and emulsion packet (J/(m^2 K s))

h_l: heat transfer coefficient between heat exchanger and bubble (J/(m^2 K s))

h_t: heat exchanger heat transfer coefficient (J/(m^2 K s))

$h_{s,in}$: output solid sorbent specific enthalpy (kJ/kg)

$h_{s,out}$: output solid sorbent specific enthalpy (kJ/kg)

J: superficial solid flux (kg/(m^2 s))

k: reaction rate constant

k_p: thermal conductivity of solid particles (J/(m K s))

$k_{p,a}$: thermal conductivity of emulsion packet (J/(m K s))

K: reaction equilibrium constant

$K_{ce,bs}$: cloud-wake to emulsion solids mass transfer coefficient (s^{-1})

K_{ce}: cloud-wake to emulsion gas mass transfer coefficient (s^{-1})

K_{bc}: bubble to cloud-wake gas mass transfer coefficient (s^{-1})

$K_{g,bulk}$: rate of gas bulk flow between bubble and emulsion region (kmol/(m s))

$K_{s,bulk}$: rate of solid bulk flow between cloud-wake and emulsion region (kmol/(m s))

$K_{ce,bs}$: cloud-wake to emulsion solids mass transfer coefficient (s^{-1})

k_g: gas thermal conductivity (J/(m K s))

L: reactor length (m)

n: adsorbed species concentrations in the sorbent (mol/kg)

nv: amine loading of the sorbent (mol/m^3)

N_{or}: number of orifices per square meter in distributor plate (m^{-2})

N_x: number of tubes in heat exchanger

Nu_p: Nusselt number

P: bed pressure (bar)

Re: Reynolds number

r: rate of reaction (mol/(m^3 s))

T: temperature (K)

$T_{g,in}$: Input flue gas temperature (K)

v: gas velocity (m/s)

x: height above distributor plate (m)

y: gas mole fraction

$z_{g,in}$: input flue gas mole fraction

$z_{s,in}$: input solid sorbent mole fraction

$z_{s,out}$: output solid sorbent mole fraction

ΔH: heat of reaction (J/mol)

ΔS: reaction entropy (J/mol)

ΔT_{hx}: heat exchanger temperature difference (K)

Greek characters

$delta$: volume fraction of bubbles in bed

ρ_g: gas density (kg/m^3)

ρ_s: solid density (kg/m^3)

ε: cross-sectional average voidage (m^3/m^3)

ε_d: voidage of emulsion region (m^3/m^3)

ϕ_s: particle sphericity

τ: bubble residence time at heat exchanger surface (s)

μ: gas viscosity (kg/(m s))

Subscripts

b: bubble region

c: cloud-wake region

e: emulsion region

i: adsorbed species

j: gaseous species

m: maximum

mf: minimum fluidization

t: total

0: bottom of the reactor (x=0)

L: top of the reactor (x=L)